Understanding the Glioblastoma Tumor Immune Microenvironment as Foundation for Refining Immunotherapeutic Strategies: Contributions from Tumor Cell Lineage and NF1 Alterations

by

Mollie E Chipman

A Dissertation

Presented to the Faculty of the Louis V. Gerstner, Jr.

Graduate School of Biomedical Sciences,

Memorial Sloan Kettering Cancer Center

in Partial Fulfillment of the Requirements for the Degree of

Doctor of Philosophy

New York, NY

May 2023

_____ _____

Luis F Parada, PhD Date

Dissertation Mentor

Dedication

My dissertation is dedicated to my parents, Susan and Richard Chipman, my sister and nephew, Shannon King and Chris Sylvia, my Fiancé, Jonathan Smith, and my friends, who's unconditional love and support have propelled me through my journey. I also dedicate my dissertation to Jordan Aronowitz, a beloved GSK classmate and friend whom we lost too early.

Abstract

Glioblastoma Multiforme (GBM) is an aggressive primary brain tumor with a dismal 5-year survival rate of 5-6%. The GBM tumor immune microenvironment (TIME) is composed primarily of tumor associated macrophages and has lower levels of lymphocytes (T-cells, B-cells, NK-cells) and other myeloid populations (dendritic cells, myeloid-derived suppressor cells). Recent clinical trials of immunotherapeutics in GBM have been unsuccessful. Greater strides in understanding the TIME are critical to poise current and future immunotherapies for success in GBM. Here, we discovered two factors that shape the tumor immune microenvironment in GBM: tumor cell lineage and NF1 loss.

To study the role of tumor cell of origin in shaping the immune microenvironment, we used two lineage-based models of GBM: a neural stem cell (NSC) driven model *Nst-CreER^{T2}; Nf1$^{fl/+}$; Trp53$^{fl/fl}$; Pten$^{fl/+}$* and an oligodendrocytic progenitor cell lineage (OPC) driven model *NG2-CreER^{T2}; Nf1$^{fl/+}$; Trp53$^{fl/fl}$; Pten$^{fl/+}$*. We characterized the tumor immune microenvironments of these models and found that OPC-driven GBMs recruited greater numbers of tumor-associated macrophages (TAMs) and specifically monocyte-derived macrophages (MDMs) in both spontaneous and orthotopic allograft mouse models. Given the difference in predominant TAM ontogeny in NSC and OPC driven GBMs, we depleted TAMs with a combination of genetic and pharmacologic approaches to determine the role of TAMs in tumor progression in these two tumor types. We found that TAM depletion did not extend survival in either NPC or OPC driven mouse models of GBM. Further, we examined the changes in gene expression between TAM depleted and control tumors and found that TAM depleted tumors did not up regulate any compensatory pathways to overcome TAM depletion. This suggests that GBMs do not depend on the support of TAMs for survival. Overall, we uncover tumor cell-lineage as a

driver of MDM recruitment in GBM and show that GBMs progress independent of TAMs in both lineage-based models.

NF1 is a common driver mutation of GBM and is mutated in approximately 17% of cases. Large scale transcriptomic studies of patient GBM samples have correlated NF1 loss with increased tumor immune infiltration. Here, we aimed to uncover mechanisms by which NF1 loss promotes inflammation in GBM using genetically engineered mouse models of NF1 mutant and NF1 WT GBM. We demonstrate that NF1 loss causes enhanced immune infiltration in GBM, specifically of lymphocytes and monocytic populations. Next, we used CITEseq to dissect the activation states and communication networks in the GBM TIME. This revealed that NF1 mutant GBMs have significantly increased ligand-receptor mediated crosstalk between the TIME cells compared to NF1 WT GBMs. Increased cellular crosstalk in NF1 mutant GBMs occurred primarily through greater cytokine production and receptor expression by immune cell populations. We profile cytokines using targeted proteomics in mouse and human GBMs and show that NF1 mutant GBMs have higher levels of NFKB pathway target cytokines. When comparing DEGs between NF1 mutant and WT GBM immune cell populations, enhanced TNFa signaling through NFKB was is enriched in NF1 mutant GBM, and this corresponds with increased nuclear localization of NFKB1 and CEBPB transcription factors in NF1 mutant GBM immune cells. In sum, NF1 mutant GBMs recruit greater amounts of immune infiltrates through increased secretion of pro-inflammatory cytokines mediated by NFKB1 and CEBPB transcription factor activity.

Biographical Sketch

Mollie Chipman grew up in Cohasset, Massachusetts. There, she attended the Cohasset Public School systems throughout elementary, middle, and high school. It was in Doc T's Introduction to Chemistry class in High School that she realized her passion for science. Additionally, while in high school, Mollie spent portions of her summer volunteering on the oncology floor at Children's Hospital Boston, which fueled her passion for oncology research and drug development. After high school, Mollie attended Tufts University in Medford, MA. During her sophomore year, she wanted to get involved in cancer research and excitedly joined the Amy Yee lab at Tufts Medical School. She worked in Dr. Yee's lab for the rest of the semesters and summers of her undergraduate education studying the underlying mechanisms of a drug combination therapy in triple negative breast cancer. Her work resulted in a second author manuscript published on BioRXiv and served as the foundation for a startup company, Cha Therapeutics. Mollie graduated Tufts University in May 2017, *Magna Cum Laude,* with a Bachelor of Science in Engineering Science and Biochemistry.

With the encouragement and mentorship of Dr. Amy Yee, Mollie applied to graduate schools with the goal of continuing cancer research. She excitedly joined the Gerstner Sloan Kettering (GSK) Graduate School of Biomedical Sciences at Memorial Sloan Kettering Cancer Center (MSKCC) to pursue her PhD in Cancer Biology in July 2017. Excited to study the tumor immune microenvironment of Glioblastoma, Mollie joined the lab of Dr. Luis Parada for her thesis work. During this time, Mollie was supported by the MSKCC Geoffrey

Beene Fellowship and the NIH Ruth L. Kirschstein National Research Service Award. Mollie greatly enjoyed her time at GSK/MSKCC and in the Parada Lab and will be forever grateful for her top-notch Cancer Biology training that has set the stage for the rest of her career.

Acknowledgements

I would like to thank the many mentors I have had in my life that have been instrumental to my growth as an individual and in my career. I would like to first thank my high school chemistry teacher, Dr. Ann Thomae, or “Doc T”, who helped me discover my passion for science and fostered my endless curiosities about the subject. Next, I would like to thank my undergraduate mentors, Dr. Amy Yee and Dr. Eric K Paulson. Amy and Eric took me on in their lab, taught me everything from how to pipette to running a qRTPCR experiment, and got me excited about cancer research. Amy and Eric encouraged me to pursue my PhD and offered continued support throughout the application process and beyond. If it was not for these fantastic mentors who cultivated my passion for science and research, I would not have made it to a PhD program.

Next, I would like to thank my PhD mentor, Dr. Luis Parada. I met Luis when I was interviewing for graduate school and was drawn to his passion for researching difficult to treat, rare tumors, including glioblastoma and malignant peripheral nerve sheath tumors. Luis has pushed me to think critically about all my findings and to be rigorous in my scientific approach. He has also taught me not to be afraid to challenge the status quo of a field. Additionally, Luis has taught me to have high standards for cancer research and for mouse models of disease. I hope to carry the high scientific standards, critical thinking, and boldness that I have gained from Luis in my training as a cancer biologist throughout my career.

Next, I would like to acknowledge all the Parada Lab members who were instrumental in my journey through graduate school. First, I would like to thank

Zilai Wang, who was my first post-doctoral mentor in the lab, and who taught me several technical and experimental design skills that I used throughout graduate school. I would also like to thank Daochun Sun and Swathi Iyer, who also served as post-doctoral mentors to me during my time in the lab. Next, I acknowledge Yu-Jung Chen and Chenu Jayewickreme, for being there to commiserate and work our way through graduate school together. I would also like to thank senior research technician, Alicia Pedraza, who's technical skills and support were extremely helpful in my projects. Current and former Parada Lab members Sheila Alcantara Llaguno, Xuanhua Xie, Dan Laks, Charlene Iltis, Stefan Sweha, Kacper Walentynowicz, Tao Wang, Rebecca Brown, Sameer Farouk-Sait, Sarnai Ganbold, Samhita Bapat, Chowdhury Rahman, Michelle Lien, Jing Li, and Jemma Villavieja were generous with their time, ideas, and technical know-how. Lab support staff, Aimee Cowen, Ashley Chandradat, and Tunde Frankl provided valuable research support. Finally, I thank the Parada Lab for all the fun times we have had at Luis's holiday parties, retreats, picnics, lab lunches, and happy hour drinks!

Next, I would like to thank my committee members, Dr. Adrienne Boire and Dr. Justin Perry. Adrienne and Justin gave me support and advice for graduate school and beyond. Their guidance during my thesis committee meetings was important in moving my project forward.

I would like to thank the Gerstner Sloan Kettering Graduate School (GSK) for providing an amazing community during my graduate school experience. The support from my GSK classmates has contributed significantly to making my PhD

experience positive and fun. Thank you for all the beers, ski trips, faculty club happy hours, retreats, heart to hearts, etc. I also acknowledge the GSK graduate school Deans and Assistant Deans, Ken Marians (former Dean), Michael Overholtzer (current Dead), Linda Burnley (Associate Dean), and Tom Magaldi (Assistant Dean), and graduate school support staff, David McDonagh, Raphaelle Chassagne, and Julie Masen for creating and cultivating this incredible community.

I would also like to thank Thalyana Stathis, who's career events and coaching are the reason I figured out what I wanted to do with my PhD.

Lastly, I would like to acknowledge my family and friends. I have had a fantastic network of friends in NYC and elsewhere who provided an excellent distraction from failing experiments. I would like to thank my Fiancé, Jonathan Smith, who I met in the months leading up to my qualifying exam, for supporting me and putting up with all my complaining during this journey. And finally, I would like to thank my family, who provided love, support, and encouragement throughout my whole life and time as a student.

Table of Contents

List of Figures

List of Abbreviations

GBM: Glioblastoma

TIME: Tumor immune microenvironment

Chapter 1 Introduction

Glioblastoma

Glioblastoma (GBM) is the most commonly occurring malignancy of the central nervous system (CNS). GBM is a Grade IV, highly invasive brain tumor that has a dismal 5-year survival rate of 5%[1, 2]. Standard of care includes surgery followed by radiotherapy and chemotherapy, with tumor treating fields[3]. Of over 400 clinical trials since 2005, encompassing over 32,000 patients, testing many therapies, only one Phase III and no Phase III trials have demonstrated success for newly diagnosed and recurrent GBM respectively[4]. Thus, targeted therapies so far remain ineffective in GBM[5]. Overall, the prognosis for GBM patients remains bleak, and new therapies are urgently needed.

Cell of Origin

Several cell populations in the adult human brain serve as candidates for the cell of origin for GBM. Subventricular zone (SVZ) neural stem cells (NSCs) and oligodendrocyte progenitor lineage cells (OPCs) are both populations present in the adult brain that can proliferate throughout life[6, 7]. As such, our group and others have demonstrated that mouse GBM can arise from SVZ NSCs and OPCs[8, 9, 10], and that GBMs are far less likely to arise from more differentiated cell types[11]. Additionally, the SVZ region in GBM patients has been shown to harbor low level GBM driver mutations that are represented at high levels in the

patient tumor, suggesting that human GBMs can also be derived from SVZ NSCs[12].

Stratification Methods

Patient disease stratification methods can improve the outcome of clinical trials. There have been several strategies proposed to subclassify GBM. In one strategy by the TCGA, hundreds of patient GBM samples were bulk RNA-sequenced and four transcriptional subtypes, Classical, Mesenchymal, Proneural, and Neural were derived by hierarchal clustering[13, 14]. Later, the Neural classification was dropped due to contamination of normal brain tissue in these samples[15]. The three remaining subtypes were correlated with certain GBM driver mutations; the Classical, Mesenchymal, and Proneural subtypes were correlated with EGFR, NF1, and PDGFRA alterations respectively[13, 15]. Additionally, Mesenchymal tumors were correlated with increased GBM immune infiltration[15]. NF1 loss has previously been shown to play an important role in shaping the tumor immune microenvironment in Neurofibromatosis Type 1-associated tumors as well[16], highlighting the potential role of NF1 in several tumor types in promoting tumor immune infiltration and activation. Despite the strong correlation between NF1 alterations and enhanced GBM immune infiltration, it remains unknown how NF1 loss contributes to enhanced immune infiltration. Although the TCGA classifications have been studied extensively preclinically, the clinical relevance remains in question[5].

Aside from subtyping GBMs based on transcriptomic classifications and driver mutations, evidence has demonstrated a role for GBM tumor cell-lineage in shaping the molecular and histological features of GBM[9, 10]. SVZ NSC-derived and OPC-derived GBMs have been demonstrated to have distinct therapeutic vulnerabilities[10], thus providing strong rational to potentially stratify future clinical trials by GBM cell lineage.

Tumor Immune Microenvironment

The GBM tumor immune microenvironment (TIME) is primarily cold: characterized by extensive tumor-associated macrophage (TAM) infiltration, and to a lesser extent other myeloid populations, T-cells, B-cells, and NK-cells[17]. The function of the TIME in GBM is context dependent; roles for the myeloid and lymphoid populations have varied across experimental model systems and remain an area of active investigation[18].

TAMs can account for up to 40% of the GBM tumor mass and thus have been widely studied to further understand their function and potential to be therapeutically targeted in GBM[19]. TAMs have primarily been shown to support tumor growth through secretion of cytokines, chemokines and growth factors that enhance tumor cell proliferation, invasion, angiogenesis, and suppression of anti-tumor immune responses[20, 21, 22, 23, 24, 25]. As such, CSF1R inhibition, which targets an important growth/survival pathway in TAMs, has been studied both preclinically and clinically in GBM[26, 27, 28]. In several preclinical studies in PDGFB-

driven GBM models, CSF1R inhibitor dramatically extended mouse survival[26]. However, population-wide responses were not seen in Phase II studies of CSF1R inhibitor in human patients[28]. More recently, studies have shown that treatment with CSF1R inhibitor can hinder survival or have no impact on survival in HRas-driven and PDGFRA-driven mouse models of GBM, respectively[29]. These studies highlight the context-dependent roles for TAMs in GBM and prompt the need for more studies determining how TAM function varies across GBMs.

Recent single cell sequencing studies have highlighted the complexity of TAM populations in the tumor immune microenvironment[30, 31, 32]. One study comparing TAM populations using scRNAseq between a mouse model of GBM, and newly diagnosed and recurrent human GBM highlighted the heterogeneity of TAM populations; they found an interferon-gamma response cluster, a phagocytic/lipid metabolism cluster, and a hypoxic cluster, among others[30]. To dissect the function of these TAM populations, they will either need to be depleted to examine effects on the microenvironment and tumor progression or sorted from the tumor to assess functionality in vitro. Moreover, a recent study identified a population of CD169+ macrophages that supported anti-tumor immunity[33]. Further, they showed that depleting this CD169+ TAM population caused decreased survival in mice, decreased tumor immune infiltration, and decreased pro-inflammatory cytokine secretion[33]. Overall, the role of TAMs in GBM is

complex, and should be studied further in several contexts and model systems to enhance the knowledge of the field.

Other myeloid populations have also been shown to be present in the GBM TIME including myeloid-derived suppressor cells (MDSCs) and dendritic cells. MDSCs have been shown to have a sex-dependent role in GBMs, with depletion of granulocytic-derived MDSCs extending survival in female but not male GBM-bearing mice, again highlighting the context-dependent function of the tumor immune microenvironment[34]. MDSCs are not present in all single cell studies of the GBM TIME[30, 31, 32], making assessing their functionality challenging. This could be due partly to the lack of markers characterizing the population. Several dendritic cell populations have been identified in the GBM TIME, including conventional dendritic cells, migratory dendritic cells, plasmacytoid dendritic cells, and pre-dendritic cells[30]. They appear to share some transcriptional similarity to TAMs in GBM, but their function in the microenvironment is still under investigation[18]. Early studies have shown that either increasing conventional dendritic cell recruitment or activation can augment immune checkpoint therapies in GBM[35]. More studies are necessary to fully understand the functionality of dendritic cells in the GBM TIME.

CD8 cytotoxic T-cells, CD4 T-helper cells, and regulatory CD4+, FOXP3+ T-cells are all present in the GBM tumor immune microenvironment. For the most part, CD8 and CD4 T-cells are exhausted and non-functional in the GBM TIME, and

regulatory T-cells (T-regs) are immunosuppressive[25]. Effector T-cells can be exhausted by TAMs, tumor cells, and T-regs, and often express markers of exhaustion such as PD1, CTLA4, TIM-3 and/or LAG-3[36]. Myeloid cells and tumor cells in GBM and in other cancers often express high levels of PDL1, which contributes to the exhaustion of T-cells in the TIME[36]. Additionally, T-cells can also be exhausted by tumor and other TIME cells through immune suppressive cytokine secretion. Recently, one report demonstrated that myeloid cells in the GBM TIME can exhaust T-cells through release of IL-10[37]. Like many cancers, there is a lack of an anti-tumor immune response from T-cells in GBM.

T-regs primarily function to suppress anti-tumor immunity in GBM. However, there is no clear correlation between T-reg abundance and GBM patient survival, suggesting that there may be some populations of T-regs that are less immunosuppressive than others[18, 38]. Another possibility is that GBMs do not rely on the immunosuppressive ability of T-regs for tumor progression. GBMs that have greater proportions of T-regs in their TIME will likely be better candidates for T-reg targeting immunotherapies[18]. Further study of T-reg functionality in the GBM TIME is necessary for optimization of T-reg targeting therapies for use in GBM.

Mouse Models of GBM

In the Parada Lab, we use spontaneous and allograft genetically engineered mouse models (GEMMs) of GBM with clinically relevant driver mutations and differing cells of origin[9, 10]. In the spontaneous model, tumor suppressor loss is

induced in the adult SVZ by tamoxifen induction of Nst-CreER^{T2}; Nf1$^{fl/+}$; Trp53$^{fl/fl}$; Pten$^{fl/+}$ mice to form Type 1 GBM[8, 9]. Alternatively, tumor suppressor recombination is induced in stem cells of the oligodendrocytic lineage by tamoxifen induction of NG2-CreER^{TM}; Nf1$^{fl/+}$; Trp53$^{fl/fl}$; Pten$^{fl/+}$ mice to form Type 2 GBM[9]. *NF1*, *TP53*, and *PTEN* represent commonly altered tumor suppressor genes in human GBM, and are altered in 18%, 35%, and 38% of tumors respectively[39]. Primary cultures from Type 1 and Type 2 spontaneous tumors can be grown in defined serum free medium and orthotopically injected into immunocompetent mice, forming tumors that resemble the molecular and histological features of spontaneous Type 1 and Type 2 GBM respectively[9, 10]. Primary cells are kept at low passage to reduce the gain of mutations through extensive serial passaging. Because spontaneous GBM mice are maintained on a mixed background (129/S and C57BL/6), the injection of cultured primary Type 1 and Type 2 spontaneous GBM cultured cells is an allograft model rather than a syngeneic model, and this is a shortcoming of this system[9, 10]. However, a similar allograft system, using spontaneous cultured GBM tumor cells orthotopically injected into immunocompetent mice[40], was reported to resemble human GBM and thereby serve as a relevant model system to study the TIME of GBM[41]. Ultimately, the allograft models presented here have been extensively characterized and offer a physiologically relevant system to study the TIME in GBM.

Several syngeneic models are used to study the tumor immune microenvironment of GBM as well. The most used models include the GL261 model[42], the C2TA model[43], and the RCAS system[44]. The GL261 model was generated in 1970 by the injection of the chemical carcinogen methylcholanthrene into the brains of C57BL/6 mice and was reported to histologically resemble ependymoblastomas (rare embryonic brain tumors)[42]. The GL261 model is highly immunogenic due to the artificially high number of mutations, with a tumor mutational burden of 4978 mutations compared to 2.7 mutations in human GBM[45]. GL261 tumors carry point mutations in *K-ras* and *Trp53*, and although *TP53* is commonly mutated in human GBM, only 1.5% of human GBMs have alterations in *K-ras (C-Bio portal)*[39, 46]. Consistent with the high mutational burden, GL261 tumors have been shown to have greater infiltration of CD8+ T-cells than is found in human GBMs[47]. Not surprisingly, given the artificially high mutational burden and large CD8 T-cell infiltration, several studies using the GL261 model have shown responses to checkpoint blockade therapy[45, 48, 49], which did not translate into the clinic[50]. The GL261 model has been the single most used model system to study the TIME of GBM, and it is unknown whether these findings will translate to the clinic[51]. Overall, the GL261 brain tumor model has several shortcomings, including not histologically resembling GBM, derivation by chemical carcinogenesis, high tumor mutational burden, the less physiologically relevant point mutation of *K-ras,* and the artificially high infiltration of CD8+ T-cells*.* Given these shortcomings, the GL261

model should not be relied upon for clinically translatable findings regarding the GBM TIME.

Similar to the GL261 model, the C2TA model was chemically derived via injection of methylcholanthrene into C7BL/6 mice[43]. C2TA tumors resemble anaplastic astrocytomas, and share several high-grade histological features with GBMs, such as high cell density, pseudopalisading necrosis, and microvascular proliferation[51, 52]. Although the data is not readily available, C2TA tumors likely have a high mutational burden, similar to GL261 tumors, due to their derivation through chemical carcinogenesis and continueous serial passaging[51]. C2TA tumors are deficient in Pten, like many human GBMs. Studies have classified C2TA tumors as more immunologically inert than GL261 tumors[47]. Shortcomings of the C2TA model include derivation by chemical carcinogenesis, likely high mutational burden, and lack of characterization. Overall, C2TA tumors may present a less immunogenic alternative to the GL261 model, however, further characterization is required to better understand this model system and its physiologic relevance.

The RCAS/*tv-a* system is another widely used model to study the TIME of GBM[44]. RCAS/*tv-a* is a somatic gene transfer system: gene transfer is mediated by delivering cells expressing *RCAS-gene* to cells expressing the RCAS receptor, *tv-a,* thus allowing cell-type specific gene transfer[44]. To model GBM, *Tv-a* expression is driven by the Nestin transgene (*Ntv-a*), and thereby likely

expressed in the SVZ NSCs, but this has not been fully characterized[44]. Then, DF-1 chicken fibroblast cells are engineered to secrete RCAS-PDGFB, and injected into the brains of mice[44]. This model system is used on *Cdkn2a* germline deficient mice (*Cdkn2a*$^{-/-}$) to accelerate tumor formation[44]. The impact of germline deletion of Cdkn2a on tumor infiltrating immune cells has not been described. This model system was used in several important studies examining the role of TAMs in GBM tumor progression and survival[26, 27]. More recent studies have incorporated RCAS-shRNAs to add GBM relevant deletions of tumor suppressors such as *Nf1* and *Trp53* to the tumors, which has allowed the modeling of various TCGA GBM subtypes[53]. The prominent shortcomings of this system include the potential inflammatory effects of delivering chicken fibroblasts to the brain and unknown impact of germline deletion of *Cdkn2a* on TIME cells. Overall, our spontaneous and allograft GBM models have the fewest shortcomings and represent the most physiologically relevant system to study the tumor immune microenvironment of GBM.

Immunotherapy in GBM

In the last decade, immunotherapy has become a main stay in cancer treatment, and has been incredibly successful in certain tumor types[18]. One of the most successful therapies thus far is checkpoint blockade therapy. These therapies work by interfering with the T-cell immune checkpoints: PD1 and CTLA4[54]. Therapies targeting other immune checkpoints are also under development. Antibodies bind either PD1 (Nivolumab and Pembrolizumab), PDL1

(Atezolizumab and Avelumab), or CTLA4 (Ipilimumab and Tremelimumab) to prevent CD8 T-cells from being exhausted via immune checkpoint binding by tumor cells and immune-suppressive myeloid cells among others[54]. Unfortunately, Checkpoint blockade therapy using PD1 inhibitor Nivolumab failed to produce population-wide responses in both newly diagnosed[50] and recurrent GBM[55]. No relevant patient segmentation was used in either of these trials, aside from MGMT methylation status, which to my knowledge, has not been shown preclinically to influence GBM response to immunotherapy.

Aside from checkpoint blockade therapy, CSF1R inhibition has been tested in Phase II clinical trials for GBM[28], due to promising preclinical studies[26, 27]. Unfortunately, this also did not produce population-wide responses[28]. Again, no relevant patient segmentation strategy was employed.

Despite many failures of immunotherapies in GBM, there has been recent success with oncolytic viral therapy[56], and dendritic cell vaccines[57]. In a clinical trial of oncolytic herpes virus G47Δ, the median overall survival (OS) and progression free survival (PFS) was 20.2 months and 4.7 months, compared to historic controls of standard of care of 5.0 months and 1.8 months[56]. Some shortcomings of this study include a small N (19 patients), and lack of a control study arm and patient segmentation[56]. In the Phase III study of autologous tumor lysate-loaded dendritic cell vaccines, newly diagnosed GBM patients treated with vaccines had an OS of 19.3 months since randomization, and externally matched

controls had an OS of 16.4 months since randomization[57]. For recurrent GBM, vaccine treated patients and externally matched controls has an OS of 13.2 months and 7.8 months since relapse respectively[57]. A limitation of this study includes use of externally matched controls without patient level data for optimal comparison[57]. Despite the limitations, both studies are exciting for the future of immunotherapy in GBM.

As discussed above, the TIME of GBM is cold, making it less likely for GBMs to respond to certain immunotherapies that work better in “hot” tumors containing T-cell infiltration and elevated immune activity. Several studies have investigated potential strategies to make GBM tumors hot. For example, a recent report proposes that the cold nature of GBM tumors may have to do with the lack of draining of tumor antigens to the cervical draining lymph nodes[58]. They showed that treatment with VEGF-C endows greater priming and infiltration of CD8 T-cells, and enhanced survival of mice bearing GBMs alone or in combination with checkpoint inhibitor therapy[58]. Another strategy that has been effective preclinically is engineering oncolytic viral therapies to express and secrete a cetuximab-CCL5 fusion protein for the targeted delivery of pro-inflammatory CCL5 cytokine[59]. This treatment enhanced the infiltration and activation of several immune populations, inhibited EGFR signaling, and offered a survival improvement compared to oncolytic viral therapy alone[59]. In another study, administration of antibody conjugated TNFa was safe and increased CD4 and CD8 T-cell infiltration in GBM patients in a Phase 1 study[60]. Recent clinical trial

successes of oncolytic viral therapy and dendritic cell vaccines, along with improved strategies to make GBMs hot, offer exciting possibilities for the future of immunotherapies in GBM.

Expanding Patient Stratification Strategies

Thus far, the use of patient segmentation strategies in Glioblastoma immunotherapy clinical trials has been lacking. To maximize the potential of immunotherapies in GBM, it is important to examine biomarkers that could predict patient response to treatments. Here, we examined the impact of glioblastoma cell lineage and NF1 loss on shaping the tumor immune microenvironment. We have shown previously that glioblastoma cell lineage can impact the molecular and histological features of the tumor, and response to targeted therapies[10]. Therefore, it is logical to investigate if cell lineage can also influence the composition of the TIME and response to microenvironment targeting therapies. Several studies have reported the correlation between NF1 loss and increased immune infiltration in GBM[15, 61]. Thus, we seek to understand potential mechanisms by which NF1 loss shapes the tumor immune microenvironment. Overall, we aim to gain a better basic understanding of the GBM TIME and to propose potential patient segmentation strategies for GBM clinical trials.

Chapter 2 Tumor progression is independent of tumor-associated macrophages in cell-lineage based mouse models of glioblastoma

Abstract

Macrophage targeting therapies have had limited clinical success in glioblastoma (GBM). Further understanding the GBM immune microenvironment is critical for refining immunotherapeutic approaches. Here, we use genetically engineered mouse models and orthotopic transplantation-based GBM models with identical driver mutations and unique cells of origin to examine the role of tumor cell lineage in shaping the immune microenvironment and response to tumor-associated macrophage (TAM) depletion therapy. We show that oligodendrocyte progenitor cell lineage-associated GBMs (Type 2) recruit more immune infiltrates and specifically monocyte-derived macrophages than subventricular zone neural stem cell-associated GBMs (Type 1). We then devise a TAM depletion system that offers a uniquely robust and sustained TAM depletion. We find that extensive TAM depletion in these cell lineage-based GBM models affords no survival benefit. Despite the lack of survival benefit of TAM depletion, we show that Type 1 and Type 2 GBMs have unique molecular responses to TAM depletion. In sum, we demonstrate that GBM cell lineage influences TAM ontogeny and abundance, and molecular response to TAM depletion.

Introduction

Glioblastoma Multiforme (GBM) is an aggressive primary brain tumor with a dismal five-year survival rate of five percent[1]. Standard of care therapy is surgery

followed by radiation and chemotherapy with tumor treating fields[3]. Given that TAMs can constitute up to forty percent of live cells in GBM, it's logical to examine their functions in tumor development and progression to assess their value as possible therapeutic targets[17].

In GBM, TAMs are composed of both tissue resident microglia and monocyte-derived macrophages (MDMs) infiltrating from the periphery[19]. TAMs have been reported to exhibit pro-tumorigenic functions, including promoting angiogenesis, secreting tumor supportive growth factors, and suppressing anti-tumor immunity[20, 21, 22, 23]. However, recent single-cell RNA sequencing studies have highlighted the heterogeneity of TAM populations in GBM[30, 31, 32], and certain subpopulations have been reported to support anti-tumor immunity[33]. Overall, the role of TAMs in GBM is complex[62] and incompletely understood.

Because TAMs rely on CSF1-CSF1R signaling for proliferation and survival, several studies have tested the effect of CSF1R inhibition on GBM survival. Targeting TAMs with CSF1R inhibitor was reported as highly effective in RCAS PDGFB-driven models of GBM[26, 27]. However, despite promising preclinical studies, CSF1R inhibitor therapy did not show population-wide success in GBM clinical trials[28]. In this clinical trial[28], two patients showed an extended progression free survival, suggesting that subsets of GBM may indeed respond to CSF1R therapy. More recently, CSF1R inhibitor therapy was tested in several mouse models of GBM with differing driver mutations; success was again seen in PDGFRB-driven GBM, but not in H-Ras or PDGFA-driven

models[29]. These studies highlight the diversity of models, and that a more basic understanding of the GBM tumor immune microenvironment as well as more cohesive preclinical data are needed.

Here, we explore GBM cell lineage association as a potential patient segmentation strategy for TAM targeted therapy using mouse models harboring identical and physiologically relevant driver mutations (*Nf1*, *Trp53*, and *Pten*) with unique cells of origin[10]. We show that while both tumor types exhibit immune infiltration, oligodendrocyte progenitor cell (OPC) lineage-derived GBMs recruit significantly greater numbers of MDMs compared to subventricular zone (SVZ) neural stem cell (NSC) derived GBMs. To examine the role of TAMs in tumor development and progression, we combine a genetic and pharmacologic approach to achieve effective and sustained TAM depletion beyond the effects of CSF1R inhibitor therapy alone. Acute and chronic TAM depletion in our lineage-based models of GBM show no significant modulation of tumor initiation, progression, or survival extension.

Results

Cell of origin impacts immune microenvironment.

To investigate the impact of cell of origin on the tumor immune microenvironment in GBM, we used two experimental systems: spontaneous genetic models and allograft models. In the spontaneous model, tumor suppressor loss is induced in the adult SVZ by tamoxifen induction of *Nst-CreER^{T2}; Nf1$^{fl/+}$; Trp53$^{fl/fl}$; Pten$^{fl/+}$*

mice to form Type 1 GBM[9]. Alternatively, tumor suppressor recombination is induced in progenitor cells of the oligodendrocytic lineage by tamoxifen induction of *NG2-CreER^{TM}; Nf1$^{fl/+}$; Trp53$^{fl/fl}$; Pten$^{fl/+}$* mice to form Type 2 GBM[9] (Figure 2-1A). Primary cultures from the Type 1 and Type 2 tumors can be grown in defined serum free medium and orthotopically injected into immunocompetent mice[9] (Figure 2-2A). These models have been extensively characterized[10] and offer a physiologically relevant and immunocompetent system to study the tumor immune microenvironment.

TAM morphology and quantity was assessed in the spontaneous tumor cores using immunohistochemical staining with IBA1 antibody. Type 1 (SVZ) tumors exhibited fewer TAMs albeit with a greater number of processes than Type 2 (oligodendrocyte lineage) GBM TAMs (Figure 2-1B, C). MDMs are known to have fewer processes compared to resident microglia[63], thus suggesting that Type 2 GBMs have greater MDM infiltration. We also examined the TAM composition in orthotopically transplanted tumors and found similar results as the spontaneous tumors with greater number of TAMs in the oligodendrocyte lineage associated (Type 2) tumors (Figure 2-2B). To assess the ontogeny and spatial distribution of TAMs in spontaneous Type 1 and Type 2 GBMs, CD44, a marker of MDMs[30], was used in conjunction with IBA1. We observed a significant increase in IBA1+, CD44+ cells in the tumor core and IBA1, CD44- cells in the parenchyma of Type 2 GBMs, consistent with our observations on the morphology difference of Type 1 and Type 2 GBM TAMs (Figure 2-2C). Overall,

the majority of MDMs are in the tumor cores of Type 1 and Type 2 GBMs, while microglia are present in the tumor core, border, and brain parenchyma, likely reflecting preferential tumor entry zones with MDMs entering via neoangiogenic vessels (Figure 2-2C). To assess TAM ontogeny and spatial distribution in Type 1 and Type 2 transplanted GBMs, lineage tracing was employed using *Cx3cr1-CreER-Ires-Yfp; Lsl-Tdt* mice. Microglia retain Tdt positivity over time and were quantified as Tdt+, IBA1+ cells, while MDMs loose Tdt positivity over time, and were thus quantified as Tdt-, IBA1+ cells. Again, Type 2 GBMs had significantly greater amounts of IBA1+, Tdt- MDMs in the tumor core (Figure 2-2D). The spatial distribution of TAMs mirrored that seen in spontaneous GBMs, as the majority of MDMs are localized to the tumor core, while microglia are distributed throughout the tumor core, border, and brain parenchyma (Figure 2-2D).

To further characterize the microenvironments of spontaneous Type 1 and Type 2 GBM, multi-color flow cytometry was used to quantify myeloid and lymphoid populations (Figure 2-3A). Type 2 GBM showed significantly higher levels of CD45+ immune infiltrates, characterized by increased levels of MDMs, microglia, monocytes, and neutrophils (Figure 2-1D). Increased levels of MDMs were verified using an independent MDM marker, CD49D[64] (Figure 2-1D). In contrast, relative lymphoid cell levels were not significantly different between Type 1 and Type 2 tumors (Figure 2-3B). We next examined transplanted tumors and found similar immune microenvironment composition with Type 2 tumors exhibiting higher levels of MDMs and neutrophils and trending higher levels of monocytes and microglia (Figure 2-2E).

Again, increased levels of MDMs were verified with the independent MDM marker, CD49D[64] (Figure 2-2E). We note that although the TAM trends in spontaneous tumors are mirrored in transplanted tumors, we do see a higher recruitment of MDMs and almost all peripherally derived immune cell types in transplanted tumors. This is likely due to the higher growth rate of transplanted tumors (~6-8 weeks for transplanted tumors compared to ~6-12 months for spontaneous tumors) and was also seen in another report comparing the immune infiltration of transplanted vs. spontaneous GBM mouse tumors[41]. In aggregate, these data indicate that in the context of identical driver mutations, cell of origin and lineage influence the microenvironment composition wherein Type 2 GBMs recruit more TAMs, and particularly MDMs, than Type 1 tumors.

Having previously identified cohorts of Type 1 and Type 2 GBM in the TCGA GBM data repository, we probed these datasets for expression of TAM-associated genes[10, 13, 14]. We found, consistent with the mouse modeling data, that expression of the pan-TAM marker gene *AIF1*, pan-immune infiltrate marker *PTPRC*, and MDM marker genes, *ITGA4* and *ITGAL*[64], were significantly higher in human Type II tumor data (Figure 2-1E). This suggests that human Type II GBMs have more total immune infiltration and specifically derived from MDMs than human Type I GBMs. Additionally, *SALL1*, a microglial marker gene[65], was significantly higher in Type I human tumors (Figure 2-1E). Overall, these analyses demonstrate that oligodendrocyte lineage-associated GBMs contain

substantially greater MDM numbers in both mouse human Type II GBM.

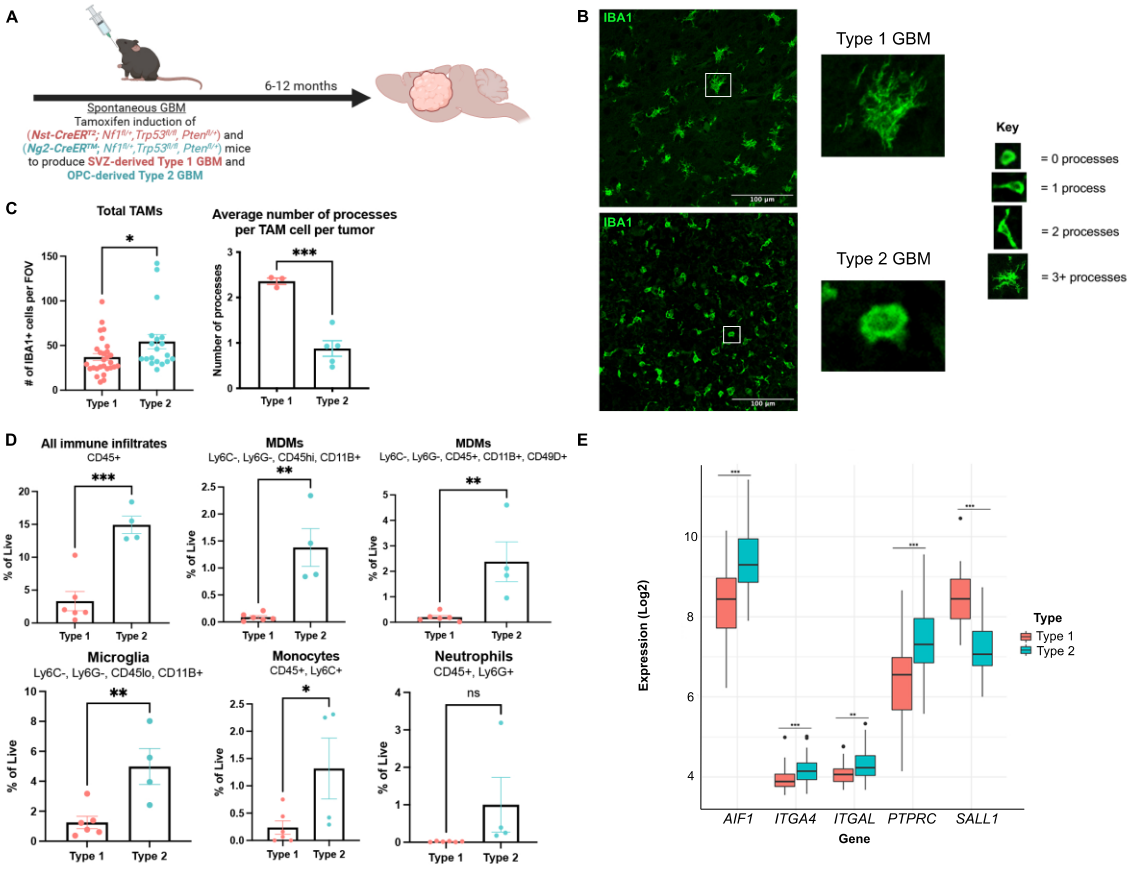

Figure 2-1 Cell of origin influences TAM ontogeny in spontaneous GEMMs of GBM.

(**A**) Schematic illustrating the spontaneous GEMMs used to examine the impact of GBM cell of origin on the tumor immune microenvironment. (**B**) IF images and quantification of the total TAMs in Type 1 and Type 2 spontaneous GBMs (N= 6 Type 1, 4 Type 2 tumors, data represented as mean with SEM, p= 0.0379, unpaired t-test, each dot represents one FOV) and the average number of processes per TAM cell per tumor (N=3 Type 1, 5 Type 2, data represented as mean with SEM, p= 0.0007, unpaired t-test, each dot represents one mouse). (**C**) Multi-color flow cytometry measuring the levels of all immune infiltrates (p=0.0006), MDMs (p=0.0017 $CD45^{hi}$, $CD11B^{+}$, p=0.0082 $CD45^{+}$, $CD11B^{+,}$ $CD49D^{+}$), Microglia (p=0.0086), Neutrophils, and Monocytes (p=0.0489), data represented as mean with SEM, unpaired T-test, each dot represents one mouse. (**D**) mRNA expression levels of pan-TAM (AIF1), MDM-associated (ITGA4, ITGAL), pan-immune (PTPRC), and microglia-associated (SALL1) genes in Type 1 and Type 2 subtyped human TCGA GBM samples.

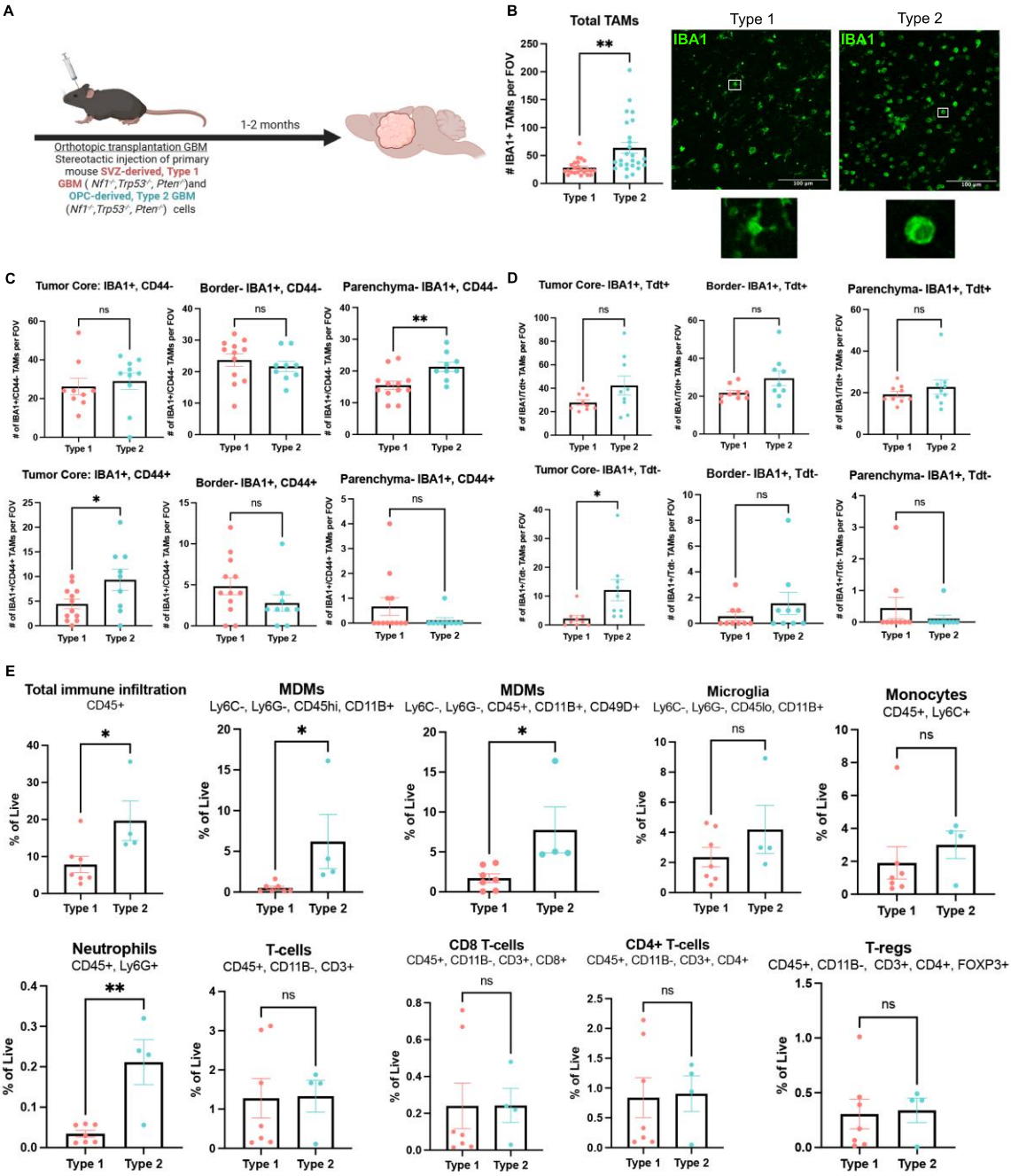

Figure 2-2 Cell of origin influences TAM ontogeny in transplantation-based mouse models of GBM

A) Schematic illustrating the orthotopic, transplanted mouse model used to examine the impact of GBM cell of origin on the tumor immune microenvironment. (**B**) IF staining quantification of the total TAMs in Type 1 and Type 2 transplanted GBMs, N= 4 Type 1, 5 Type 2, data represented as mean with SEM, 5 FOV per sample, p=0.0013, unpaired t-test. (**C**) Multi-color flow cytometry measuring the levels of total immune infiltrates (p=0.038), MDMs (p=0.043 $CD45^{hi}$, $CD11B^{+}$, p=0.023 $CD45^{+}$, $CD11B^{+,}$ $CD49D^{+}$), Microglia, Monocytes, Neutrophils (p=0.0022) and lymphoid cell populations in Type 1

vs. Type 2 transplanted GBMs, data represented as mean with SEM, unpaired t-test, each dot represents one mouse.

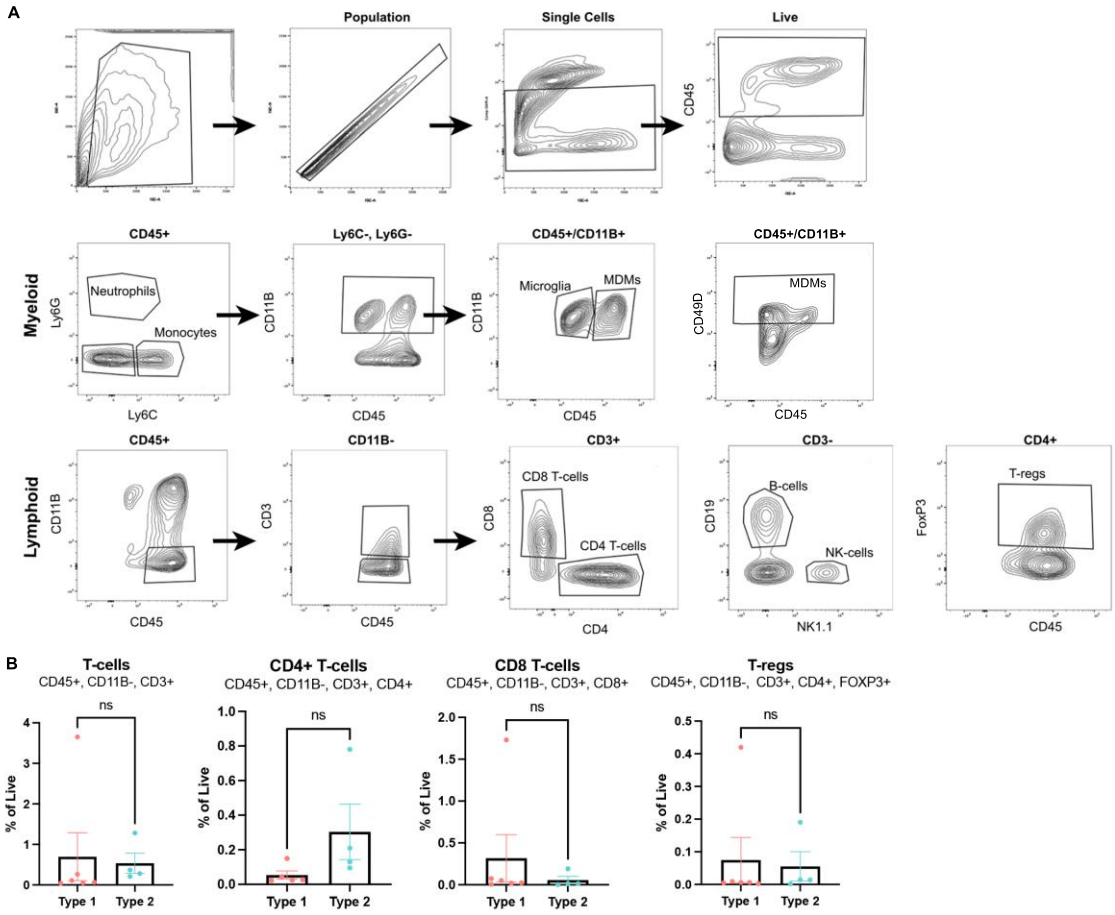

Figure 2-3 Gating strategy and lymphoid populations in spontaneous GBM

(**A**) Gating strategy used for all flow cytometry. (**B**) Levels of lymphoid populations in spontaneous Type 1 and Type 2 GBMs, data represented as mean with SEM, unpaired T-test, each dot represents one mouse.

Transcriptional TAM cohesion in transplanted and spontaneous GBM.

To determine the transcriptional states of TAMs in spontaneous and transplanted GBM, we performed bulk RNA-sequencing on sorted MDMs (Ly6C-, Ly6G-, $CD45^{hi}$, CD11B+) and microglia (Ly6C-, Ly6G-, $CD45^{lo}$, CD11B+). Tumors were

dissociated on ice prior to sorting to avoid acute transcriptome modifications (Figure 2-4A)[66]. Samples underwent principal component analysis and the data revealed that the most significant driver of TAM transcriptional grouping was ontogeny (MDM vs. Microglia) and not whether the tumors arose spontaneously or were subjected to allograft transplantation[17, 64] (Figure 2-4B). Consequently, levels of genes known to mark MDMs (*Itga4, Cd44, Itgal*)[30, 64] and microglia (*Tmem119, Sall1, Cx3cr1, P2ry12*)[65, 67] were elevated in their respective samples (Figure 2-4C). We noted 4,199 differentially expressed genes between all MDM vs. all microglia samples (Padj < 0.05, LFC >1.5 or LFC < -1.5), with 1,728 enriched in microglia and 2,471 enriched in MDMs (Figure 2-4D, Supplementary Dataset 1). Genes enriched in microglia were associated with gene ontology terms for neurological processes and angiogenesis, while genes enriched in MDMs were associated with cell adhesion, antigen presentation, and lymphocyte activation, consistent with previous reports[17, 68]. We also examined the influence of cell of origin on TAM transcriptome and found no appreciable differences (data not shown). Thus, because TAMs in spontaneous and orthotopically transplanted GBMs are transcriptionally similar, we moved forward with the orthotopic transplantation model to examine the role of TAMs in tumor progression.

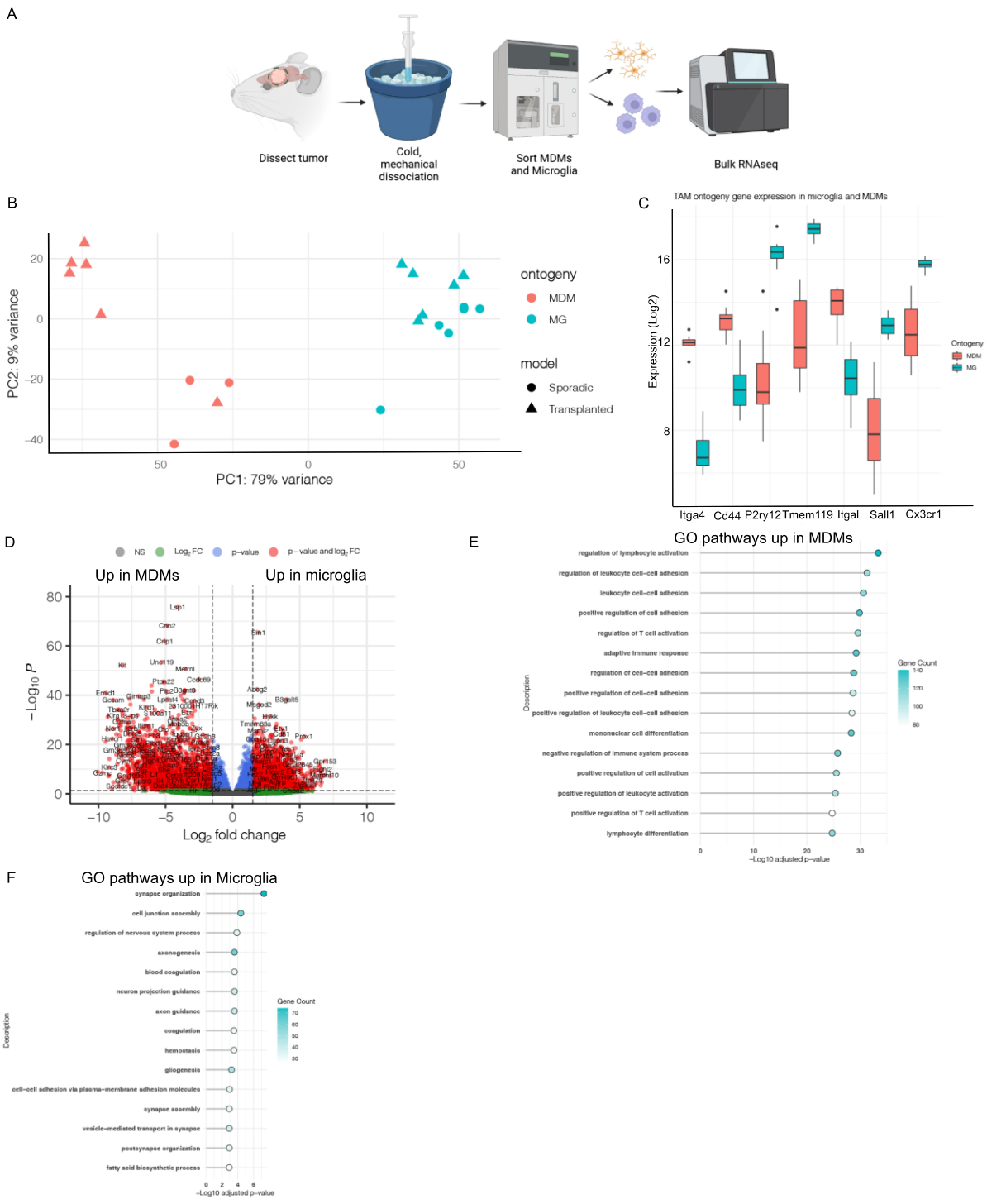

Figure 2-4 TAMs from spontaneous and transplanted GBMs are transcriptionally similar.

(**A**) Schematic demonstrating the dissociation and sorting method for bulk RNAseq of MDMs and Microglia from normal brains, Type 1 spontaneous tumors, Type 1 transplanted tumors, Type 2 spontaneous tumors, and Type 2 transplanted tumors. (**B**)

PCA plot showing all TAM samples, as well as their ontogeny and associated model. (**C**) Gene expression of common microglia markers (P2RY12, TMEM119, SALL1, CX3CR1) and MDM markers (ITGA4, CD44, ITGAL) in all MDM and microglia TAM samples. (**D**) Volcano plot showing DEGs when comparing all microglia TAM samples vs. all MDM TAM samples (padj<0.05, LFC>1.5 or <-1.5). Plots showing GO biological processes enriched in MDMs (**E**) and Microglia (**F**).

A robust TAM depletion system.

To investigate the potential role of TAMs in GBM development, we evaluated different strategies for effective TAM depletion. We first employed a TAM-specific promoter *Cx3cr1-CreER^{T2}; Ires-Eyfp* transgene to drive homologous recombination[69] of a Cre dependent diphtheria toxin receptor (*R26-Lsl-iDTR*) and Td-Tomato reporter (*R26-Lsl-Tdt*) cassettes thus permitting TAM visualization and rendering them diphtheria toxin (DT) sensitive. Tamoxifen dosing was optimized for high iDTR recombination efficiency and approximately 90-95% recombination was achieved with two doses given 24 hours apart (Figure 2-6A, B). We next treated non-tumor bearing mice with three initial DT doses, 24 hours apart, and continued dosing every three days thereafter for two weeks to maintain TAM depletion. TAM depletion was effective for up to 72 hours after the initial DT doses; however, the maintenance regimen was unsuccessful as we observed rapid repopulation by DTR non-expressing TAMs (Figure 2-6C). This effect of rapid TAM repopulation was likely due to Cre recombination inefficiency that allowed a few remaining iDTR- microglia to mediate reconstitution. To improve maintenance of TAM depletion, the mice were placed on CSF1R inhibitor (PLX5622; CSF1Ri) containing chow following the initial three doses of DT (Figure 2-6D). This combined TAM targeting approach resulted in robust microglia depletion in normal brains (87% cortex depletion after 1 week of

treatment, 86% after two weeks of treatment) and worked better than CSF1R inhibition alone, particularly in the first week of treatment (66% cortex depletion after 1 week, 81% cortex depletion after 2 weeks) (Figure 2-5A, B). The combined depletion strategy in Type 1 and Type 2 GBMs also achieved significant depletion of total TAMs (~84% in Type 1, ~97% in Type 2) and depletion of monocytes, with no evident changes neutrophil levels, or significant impact on the lymphoid compartment (Figure 2-5C, Figure 2-6E). In sum, our TAM depletion system has greater efficacy and sustainability than previously reported strategies[26, 29, 30, 70].

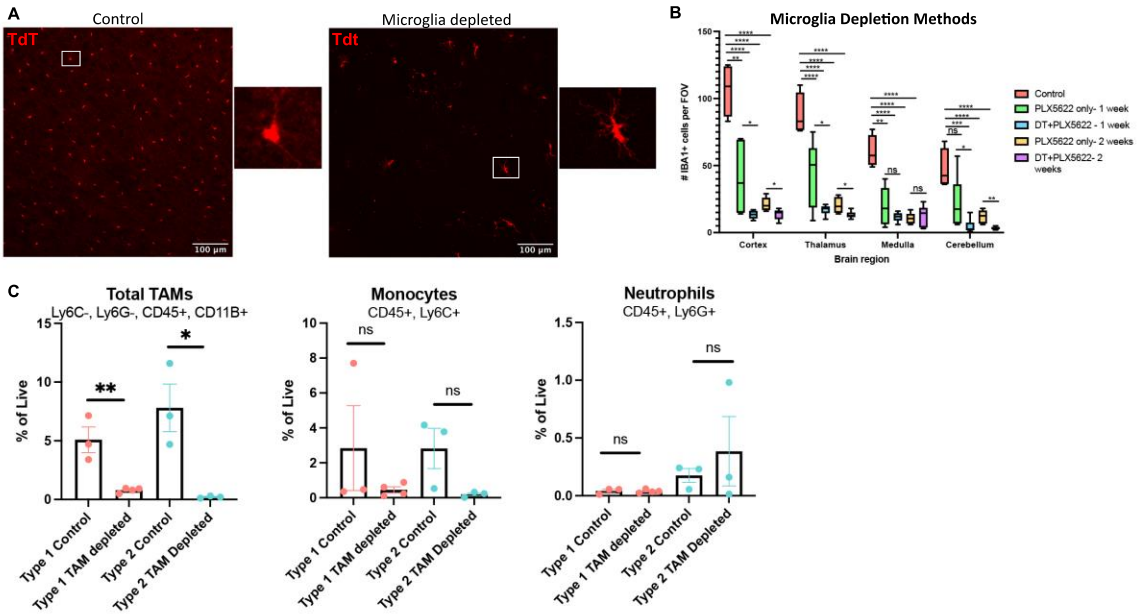

Figure 2-5 Combination of a genetic and pharmacologic system robustly depletes TAMs.

(A) Representative IF images of TAM depleted vs. Control brains. (**B**) Box and whisker plot comparing TAM depletion strategies (N=2 mice per group, 3 images quantified per mouse per brain region, middle line displays median value, whiskers display min and max values). Comparing the median values for the Cortex region gives the following TAM depletion percentages by treatment; 66% (CSF1R only 1 week), 81% (CSF1R only 2 weeks), 87% (DT+CSF1R 1 week), 86% (DT+CSF1R 2 weeks). All p-values with 4 stars indicate p<0.0001. Other p-values for comparisons are Cortex 1 week

DT+PLX5622 vs. PLX5622 only (p=0.041), Cortex 2 weeks DT+PLX5622 vs. PLX5622 only (p=0.016), Thalamus 1 week DT+PLX5622 vs. PLX5622 only (p=0.023), Thalamus 2 weeks DT+PLX5622 vs. PLX5622 only (p=0.019), Cerebellum 1 week DT+PLX5622 vs. PLX5622 only (p=0.05), Cerebellum 2 weeks DT+PLX5622 vs. PLX5622 only (p=0.0015), Cortex 1 week control vs. PLX5622 only (p=0.0037), Medulla 1 week control vs. PLX5622 only (p=0.0014), and Cerebellum 1 week control vs. DT+PLX5622 (p=0.0002). (**C**) Multi-color flow cytometry levels of Total TAMs (Type 1 p=0.0056, Type 2 p=0.02), Monocytes, and Neutrophils in control vs TAM depleted Type 1 and Type 2 GBMs, data represented as mean with SEM, unpaired t-test, each dot represents one mouse. TAM depletion percentage was estimated by comparing the percentages of total TAMs between TAM depleted and control samples (84% for Type 1, 97% for Type 2).

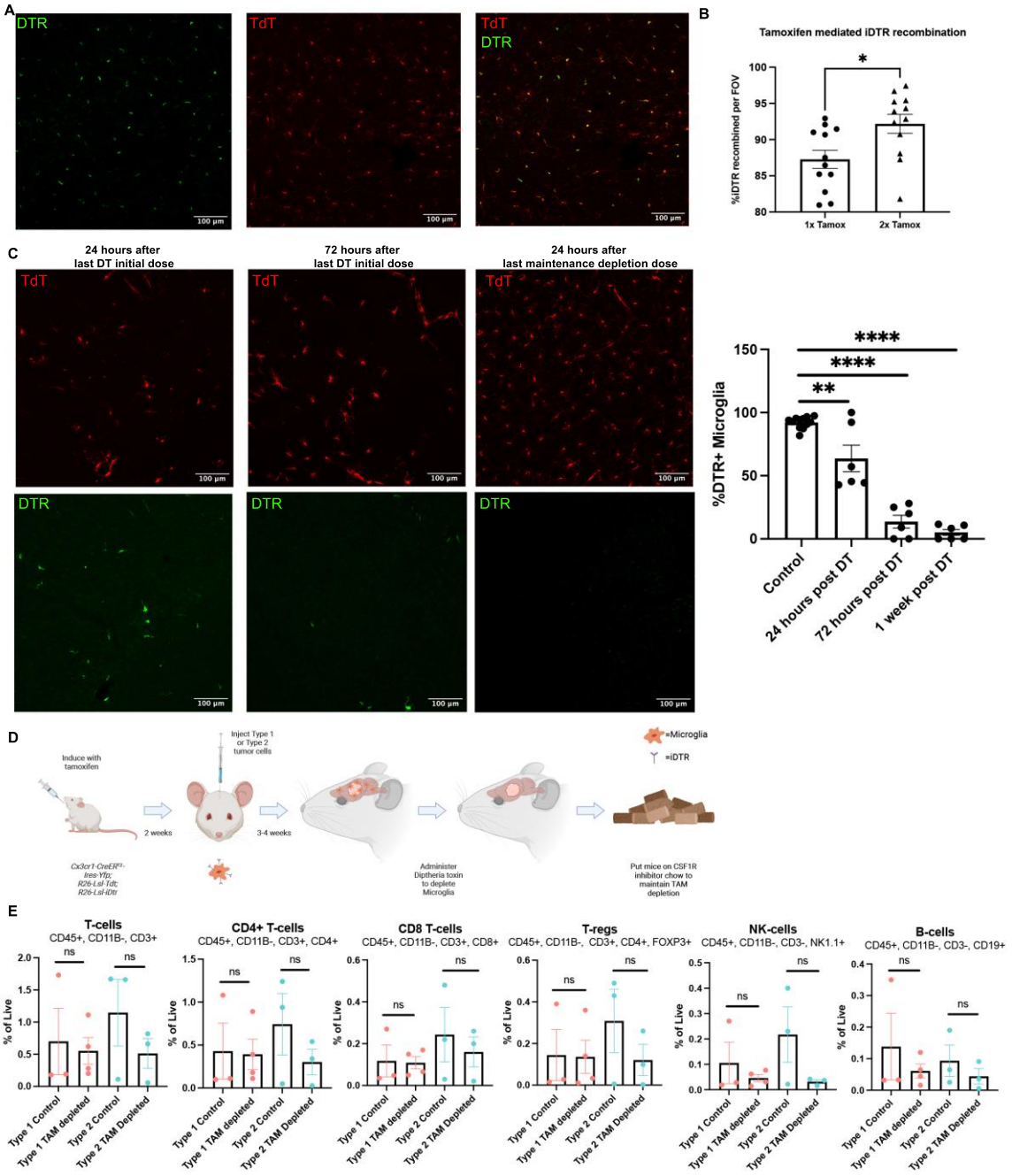

Figure 2-6 Generating a TAM depletion system.

(**A**) Images showing Tdt and iDTR IF staining 48 hours after 2x doses of tamoxifen (**B**) Quantification of iDTR recombination efficiency from one vs. two doses of tamoxifen, data represented as mean with SEM, N= 2 mice per group, 6 FOVs per mouse, p=0.012, unpaired t-test. Each dot represents one FOV. (**C**) IF staining images and quantification showing TdT and iDTR 24 hours after the last initial DT dose, 72 hours after the last DT initial dose, and 24 hours after the last DT maintenance dose (N= 4 mice in control group, 2 mice per treatment group, 3 images per mouse, p=0.0015, p<0.0001, p<0.0001, unpaired t-test). Each dot represents one FOV. (**D**) Schematic of TAM depletion strategy for transplanted Type 1 and Type 2 GBMs. (**E**) Multi-color flow

cytometry measuring levels of lymphoid populations in TAM depleted Type 1 and Type 2 GBMs vs. controls, data represented as mean with SEM, unpaired t-test, each dot represents one mouse.

TAM depletion does not extend survival.

Following TAM depletion in Type 1 and Type 2 GBM we examined tumor progression (Figure 2-6D). In a first set of experiments, TAM depletion was initiated approximately 3-4 weeks after tumor implantation allowing for GBM establishment. We observed no effects, either acceleration or delay, in survival of either Type 1 or Type 2 GBM models (Figure 2-7A, B). Additionally, TAM depletion did not impact tumor cell proliferation, as measured by phospho-histone H3 (PH3) and Ki67 staining (Figure 2-7C; Figure2-8A); or tumor histology (Figure2-8B, C). To examine the impact of TAM depletion on early stages of tumor initiation, TAM depletion was implemented in Type 2 tumors 1 week after tumor implantation. This protocol also failed to modify tumor bearing mouse survival (Figure 2-7D). These results are consistent with recent reports that Ras-driven GBMs do not respond to TAM depletion therapy[29].

We also employed our TAM depletion strategy on a Ras-independent GBM model using a primary tumor line generated from a spontaneous GBM mouse with the genetic configuration: *Nst-CreER^{T2}; Qk$^{fl/fl}$; Trp53$^{fl/fl}$; Pten$^{fl/fl}$* [40, 41]. TAM depletion was also unsuccessful in extending mouse survival in NF1 sufficient GBM (Figure 2-7E). Taken together, our data indicate that in a setting where we maximally deplete TAMs, either early in tumor initiation or during progression, tumor development remains unimpeded.

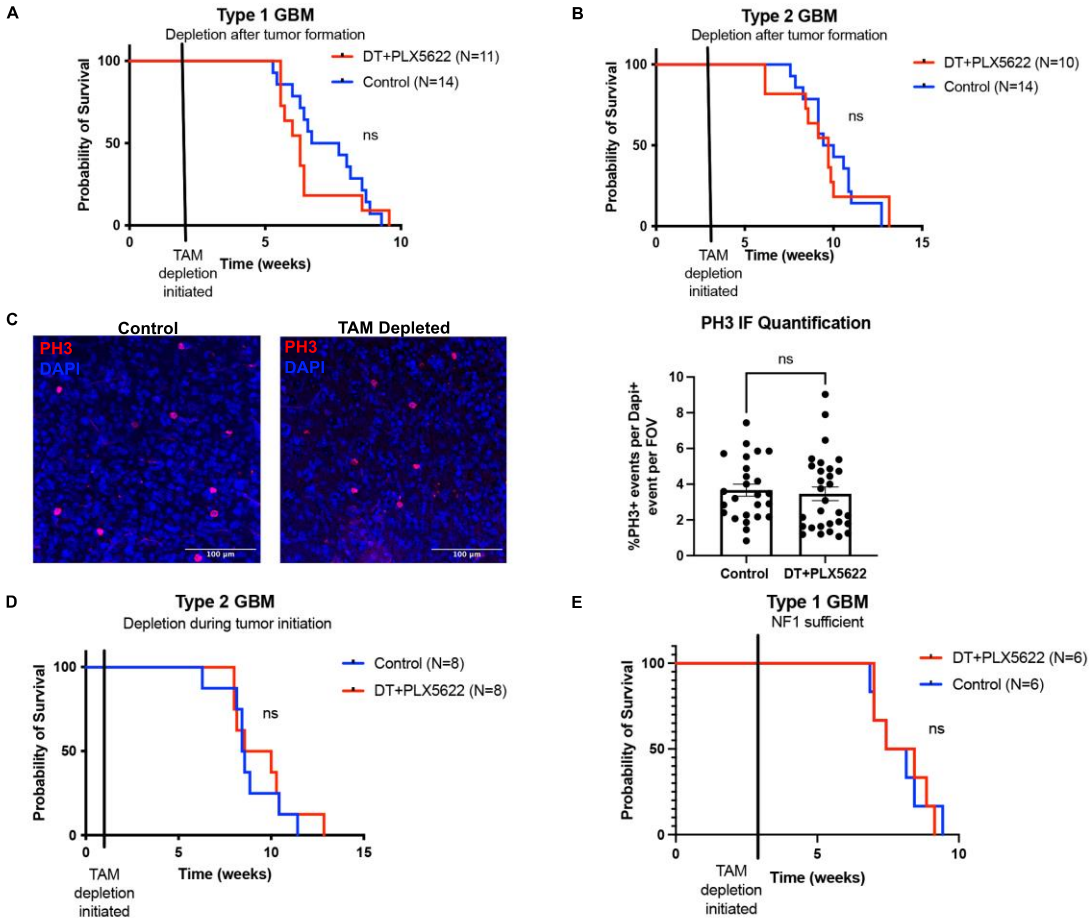

Figure 2-7 TAM depletion does not extend survival in Type 1 and Type 2 GBM.

Kaplan-Meier survival curves of TAM depleted vs. control (treatments initiated 3-4 weeks after tumor implantation) Type 1 (DT+PLX5622 N=11, Control N=14) (**A**) and Type 2 (DT+PLX5622 N=10, Control N=14) (**B**) GBM mice, significance calculated with Mantel-Cox test. (**C**) Phospho-histone H3 IF staining images and quantification of TAM depleted and control GBMs, data represented as mean with SEM, N= 5 control mice, 5 TAM depleted mice, unpaired t-test, symbols represent %PH3+ events per dapi+ event for each FOV (5 FOV per mouse). (**D**) Kaplan-Meier survival curve of TAM depleted vs. control (treatments initiated 1 week after tumor implantation) Type 2 (DT+PLX5622 N=8, Control N=8) GBM mice, significance calculated with Mantel-Cox test. (**E**) Kaplan-Meier survival curve of TAM depleted vs. control (initiated 3-4 weeks after tumor implantation) NF1 sufficient (DT+PLX5622 N=6, Control N=6) GBM mice, significance calculated with Mantel-Cox test.

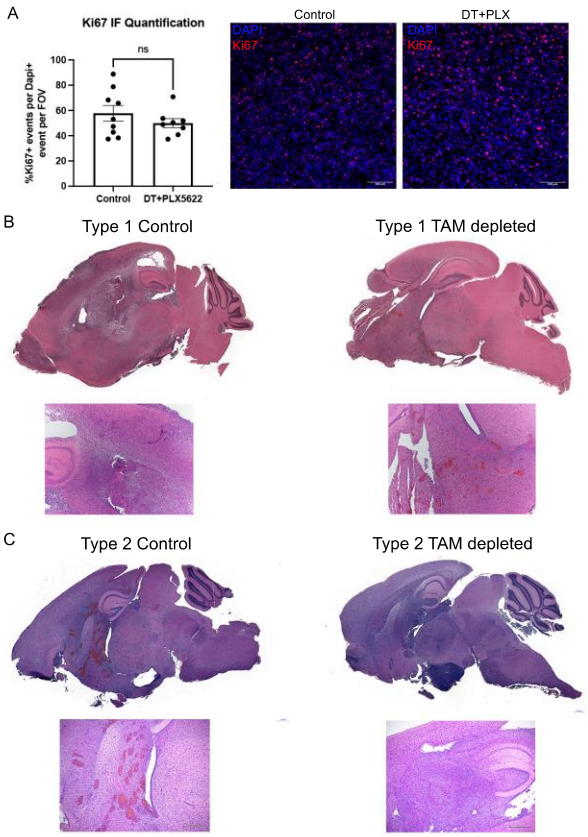

Figure 2-8 Histology of Type 1 and Type 2 control and TAM-depleted tumors.

(**A**) Quantification and images of Ki67 IF staining (N= 3 control, 3 TAM depleted tumors, 3 FOV per mouse). Whole brain and 4x images of H&E stains of Type 1 (**B**) and Type 2 (**B**) control and TAM depleted tumors.

Type 1 and Type 2 GBMs have distinct molecular responses to TAM depletion

To understand how TAM depletion impacted the GBM transcriptome, we performed bulk RNA sequencing of Type 1 and Type 2 TAM depleted vs. control GBM bulk tumor tissue. All samples were analyzed by principal component analysis and as illustrated by PCA plot, Type 1 and Type 2 GBMs still group separately on the plot, regardless of TAM depletion status (Figure 2-10A). We found 1,185 differentially expressed genes between all TAM depleted vs. control GBMs (Padj < 0.05, LFC >1.5 or LFC < -1.5). 272 genes were enriched in TAM depleted GBM transcriptomes while the remaining 913 DEGs were decreased

(Figure 2-10B, Supplementary Dataset 2). The transcriptionally decreased genes were primarily immune related, consistent with depletion of TAMs, and pathways such as Hallmark Interferon Alpha Response and Hallmark Interferon Gamma Response were significantly reduced (Figure 2-10C-E, Supplementary Dataset 2). Examining the transcriptionally increased genes revealed the enrichment of pathways related to tumor growth, such as Hallmark Hedgehog signaling and Hallmark Mitotic Spindle, consistent with previous reports[29] (Figure 2-10D, F).

Next, we analyzed the Type 1 and Type 2 samples separately for their transcriptional response to TAM depletion. When analyzed independently, TAM depleted samples separated from control samples in both Type 1 and Type 2 GBMs (Figure 2-9A, B). 192 genes were enriched and 3756 genes decreased in Type 1 TAM depleted GBMs, and 843 genes were enriched and 311 genes decreased in Type 2 TAM depleted GBMs (Padj < 0.05, LFC >1.5 or LFC < -1.5) (Figure 2-9C, D, Supplementary Dataset 2). We performed GSEA and found that Type 1 GBMs up regulated more pro-growth-related pathways than Type 2 GBMs, while Type 2 GBMs only significantly up-regulated Hallmark Oxidative Phosphorylation (Figure 2-9E, F). Type 2 GBMs had more immune related hallmark pathways significantly decreased compared to Type 1 GBMs, consistent with Type 2 GBMs having a greater immune component than Type 1 GBMs (Figure 2-9E, F). Overall, this analysis suggests that while there was no survival benefit afforded to either Type 1 or Type 2 TAM depleted GBMs, Type 1 and Type 2 GBMs responded differently to TAM depletion.

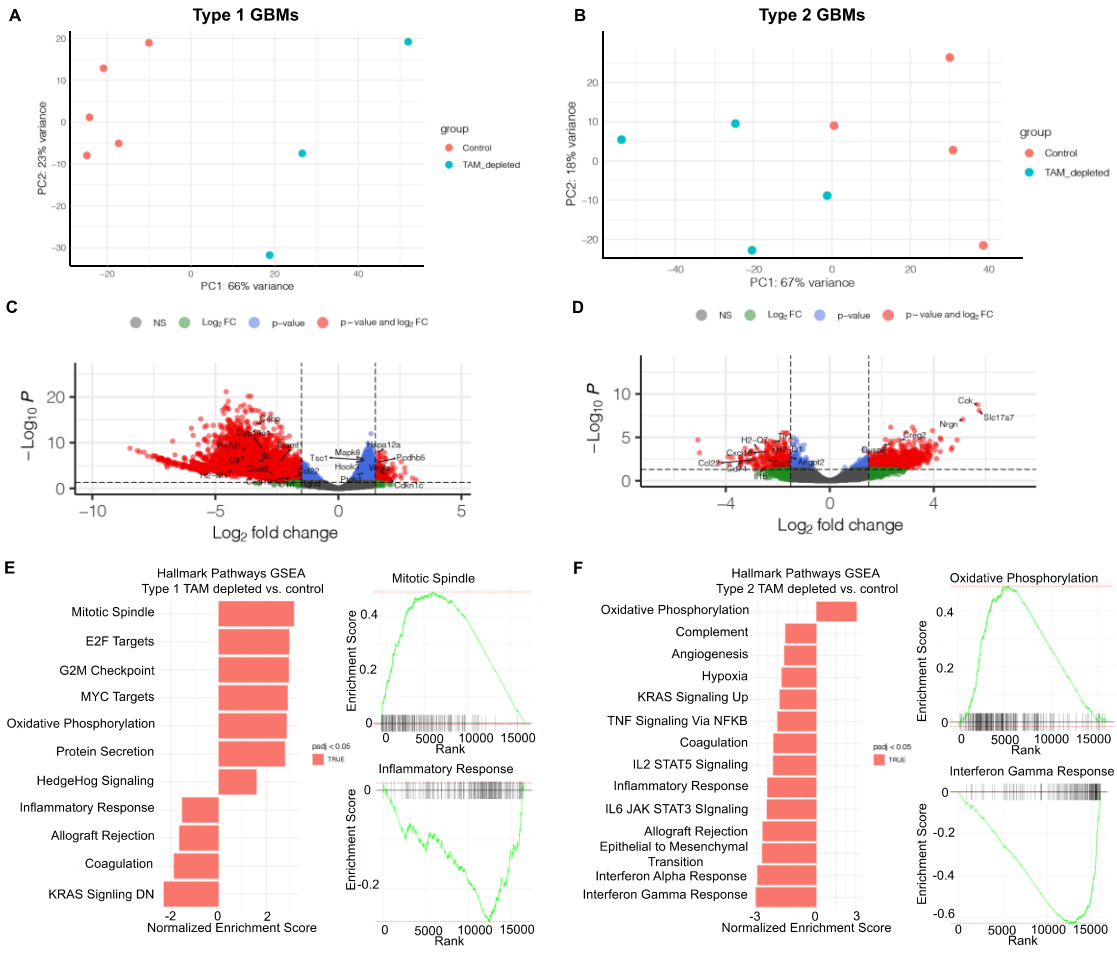

Figure 2-9 Type 1 and Type 2 GBMs have distinct molecular responses to TAM depletion therapy

(A) PCA plot showing Type 1 TAM depleted vs. control samples. (**B**) PCA plot showing Type 2 TAM depleted vs. control samples. (**C**) Volcano plot showing the DEGs when comparing Type 1 TAM depleted vs. all control tumors (padj<0.05, LFC>1.5 or <-1.5). (**D**) Volcano plot showing the DEGs when comparing Type 2 TAM depleted vs. all control tumors (padj<0.05, LFC>1.5 or <-1.5). (**E**) Hallmark pathway GSEA of Type 1 TAM depleted vs. control tumors. Select enrichment plots for Mitotic Spindle and Inflammatory Response shown. (**F**) Hallmark pathway GSEA of Type 2 TAM depleted vs. control tumors. Select enrichment plots for Oxidative Phosphorylation and Interferon Gamma Response shown.

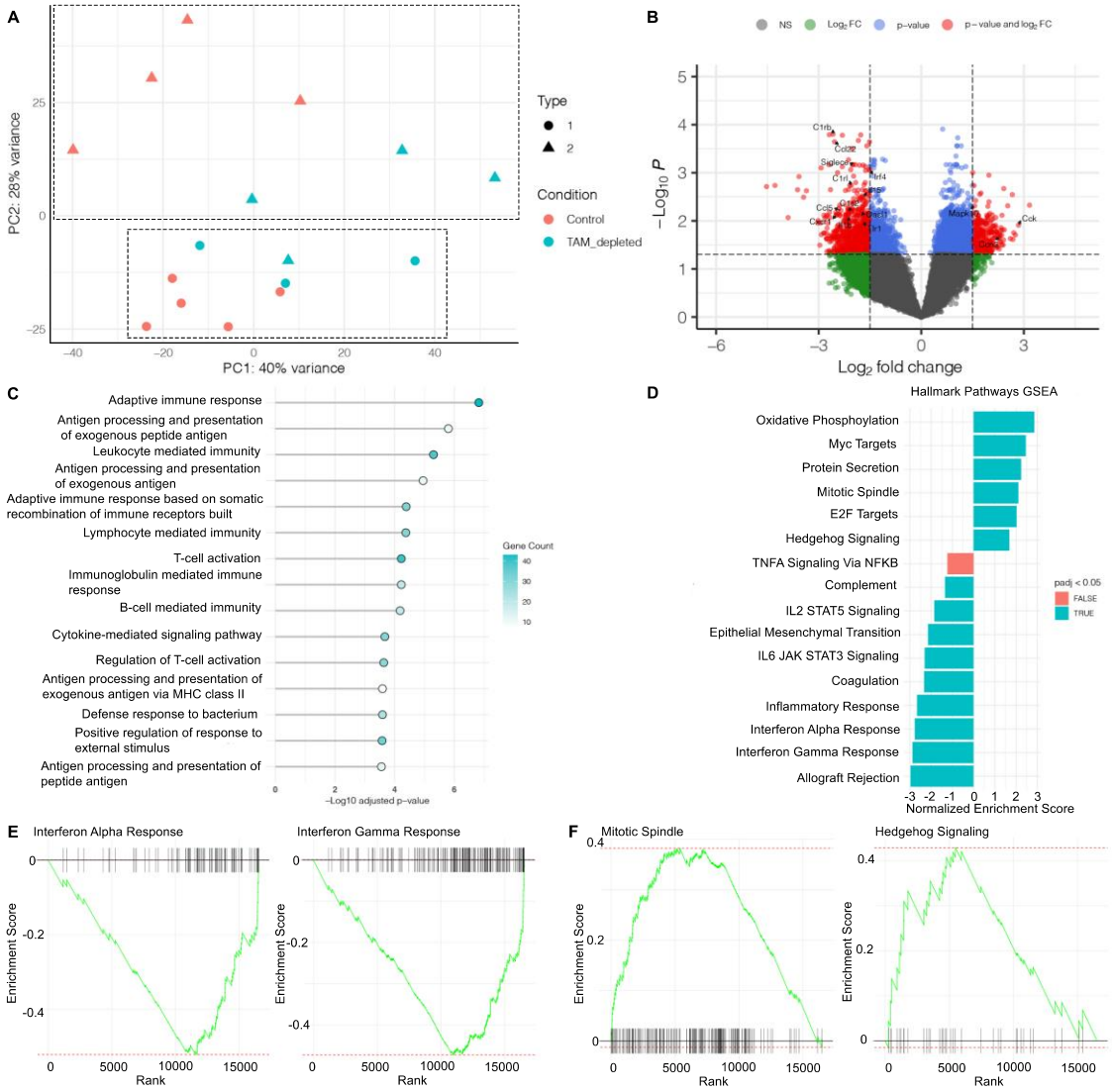

Figure 2-10 RNAseq analysis between all TAM depleted and control tumors

(**A**) PCA plot showing all Type 1 and Type 2 TAM depleted vs. control samples with colors and symbols showing the treatment condition and tumor type respectively. (**B**) Volcano plot showing the DEGs when comparing all TAM depleted vs. all control tumors (padj<0.05, LFC>1.5 or <-1.5.) (**C**) GO Plot showing the top 15 significantly enriched biological process GO terms in the genes decreased in TAM depleted tumors. (**D**) GSEA of hallmark pathways in TAM depleted vs. control tumors. (**E**) GSEA enrichment plots of Interferon Alpha Response and Interferon Gamma Response hallmark pathways in TAM depleted vs. Control GBMs. (**F**) GSEA enrichment plots of Mitotic Spindle and Hedgehog Signaling hallmark pathways in TAM depleted vs. Control GBMs.

Discussion

The tumor microenvironment has diverse influences on tumor development and progression in many cancers[71]. In particular, promising therapeutic advances have been achieved by the successful harnessing of the anti-tumor capabilities of the immune system. In GBM, immunotherapy clinical trials have not been successful[28, 50, 55]. It is noteworthy that such trials are all encompassing and did not attempt patient stratification based on mutational status, burden, or the composition of the tumor microenvironment. Thus, in some instances treatment failure may be partially explained by a cold tumor immune microenvironment. Our results suggest that a better understanding of the tumor immune microenvironment and attention to patient stratification based on the immune infiltration state may poise current and future immunotherapies for success in GBM.

Here, we investigated GBM cell of origin (or transcriptional lineage association) as a potential stratification. GEMMs that developed spontaneous GBM by initiation in SVZ stem cells or oligodendrocytic progenitor cells gave rise to GBM with distinguishable molecular and histological features[10]. We found that these distinguishing features extend beyond tumor cells to the tumor immune microenvironment. We identified marked differences in TAM ontogeny, with oligodendrocytic-derived Type 2 GBM exhibiting substantially greater recruitment of peripherally derived MDMs, while Type 1 GBM primarily recruited resident microglia. We further extended these findings from spontaneous GEMMs to orthotopic transplantation models and finally in human

patients using the Type I and Type II subtyped samples in the TCGA dataset[10]. These results could have implications for immunotherapy approaches which may have more favorable outcomes if confined to the more MDM-rich Type II tumors.

A central question addressed in this study was to evaluation of the extent of TAM contribution to tumor development and progression as previous GBM mouse model studies have reported contrasting results and employed models of varying relatedness to stereotypic mutations found in GBM[26, 29, 30, 70]. Using the GBM relevant mutations at the *Nf1*, *Trp53* and *Pten* loci to generate GBM in two separate cells of origin, for each tumor type we compared TAM transcriptomes isolated from spontaneous versus allografted tumors. The results demonstrated that TAM transcriptional differences were driven primarily by ontogeny and not by model type. Thus, the orthotopic transplantation models can be considered physiologically relevant models for TAM studies.

We initiated studies for *in vivo* TAM depletion using two previously described methods: diphtheria toxin mediated ablation[69, 72] and CSF1R receptor inhibition[26]. We found that either method alone had limitations. Diphtheria toxin receptor expression, activated by Cre mediated recombination of the silenced floxed allele in TAMs results in rapid depletion to >85% levels by 24 hours. However, within 72 hours, we observed robust TAM repopulation by microglia that were not expressing the CX3CR1 driven Cre recombinase iDTR transgene. The result was complete repopulation of a DT resistant microglial population within one week and thus only

provided transitory TAM depletion. The alternative approach of CSF1R inhibition provided different outcomes. Constant exposure to the CSF1R inhibitor in the mouse chow afforded more effective chronic TAM reduction but took one week to reach maximal depletion levels of ~80%. We therefore adapted a combined protocol in which mice were fed CSF1R inhibitor chow after exposure to DT. This combined approach allowed us to achieve immediate and sustained TAM depletion to around 85-95% over the course of our experiments.

Our data indicate Type 1 and Type 2 GBM does not depend on the tumor supportive functions of TAMs for growth and survival. We did not observe significant tumor specific gene expression changes in TAM depleted Type 1 and Type 2 tumors that would suggest compensatory gene activation or repression as an explanation for mechanism to overcome the absence of TAMs. Additionally, there is no initial response to TAM depletion treatment that suggests the requirement of tumor adaptation for continued progression. Thus, to the extent that TAMs may have many tumor-supportive functions, they are not essential and GBM can easily adapt to their absence.

As our tumor models have an *Nf1* deletion, this adds to previous observations made in an H-Ras driven model of GBM that are inherently nonresponsive to TAM depletion[29]. Here, we also performed DT plus CSF1R inhibitor mediated TAM depletion in a GBM model system that lacks an *Nf1* mutation (*Nst-CreER^{T2}; Qk$^{fl/fl}$; Trp53$^{fl/fl}$; Pten$^{fl/fl}$*)[40], and tumors progressed equivalently in the absence of TAMs.

Taken together, these results suggests that possibly only a specific subset of GBM models, such as PDGFB-driven GBMs[26], require TAMs for optimal tumor progression. However, there were no statistically significant correlations found between tumor genetics and responses to CSF1R therapy in the Phase I/II clinical trial mentioned here[28]. One patient that had an extended PFS had an NF1 alteration, but the N of the trial is not large enough to conclude if this is a statistically significant result. A larger trial will be needed to determine if there are any statistically significant correlations with GBM genetic alterations. Alternatively, there may exist intrinsic biological features of different model systems that add complexity to the tumor immune microenvironment and continued vigilance to adhere to physiologically relevant model systems will be an ever-increasing priority. Taken together, these studies highlight that the immune microenvironment may have distinct functions depending on tumor cell lineage transcriptional associations and also on tumor driver mutations.

Our results put into question the relevance of therapies aimed at ablating TAMs in the GBM tumor immune microenvironment and indicate a possible explanation for the failure of TAM depletion therapy in clinical trials. However, potentially impactful insights come from the observation that Type 2 tumors have a particularly high level of MDM infiltration. This suggests the possibility that therapeutics harnessing MDMs may have a unique and selective therapeutic efficacy on patients harboring Type II GBM.

Methods

Mice.

All mouse experiments were approved and performed according to the guidelines of the Institutional Animal Care and Use Committee of Memorial Sloan Kettering Cancer Center. Tumor suppressor mice with Nestin-CreER^{T2} [8, 73, 74] or NG2-CreER^{TM} [9, 75] transgenes were crossed with conditional *Trp53* allele. Nestin-CreER^{T2}*; Nf1*$^{fl/+}$*; Trp53*$^{fl/fl}$; *Pten*$^{fl/+}$ mice or NG2-CreER^{TM}; *Nf1*$^{fl/+}$*; Trp53*$^{fl/fl}$; *Pten*$^{fl/+}$ mice were generated by breeding Nestin-CreER^{T2};*Trp53*$^{fl/fl}$ or NG2-CreER^{TM};*Trp53*$^{fl/fl}$ mice with *Nf1*$^{fl/fl}$*; Trp53*$^{fl/fl}$; *Pten*$^{fl/fl}$ mice. All mice were maintained under formal MSKCC IACUC protocols.

Cx3cr1-CreER^{T2}-Ires-Eyfp mice[69] (JAX Stock #: 021160) were bred to *Rosa26-Lsl-Tdt* mice (JAX Stock#: 007908). These mice were then bred to *Rosa26-Lsl-iDTR* mice[76] (JAX Stock#: 007900) *to get Cx3cr1-CreER^{T2}-Ires-Eyfp; Rosa26-Lsl-Tdt/iDTR* mice.

Mouse primary cell culture.

Mice with tumor suppressor alleles were induced with tamoxifen at 4-6 weeks of age and aged until they developed symptoms of GBM as described previously[10]. Symptomatic mice were anesthetized and transcardially perfused with ice cold HBSS and tissues were harvested. Tissues were chopped and incubated with Accutase in 37C water bath for 20 minutes, dissociated, and cultured in serum free medium supplemented with B27 and N2 (serum-free media), plus EGF, FGF

and PDGF-AA (10 ng/ml each) for Type 1 GBMs (both $NF1^{-/-}$ and NF1 WT), and EGF, FGF and Neuregulin (10 ng/ml each) for Type 2 GBM. Cells were kept in 5% oxygen, 37C incubator. Primary cultures were established as tumor spheres at P0, later passages were as spheres in non-coated plates, or as monolayer in laminin pre-coated plates (10 ng/mL Laminin diluted in DPBS with Ca2+/Mg2+).

Mouse stereotactic GBM cell injection.

The Type 1 and Type 2 GBM cell lines were derived from spontaneous GBM mice and cultured as described above. For intracranial injection, mice were anesthetized (Isoflurane) and placed on a stereotactic frame. A midline incision was made on the skin to expose the skull, and a microdrill was used to perform craniotomy. For intracranial injection, 1×10^4 cells were injected in the striatum (coordinates: 1.0 AP, -1.8 ML, 4.5 DV with respect to the bregma). Minimum cells were injected to avoid inducing inflammation and to model physiologic conditions as closely as possible. Mice were monitored and euthanized for tissue collection when neurologic symptoms were evident.

Tumor dissociation.

Mice were anesthetized and transcardially perfused with ice cold HBSS. Tumors were dissected, chopped up on ice, and dissociated using the Miltenyi Brain Tumor Dissociation Kit. Following dissociation, the myelin was removed with the Miltenyi myelin removal beads and magnetic separator. Next, red blood cells were removed with red blood cell lysis buffer (Sigma). Tumor cell suspensions

were frozen with BamBanker cell freezing media and placed at -80 for < 1 month prior to flow cytometry studies.

Histology and immunohistochemistry.

Mice were perfused with PBS and brains were fixed in 4% paraformaldehyde, processed, and embedded into paraffin blocks. Blocks were sectioned into 10µM sections and stored at 4 degrees until staining. DAPI was used to stain the nucleus (ThermoScientific, 1ug/ml). All immunofluorescent antibodies used are Iba1 (Wako, #019-19741), DTR (Sigma Aldrich, #PC319L), Phospho-histone H3 (Cell Signaling Technology, #9706). The sections were then imaged with a Zeiss LSM 510 confocal microscopy using Argon 488, He543, and He 633. Images were quantified using Fiji.

Multicolor Flow Cytometry.

Tumor cell suspensions were dethawed and stained with a fixable viability dye. Cells were then washed, blocked with CD16/32 Fc block for 5-10 minutes, and stained with extracellular antibodies for 20 minutes on ice. Cells were then washed and either resuspended in FACS buffer or FluoroFix buffer (BioLegend) for analysis (myeloid panel) or moved on for staining with intracellular antibody FoxP3 (lymphoid panel). For intracellular staining, cells were fixed and permeabilized with the FoxP3/transcription factor staining kit (eBioscience). Then, cells were stained with FoxP3 for 30 minutes on ice, washed, and resuspended in FACS buffer for analysis. Flow cytometry data was acquired

using BD Biosciences LSRFortessa analyzers and BD FACSDiva software. Data was analyzed using FlowJo. Flow cytometry antibodies used for the myeloid panel include CD45(Alexafluor 700, BD Biosciences, #56010), CD11B (BV785, Biolegend, #101243), Ly6C (APC Cy7, BD Biosciences, #560596), Ly6G (PE Cy7, Tonbo Biosciences, #60-1276-U100), MHCII (BV711, Biolegend, #107643), CD49D (BV650, BD Biosciences, #740458), and PDL1 (APC, R&D Systems, #FAB1019A-025). Flow cytometry antibodies used for the lymphoid panel include CD45(Alexafluor 700, BD Biosciences, #56010), CD11B (Alexa 647, Biolegend, #101218), CD3 (PE Cy7, BD Biosciences, 560591), CD4 (APC Cy7, BD Biosciences, #561830), CD8 (BV711, BD Biosciences, #563046), CD19 (BV786, BD Biosciences, #563333), NK1.1 (BB700, BD Biosciences, #566503), FoxP3 (PE Cy5, Thermo Fisher Scientific, #15-5773-80).

TAM depletion.

Cx3cr1-CreER^{T2}-Ires-Eyfp; Rosa26-Lsl-Tdt/iDTR mice were induced with tamoxifen (10mg/20g body weight) with oral gavage at 4-6 weeks of age twice, 24 hours apart. 1-2 weeks following tamoxifen induction, mice were stereotactically injected with 1x10^4 Type 1 or Type 2 GBM cells. Mice were monitored by bioluminescence imaging or MRI for tumor formation. Approximately 3-4 weeks following stereotactic injection, mice were treated with DT (50ng/20g body weight) or DPBS for the control group, 3 times, 24 hours apart. Following the last dose of diphtheria toxin, mice were placed on PLX5622 CSF1R inhibitor chow (Plexxicon) or control chow for the remainder of their

life. PLX5622 was incorporated into AIN-76A Rodent Diet at a 1,200 mg/kg concentration by Research Diets. Mice were monitored until neurologic symptoms emerged, and then were euthanized for tissue collection. Survival curves were made using prism and the log-rank Mantel-Cox test was used to test for significance. Data is representative of several independent experiments. TAM depletion in normal brains was estimated by comparing the median values for the cortex region. For tumor-bearing brains, TAM depletion percentage was estimated by comparing the percentages of total TAMs between TAM depleted and control Type 1 and Type 2 tumors.

Analysis of TCGA GBM data.

Gene expression data from TCGA samples previously subtyped as core Type 1 or Type 2[10] GBMs was used to look at the relative levels of immune marker genes. Significance was calculated using a Wilcox test with the R package ggsignif.

Bulk RNA-sequencing.

RNA extraction

Sorted TAM RNAseq (related to Supplementary Figure 3)

Following tumor dissection, tumors were stained with CD45, Ly6C, Ly6G, and CD11B (Supplementary Table 2) and sorted for Microglia ($Ly6C^-$, $Ly6G^-$, $CD45^{lo}$, $CD11B^+$) and MDMs ($Ly6C^-$, $Ly6G^-$, $CD45^{hi}$, $CD11B^+$) directly into Trizol LS and flash frozen at -80. RNA was then extracted by the standard Trizol LS protocol.

Bulk tumor tissue RNAseq (related to Figure 4)

At tumor dissection, a small tumor piece was flash frozen and stored at -80. Later, tumor pieces were lysed in Trizol and RNA was extracted using the Zymo Direct-zol RNA Mini Prep Kit (R2050). Samples were eluted in 20 µL RNase-free water and submitted for RNAseq.

Transcriptome sequencing

Sorted TAM RNAseq (related to Supplementary Figure 3)

After RiboGreen quantification and quality control by Agilent BioAnalyzer, 1.1-2.0 ng total RNA with RNA integrity numbers ranging from 7.2 to 10 underwent amplification using the SMART-Seq v4 Ultra Low Input RNA Kit (Clonetech catalog # 63488), with 12 cycles of amplification. Next, 1-4 ng of amplified cDNA was used to prepare libraries with the KAPA Hyper Prep Kit (Kapa Biosystems KK8504) using 8 cycles of PCR. Samples were barcoded and run on a NovaSeq 6000 in a PE50 run, using the NovaSeq 6000 S1 Reagent Kit (100 Cycles) (Illumina). An average of 59 million paired reads were generated per sample and the percent of mRNA bases per sample ranged from 77% to 88%.

Bulk tumor tissue RNAseq (related to Figure 4)

Preparation of RNA sample library and RNA-seq were performed by the Genomics Core Laboratory at Weill Cornell Medicine. Messenger RNA was

prepared using TruSeq Stranded mRNA Sample Library Preparation kit (Illumina, San Diego, CA), according to the manufacturer's instructions. The normalized cDNA libraries were pooled and sequenced on Illumina NovaSeq 6000 sequencer with pair-end 50 cycles. The raw sequencing reads in BCL format were processed through bcl2fastq 2.19 (Illumina) for FASTQ conversion and demultiplexing.

Downstream analysis of bulk RNAseq data.

Alignment

Samples were aligned using STAR to the mouse GRCm39 or GRCm38 reference genome for the sorted TAM RNAseq and the TAM depletion tumor RNAseq respectively.

DEG analysis

DESeq2[77] was used for differential gene expression analysis for all bulk RNAseq studies. DEGs were reported that had a padj< 0.05, and LFC > 1.5 or <-1.5. Volcano plots were made using the EnhancedVolcano package.

GO analysis

GO was performed using the lists of significantly increased or decreased DEGs with the ClusterProfiler, TopGO, and DOSE packages.

GSEA analysis

GSEA analysis was performed using the gene level statistic values found in the DESeq2 differential expression results file as a ranking metric. The R package fgsea was used for this analysis.

Statistical analysis.

Statistical analysis between groups was performed using two-tailed unpaired Student's t-test unless otherwise indicated. Kaplan-Meier survival curves were analyzed using log-rank (Mantel-Cox) test. Data were analyzed using GraphPad Prism v.9 and Fiji. P-values less than 0.05 were considered significant unless otherwise indicated.

Data availability.

Data is available on the GEO at . This will be added once the manuscript is accepted for publication.

Chapter 3 *Nf1* loss shapes the glioblastoma tumor immune microenvironment

Abstract

Immunotherapy has thus far been unsuccessful in glioblastoma (GBM). A greater understanding of the tumor immune microenvironment (TIME) and factors influencing its composition and activation states is critical to refine immunotherapeutic strategies in glioblastoma. *Nf1* expression has been inversely correlated with increased inflammation in human glioblastoma. However, no functional studies have investigated causality, nor explored the mechanism by which Nf1 loss may shape the TIME. Here, we use several mouse models of glioblastoma to investigate whether *Nf1* loss influences the tumor immune microenvironment. We find that compared to NF1 wildtype GBM mice, *Nf1* mutant GBM have greater influx of lymphocytes and monocytes and exhibit elevated expression of several cytokines and chemokines. Additionally, *Nf1* mutant tumors indicate enhanced pro-inflammatory crosstalk between intratumoral immune populations. We identify TNF signaling via NF-κB and CEBPB as one mechanism mediating the pro-inflammatory gene transcription in NF1 mutant TIME cells. Ultimately, we demonstrate that Nf1 loss endows the GBM tumor immune microenvironment with greater monocyte and lymphocyte infiltration and enhanced pro-inflammatory signaling potentially mediated by NF-κB and CEBPB transcription factor activity.

Introduction

Glioblastoma multiforme (GBM) is the most common and aggressive adult brain tumor. The prognosis for patients is poor, with a five-year survival rate of five percent[1]. The current standard of care for GBM is surgery followed by radiation and chemotherapy, with the addition of tumor treating fields[3]. Given the poor prognosis, new therapeutics are urgently needed.

Immunotherapy has become a main stay in cancer treatment and has been highly effective in several tumor types[18]. Thus far, immunotherapy has not been successful in GBM[28, 50, 55]. This is in part due to the cold and predominantly immunosuppressive nature of the tumor immune microenvironment (TIME) of GBM[18]. Additionally, clinical trial end points have examined population-wide responses, and despite the existence of a proportion of responders[28, 78], there is a lack of biomarkers and stratification methods to identify this population. A greater understanding of the GBM TIME is fundamental to improve outcomes of immunotherapies in GBM.

NF1, a negative regulator of the Ras/MAPK pathway, is one of the most common driver mutations in GBM and is mutated in approximately 17% of cases (MSK cBio portal)[39]. Several studies have demonstrated a correlation between NF1 mutations and enhanced immune infiltration in GBM[15, 61]. Additionally, NF1 loss has been shown to promote vital tumor-microenvironment interactions in other cancers, namely in neurofibromatosis type 1-related tumors[16]. However, the

mechanisms by which NF1 loss of function mutations shape the tumor immune microenvironment in GBM remains unknown[18].

Studying the impact of a single driver mutation in human GBM patients is challenging due to the heterogeneity of tumor mutational profiles. Here, we use multiple NF1 mutant and NF1 WT orthotopic and immunocompetent transplantation-based mouse models of GBM to ask how NF1 loss shapes the GBM TIME. We demonstrate that NF1 loss preferentially elicits enhanced infiltration of lymphocytes and monocytic populations. We further identify enhanced pro-inflammatory cytokine ligand-receptor interactions among the NF1 mutant GBM TIME cells, suggesting greater overall immune activity. In sum, our data suggest that NF-κB and CEBPB induced pro-inflammatory cytokine crosstalk contribute to increased tumor infiltration of lymphocytes and monocytic cells.

Results

NF1 mutant GBMs have elevated immune infiltration.

To further understand the impact of NF1 mutations on the GBM tumor immune microenvironment, we leveraged our NF1 mutant GEMMs in which GBMs are driven by deletion of tumor suppressors in subventricular zone neural stem cells upon tamoxifen induction in *Nst-CreER^{T2}; Nf1$^{fl/+}$; Trp53$^{fl/fl}$; Pten$^{fl/+}$* mice (NPP)[9]. In parallel, we used an NF1 WT GBM model, in which GBMs are driven by deletion of tumor suppressors in subventricular zone neural stem cells upon tamoxifen

induction in *Nst-CreER^{T2}; Qk$^{fl/fl}$; Trp53$^{fl/fl}$; Pten$^{fl/fl40}$* mice (QPP). Thus, both GEMMs share loss of Trp53 and Pten but differ in the status of the NF1 gene. Following tamoxifen induction in both models, spontaneous GBM arises that can then be propagated in culture[9]. Cultured GBM cells can then be orthotopically injected into mice from the same colony, creating a transplantation-based GBM mouse model (Figure 3-1A)[9]. Prior to orthotopic injection, bi-allelic loss of tumor suppressor genes in tumor cell cultures is confirmed by genotyping. Here, two independent QPP and NPP tumor lines were used for orthotopic injection (Figure 3-1A).

We used multicolor flow cytometry to profile both myeloid and lymphoid populations in all NF1 WT and NF1 mutant GBM models (Figure 3-2A). In comparing QPP vs. NPP tumors, significant increases in monocytes, total T-cells, CD4 T-cells, regulatory T-cells (T-regs), CD8 T-cells and B-cells were observed (Figure 3-1B, Figure 3-2B). Profiling tumors from an independent set of QPP and NPP tumor lines, we similarly observed significant increases in monocytes, total T-cells, CD4 T-cells, regulatory T-cells (T-regs), and NK cells (Figure 3-2D). Additionally, we observed increased levels of TAMs (monocyte-derived macrophages and microglia) in NF1 WT tumors (Figure 3-2D). QPP and NPP tumor lines with similar overall CD45 levels were compared to reduce bias in results (Figure 3-1B, Figure 3-2D).

To further validate our findings in the models presented here, we made an additional QPP tumor line with CRISPR-mediated NF1 knockout (QPP sgNF1) to produce QPP tumors with NF1 loss (Figure 3-1C). QPP sgNF1 tumors were compared to QPP tumors transduced with non-targeting sgRNA (QPP sgNT tumors). NF1 knockout was confirmed with western blot (Figure 3-1C).

Next, we compared the TIMEs of QPP sgNT tumors vs. QPP sgNF1 tumors. Like the QPP vs. NPP comparison, we found significant increases in monocytes, total T-cells, CD4 T-cells, regulatory T-cells (T-regs), NK-cells and B-cells (Figure 3-1D, Figure 3-2C). Additionally, we found significantly increased levels of total CD45+ immune infiltrates and higher levels of total TAMs (monocyte-derived macrophages and microglia) and CD8 T-cells in QPP sgNF1 tumors (Figure 3-1D, Figure 3-2C). In sum, we demonstrate that NF1 loss causes enhanced lymphocyte and monocytic infiltration in the GBM TIME.

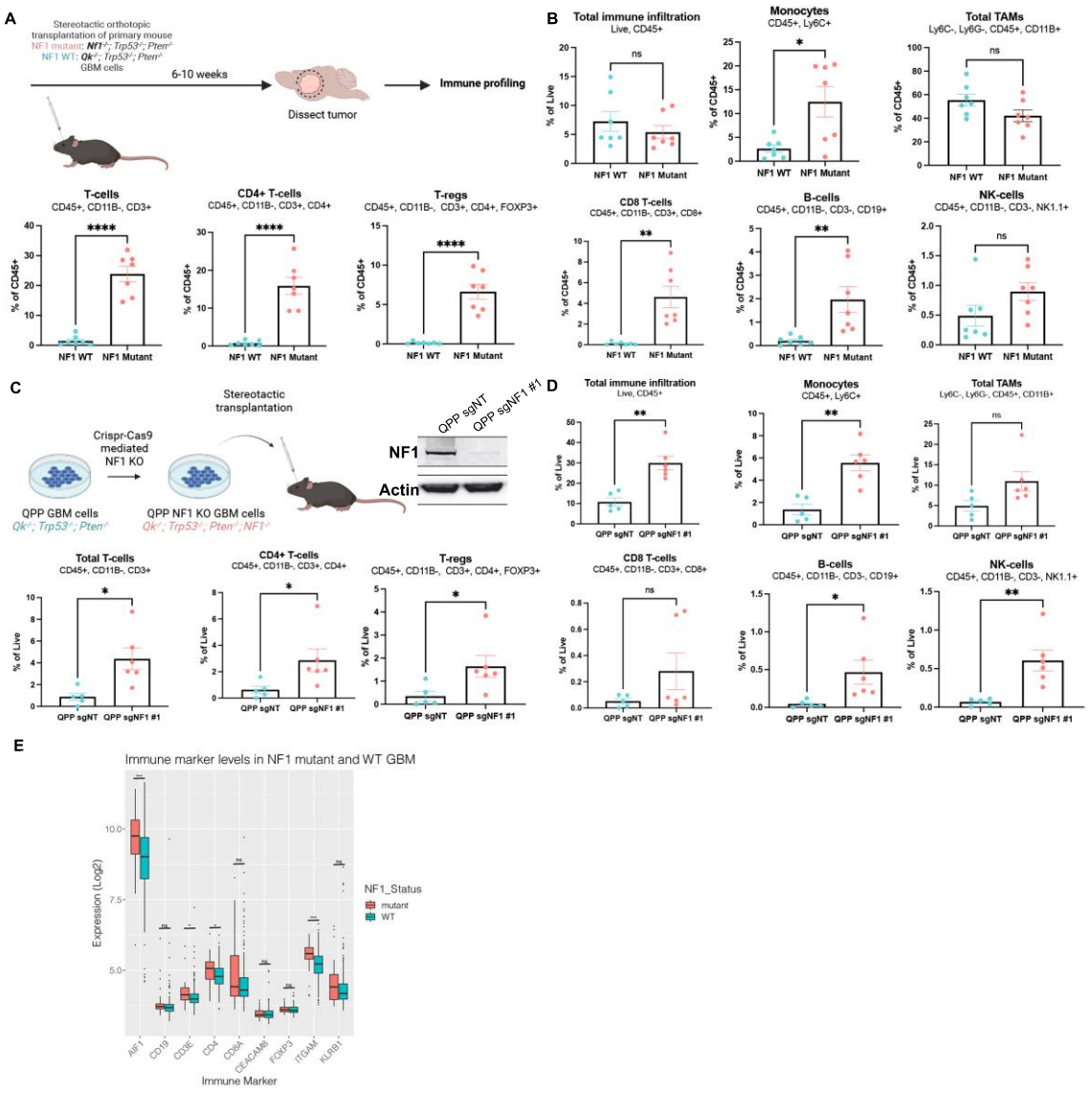

Figure 3-1 Nf1 mutant GBMs have enhanced immune infiltration.

A, Schematic outlining NF1 WT vs. Mutant mouse models. **B**, Multi-color flow cytometry measuring levels of total CD45+ immune infiltrates, Monocytes (p=0.011), Total TAMs, T-cells (p<0.0001), CD4 T-cells (p<0.0001), T-regs(p<0.0001), CD8 T-cells (p=0.0010) B-cells (p=0.0079), and NK-cells between QPP1 and NPP1. Data represented as mean with SEM, unpaired T-test, each dot is one mouse. **C**, Schematic outlining QPP sgNT vs. QPP sgNF1 mouse models and accompanying western blot to confirm NF1 KO. **D**, Multicolor flow cytometry measuring levels of total CD45+ immune infiltrates (p=0.0012), Monocytes (p=0.0012), Total TAMs, T-cells (p=0.014), CD4 T-cells (p=0.049), T-regs(p=0.045), CD8 T-cells, B-cells (p=0.043), and NK-cells (0.0060) between QPP sgNT and QPP sgNF1 #1. Data represented as mean with SEM, unpaired T-test, each dot is one mouse. **E**, mRNA expression of various immune marker genes in 28 NF1 mutant vs. 260 WT GBMs from the TCGA cohort.

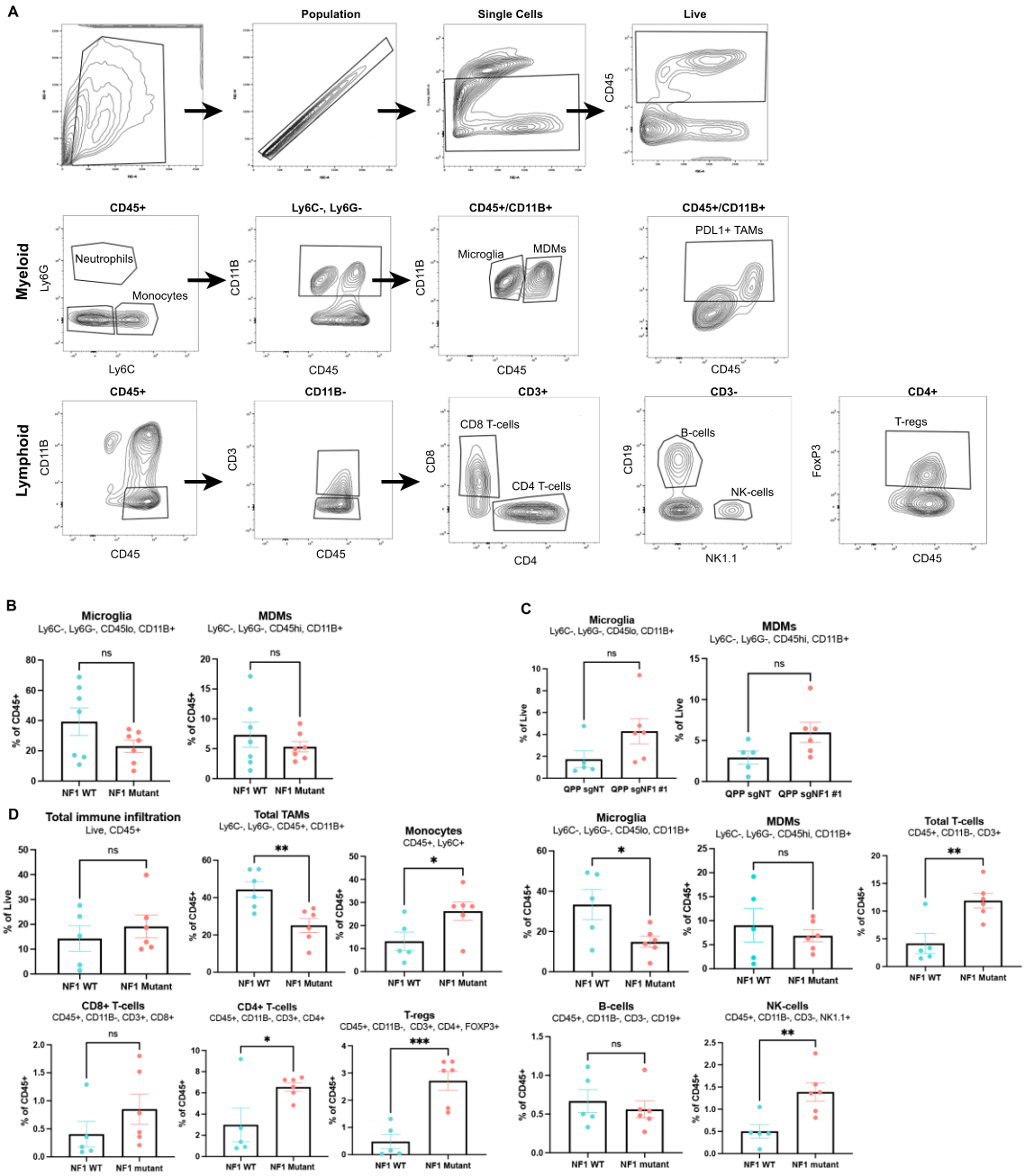

Figure 3-2 Gating scheme and flow cytometry of an independent set of NF1 mutant vs. WT GBMs.

A, Gating strategy for all flow cytometry performed in this manuscript. **B**, Muli-color flow cytometry measuring levels of Microglia and MDMs in NPP1 vs. QPP1. Data represented as mean with SEM, unpaired T-test, each dot is one mouse. **C**, Multi-color flow cytometry measuring levels of Microglia and MDMs in QPP sgNT vs. QPP sgNF1 #1. Data represented as mean with SEM, unpaired T-test, each dot is one mouse. **D,** Multi-color flow cytometry measuring levels of total CD45+ immune infiltrates, Total TAMs (p=0.0065), Monocytes (p=0.047), Microglia (p=0.034), MDMs, T-cells (p=0.0063),

CD8 T-cells, CD4 T-cells (p=0.041), T-regs(p=0.0008), B-cells, and NK-cells (p=0.0094) between QPP2 and NPP2. Data represented as mean with SEM, unpaired T-test, each dot is one mouse.

NF1 mutant mouse and human GBMs have similar immune microenvironment compositions.

To compare the proportions of immune populations seen in the mouse models used here with human GBM, we analyzed TCGA data repositories to examine the status of immune cell gene expression between human NF1 mutant and WT GBM samples[13]. Comparing microarray data from 28 confirmed NF1 mutant samples vs. 260 confirmed NF1 WT samples revealed a significant transcript elevation of genes associated with tumor associated macrophages (AIF1, ITGAM) and T-cell populations (CD3E, CD4) in NF1 mutant GBMs (Figure 3-1E). Levels of CD8A, FOXP3, CD19 and KLRB1 transcripts were unchanged in NF1 mutant vs. WT GBMs. Due to the significantly greater levels of lymphocytes and monocytes observed in mouse NF1 mutant GBM, we conclude that the models presented here represent an accurate model of human NF1 mutant GBM.

NF1 mutant GBMs have enhanced pro-inflammatory cytokine-mediated crosstalk.

To further understand the basis of increased immune cell infiltration in NF1 mutant GBM, we performed CITEseq analysis on tumors generated from two NF1 mutant tumor lines (NPP) and two NF1 WT tumor lines (QPP) (Figure 3-4A). A custom CITEseq panel was designed to measure protein levels of select immune cell markers (Supplementary Table 1). Both tumor and immune cell populations were sequenced, and samples were integrated based on NF1

mutational status (Figure 3-3A, Figure3-4B). Unsupervised clustering and uniform manifold approximation and projection (UMAP) dimensional reduction was performed, resulting in several clusters of immune cells and tumor cells identified by known cell type markers [30, 79] (Figure 3-3A, Figure 3-4C). Similar to the proportions of immune cells seen by flow cytometry, NF1 mutant GBMs had greater proportions of T lymphocytes, while NF1 WT GBMs had greater proportions of TAMs (Figure 3-3B).

Ligand-receptor interactions, specifically between cytokines and chemokines and their cognate receptors, play an important role in modulating the immune response. To further investigate the ligand-receptor interactions in NF1 mutant vs. WT GBMs, the CellChat algorithm, which predicts the probability of ligand-receptor interactions between cell types based on the gene expression of ligands and receptors in clusters in scRNAseq datasets, was used[80]. This analysis revealed that NF1 mutant GBMs have an increased number and strength of overall ligand-receptor interactions (Figure 3-3C). Upon further examination, pathways enriched in NF1 mutant tumors were pro-inflammatory cytokine/chemokine (hereafter referred to as just “cytokine”) signaling (TNF, CXCL, IL1), T-cell co-stimulatory interactions (CD86, ICOS), T-cell suppression (PD1, CTLA4), and angiogenesis promoting pathways (VEGF, ANGPTL) (Figure 3-3D, Supplementary Table 2). Together, this data demonstrates that NF1 loss induces greater pro-inflammatory microenvironment crosstalk.

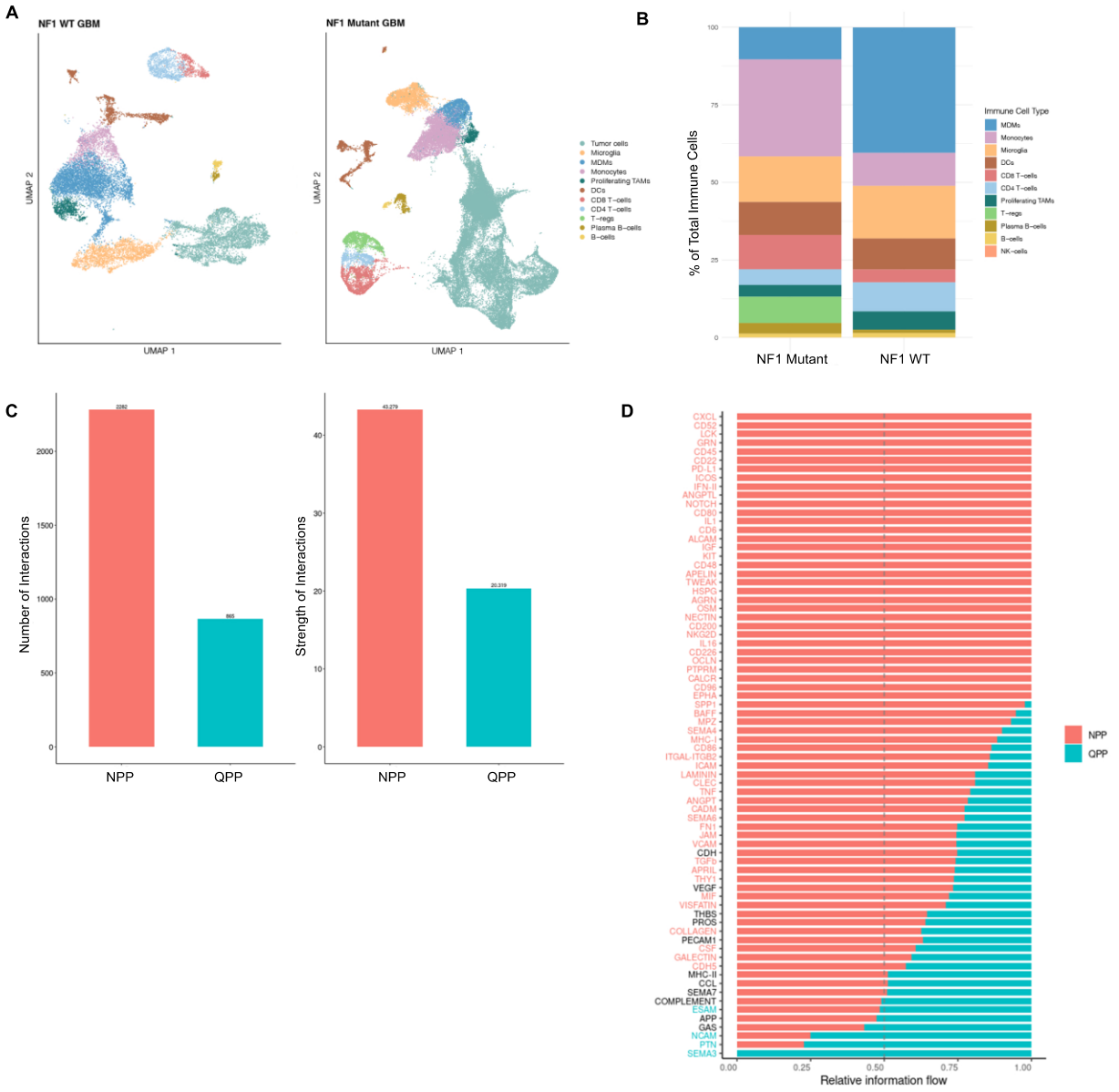

Figure 3-3 NF1 mutant GBMs have enhanced pro-inflammatory cytokine-mediated crosstalk.

A, UMAPs showing the identified cell clusters in NF1 mutant vs. WT GBMs. **B,** Stacked bar plot showing immune populations from NF1 mutant and WT immune cell scRNAseq dataset as percent of total immune cells. **C**, Graphs depicting the number and strength of ligand-receptor interactions in NF1 mutant vs. WT GBM. **D,** Graphs showing several ligand-receptor mediated signaling pathways and their relative information flow, defined by the sum of communication probability among all pairs of cell clusters in the inferred network, in NF1 mutant vs. WT GBMs.

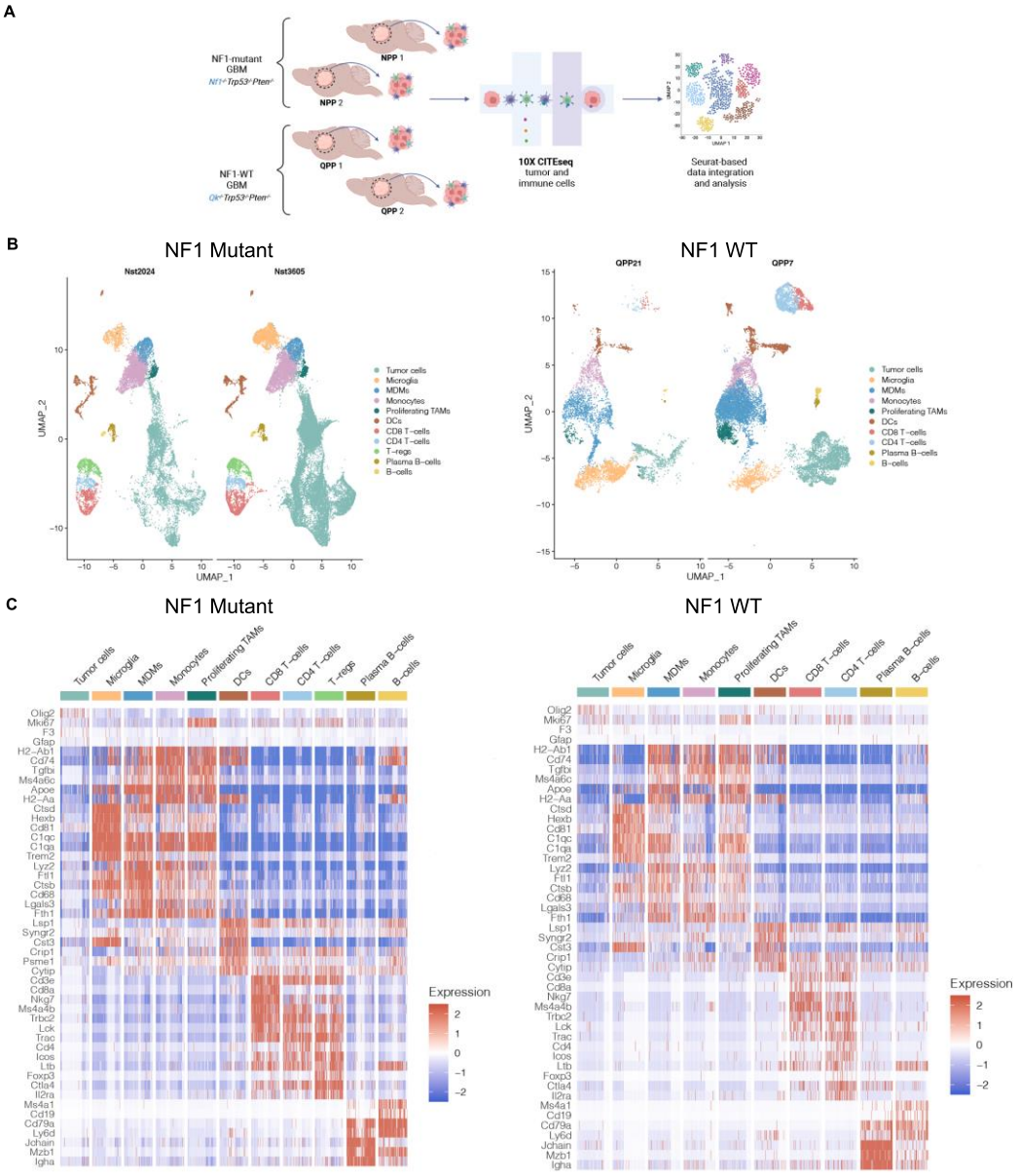

Figure 3-4 CITEseq of NF1 WT and mutant GBMs.

A, Schematic of CITEseq experiment setup to sequence NF1 mutant (NPP1, NPP2) and NF1 WT (QPP1, QPP2) GBMs (N=3-6 mouse tumors for each tumor line). **B,** UMAPs showing the contributions of each tumor type to the integrated NF1 mutant GBM dataset and the integrated NF1 WT GBM dataset. **C,** Heatmaps showing expression of various immune cell marker genes in NF1 mutant and WT GBM.

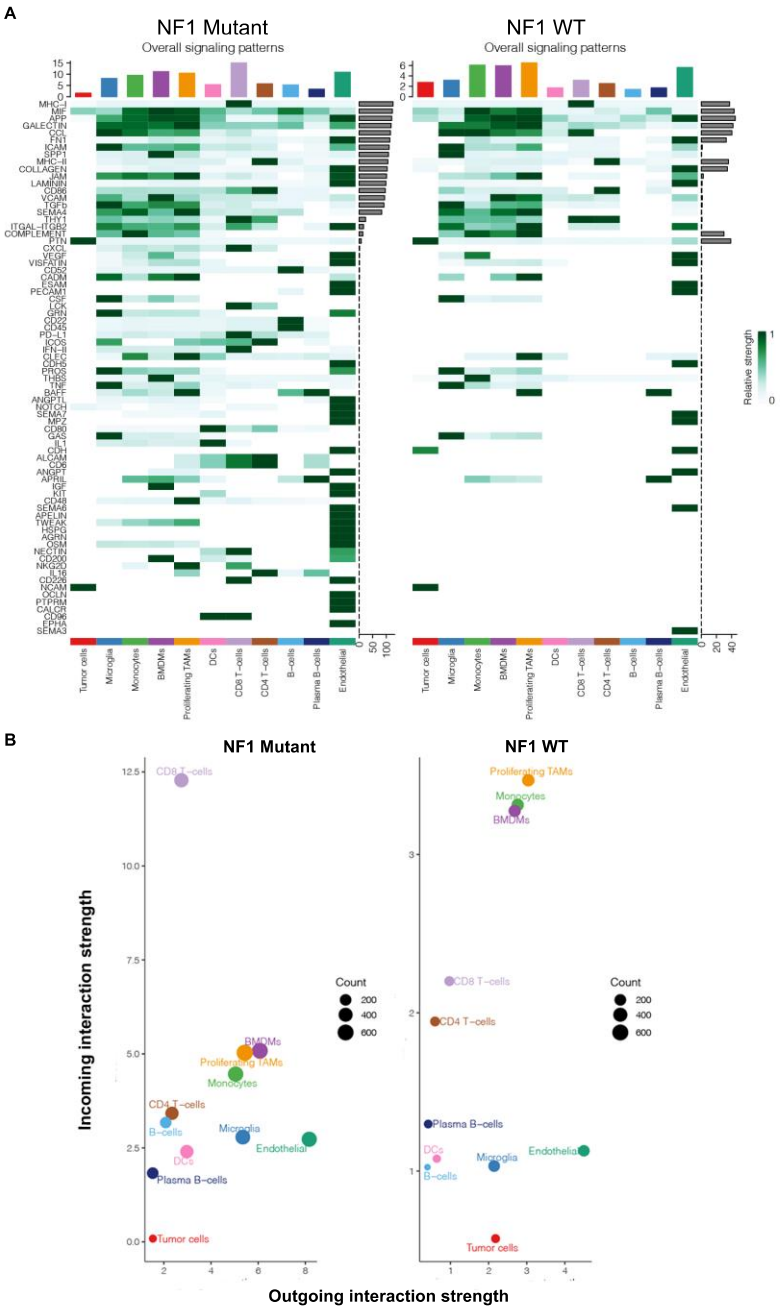

Figure 3-5 Most ligand-receptor interactions originate from TIME cells.

A, Overall signaling patterns for NF1 mutant vs. NF1 WT GBMs. Overall signaling represents all outgoing and incoming signaling added together. **B,** Outgoing and incoming interaction strength and number compared between cell types in NF1 mutant and WT GBMs.

Most ligand-receptor interactions originate from TIME cells.

We next examined which cell types appeared to be communicating in the GBM tumors. Interestingly, we observed that most of the predicted overall ligand-receptor interactions were occurring between the TIME cells rather than between tumor cells and TIME cells, especially in NF1 mutant GBMs (Figure 3-5A, B). When comparing the strength and number of sent and received signals in all cell types, it becomes evident that TAMs (monocytes, MDMs, microglia, proliferating TAMs) and endothelial cells are the dominant sources of signals, while TAMs and T-cell populations represent the dominant receivers of signals in the tumor (Figure 3-5A, B). Strikingly, CD8 T-cells are receiving 3x the amount and 6x times stronger signals in NF1 mutant tumors than CD8 T-cells in NF1 WT tumors (Figure 3-5B). Together, these results support that most ligand and receptor interactions originate from TIME cells as opposed to tumor cells.

NF1 mutant GBM T-cells engage in more ligand-receptor interactions.

Given the increased levels of T-cells in NF1 mutant GBMs, we further examined their predicted interactions in comparison to NF1 WT GBMs. We found that the dominant interactions between tumor cells and CD4 T-cells, T-regs, and CD8 T-cells were MHCII-CD4 (or MHCI-CD8), MIF-CXCR4+CD74, MIF-CD44+CD74,

and Ptn (pleiotrophin)-Ncl interactions (3-7A-C). In comparison to NF1 WT GBMs, NF1 mutant GBMs had greater T-cell TCR-MHC interactions with antigen-presenting cells, suggesting enhanced antigen-presentation activity in NF1 mutant GBMs (3-7A-C). This was further confirmed by increased levels of MHCII protein on TAM populations (Figure 3-7D). Additionally, there are more predicted T-cell stimulatory interactions such as CD86-CD28, CD80-CD28, and ICOSL-CD28 in NF1 mutant GBMs (Figure 3-6A, B, Figure 3-7A-C). However, in addition to the stimulatory interactions, there are also greater inhibitory interactions, including CD86-CTLA4, CD80-CTLA4, ICOSl-CTLA4, PDL1-PD1 occurring in the NF1 mutant TIME (Figure 3-6A, B, Figure 3-7A-C). As a result, we find greater PD1 and LAG3 protein levels on CD8 and CD4 T-cells in the NF1 mutant TIME (Figure 3-7D). PDL1 levels on TAMs was variable across mouse models in both flow cytometry analysis and by CITEseq (Figure 3-7D), suggesting that NF1 mutational status does not correlate with PDL1 levels on TAMs. In sum, comparison of the T-cell interactions between NF1 mutant and WT GBMs suggests that there is heightened T-cell activity in NF1 mutant GBMs, and that this activity likely leads to T-cell exhaustion.

NF1 mutant GBMs have enhanced TNF signaling.

Given that TAMs were among the greatest sources of signals in the tumor, we decided to focus on unique interactions between TAMs and CD4 T-cells and T-regs (Figure 3-6A, B). Among others, TNF-TNFR2 between microglia/proliferating TAMs and CD4 T-cells/T-regs was one interaction that stood out as unique to the NF1 mutant GBMs. TNF is a potent regulator of

inflammation and plays an important role in T-reg immunosuppression and expansion[81, 82]. The predicted increase in TNF-TNFR2 signaling between microglia/proliferating TAMs and T-regs may be one mechanism causing the increased presence of T-regs observed in the NF1 mutant GBM TIME.

We further examined the TNF signaling network in NF1 mutant GBMs compared to NF1 WT GBMs and found that microglia and proliferating TAMs were the main source of TNF ligand in NF1 mutant GBMs and microglia were the main source in NF1 WT GBMs (Figure 3-6C). Further, we see that TNF-TNFR1/2 signaling is predicted to occur between more TIME cell types in NF1 mutant GBM due to broader TNFR1 and TNFR2 expression (Figure 3-6D). We further validated TNFR2 expression in CD45+ cells at the protein level with immunofluorescence staining and found that the amount of TNFR2+ CD45+ cells were significantly increased in NF1 mutant GBMs (Fig. 3-6E).

Next, we explored if enhanced TNFa signaling was correlated with NF1 loss in human GBM. Using the GlioVis database[83] and the TCGA GBM RNAseq dataset[13, 14], we identified a significant negative correlation between NF1 expression and TNFR1 and TNFR2 expression levels (Fig. 3-6F). This suggests that enhanced TNF signaling may also be present in NF1 mutant human GBMs. TNF-TNFR signaling increases pro-inflammatory gene transcription via activation of the NFKB pathway[84]. This emerges as a potential mechanism by which NF1 mutant GBMs enhance inflammation in the NF1 mutant TIME. In aggregate, we

demonstrate that TNFR-TNF signaling is elevated in NF1 mutant mouse GBMs due to broader expression of TNFR1 and TNFR2 on TIME cells and that the enhanced TNFR1 and TNFR2 expression levels are correlated with decreased NF1 expression in human GBM.

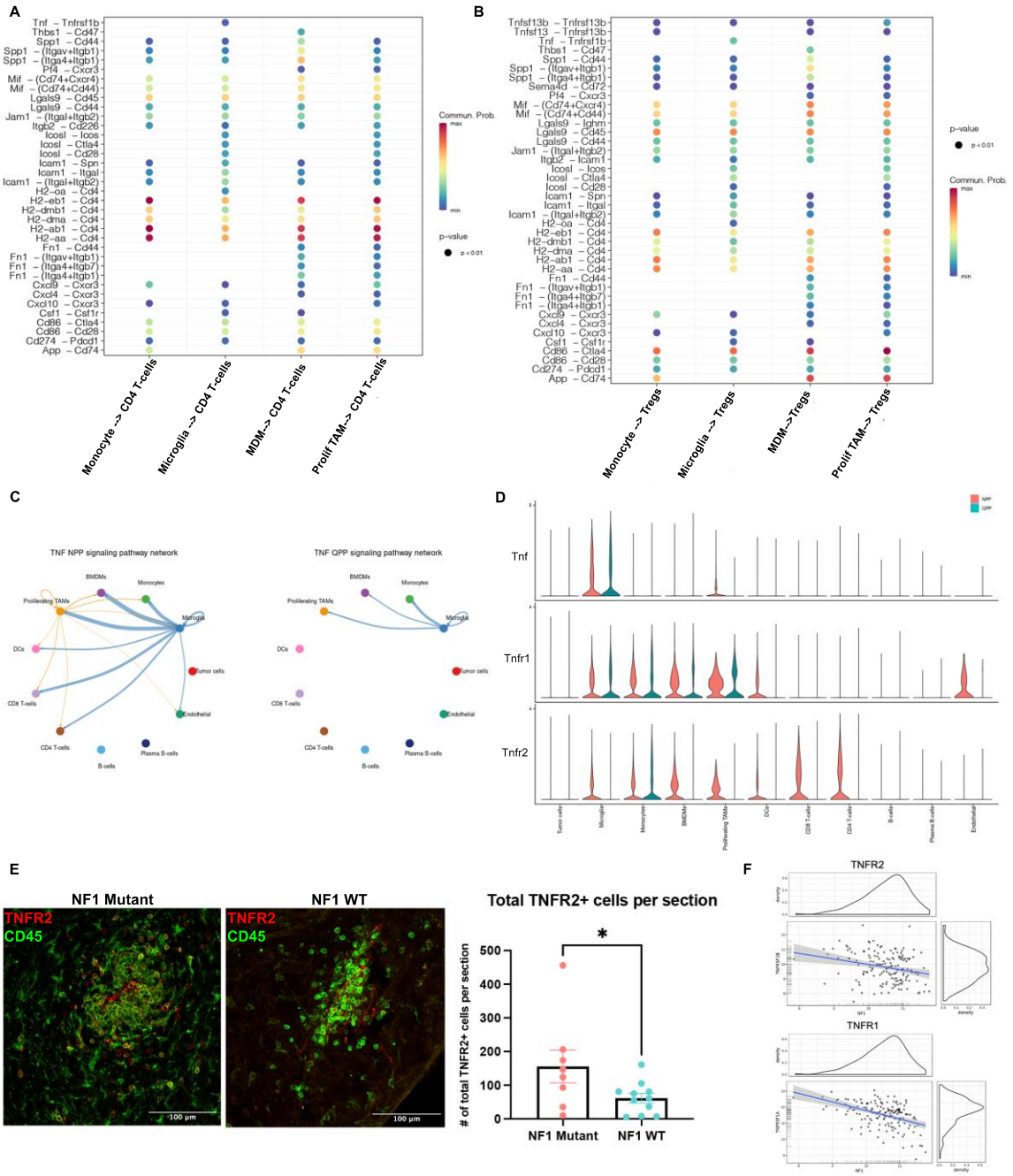

Figure 3-6 NF1 mutant GBMs have enhanced TNF signaling.

A, Interactions and communication probabilities between TAMs and CD4 T-cells. **B,** Interactions and communication probabilities between TAMs and T-regs. **C,** Circle plot illustrating the senders (indicated by a filled in circle) and receivers (indicated by an arrowhead) of TNFa signaling in NF1 mutant vs. WT GBMs. **D,** Gene expression of TNF, TNFR1 and TNFR2 in NF1 mutant vs. WT GBMs. **E**, IF staining images and quantification of total TNFR2+ cells per tumor section (N=8 NF1 Mutant tumors, 11 NF1 WT tumors, each dot represents one mouse, p=0.049). **F,** Correlation of NF1 expression with TNFR1 and TNFR2 expression. Correlation and P-values for TNFR1 and TNFR2 with NF1 respectively are correlation=-0.46, P-value=0.0, and correlation=-0.26, P-value=0.0.

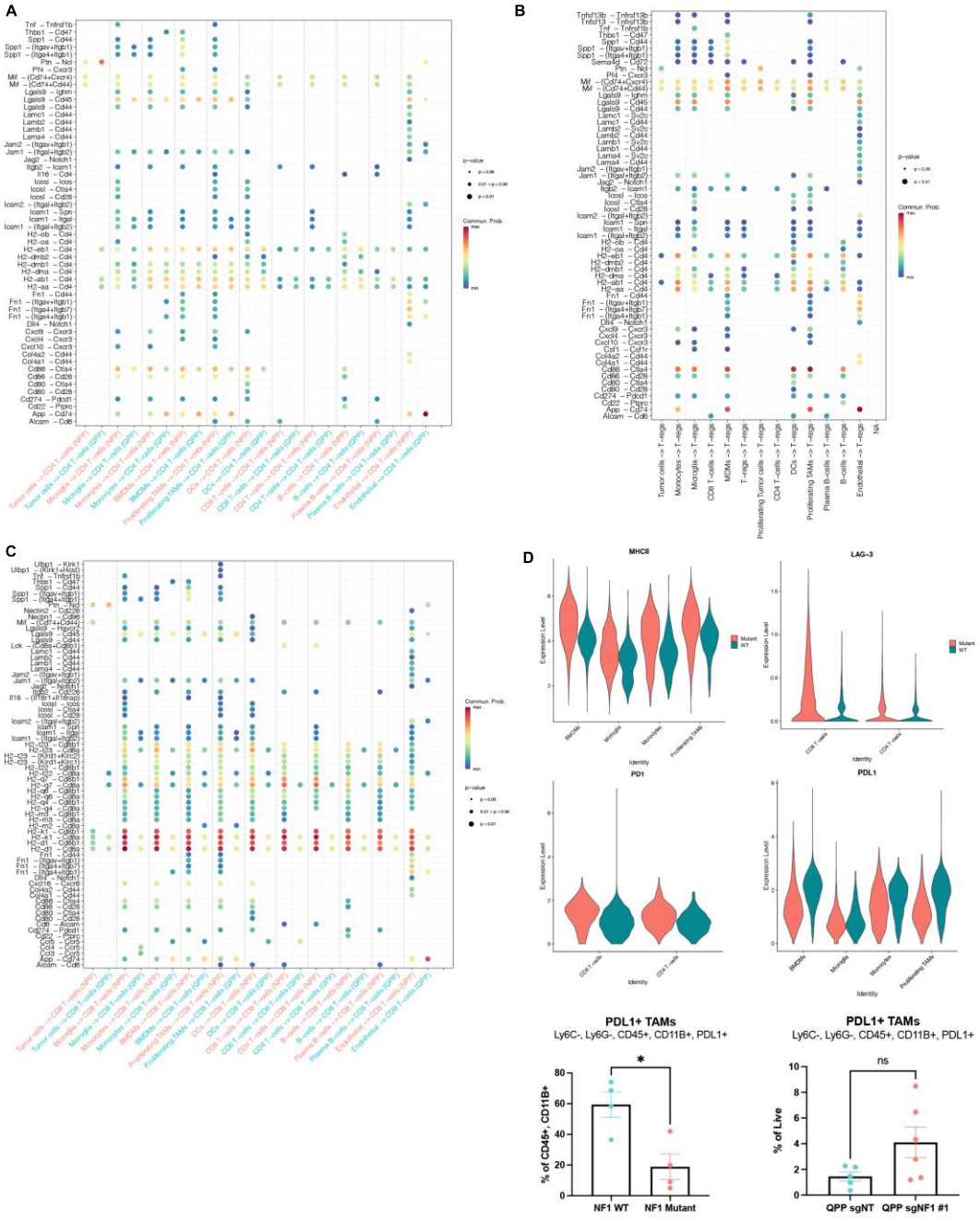

Figure 3-7 NF1 mutant GBM T-cells engage in more ligand-receptor interactions.

A, All predicted incoming signals to CD4 T-cells in NF1 mutant vs. NF1 WT GBMs. **B,** All predicted incoming signals to T-regs in NF1 mutant GBMs. There was no comparison between NF1 mutant and WT GBMs because T-regs did not cluster away from CD4 T-cells using UMAP analysis on the NF1 WT dataset. **C**, All predicted incoming signals to CD8 T-cells in NF1 mutant vs. NF1 WT GBMs. **D**, MHCII, LAG-3, PD1, and PDL1 protein levels as measured by CITEseq. **E,** PDL1 levels on TAMs as measured by flow cytometry analysis comparing NPP1 vs QPP1 (p=0.013) and QPP sgNT vs QPP sgNF1 #1 respectively. Data represented as mean with SEM, unpaired T-test, each dot is one mouse.

NF1 mutant mouse and human GBMs have higher levels of NFKB target cytokines.

To validate the increased cytokine signaling seen in NF1 mutant tumors in silico we employed targeted proteomics. To do this, we used a multiplex 44 cytokine panel on several NF1 mutant and WT mouse tumor samples, again representative of two NF1 mutant tumor lines and two NF1 WT tumor lines (Supplementary Table 3). Several cytokines were found significantly up-regulated in NF1 mutant GBMs, including IL6, TNFa, IL1B, CXCL2, CCL3, CCL5, G-CSF, M-CSF, and TIMP1 (Fig. 3-8A, Figure 3-9A). Although TNF was not predicted to be increased at the RNA level, we see it significantly increased at the protein level here, further supporting a role for TNF signaling in NF1 mutant GBMs (Figure 3-8A). Further, we examined gene expression of these cytokines in the single cell data to determine which cell populations were likely sources. We see that TIME cells are the predominant sources of significantly changed cytokines between NF1 mutant and NF1 WT GBMs, further supporting the notion that most pro-inflammatory signaling originates from TIME cells (Figure 3-9B). In looking at potential transcriptional regulators of these cytokines using TRRUST analysis[85], several NFKB family members and related transcription factors (CEBPB) were

significantly likely regulators of the increased cytokines (Figure 3-8B). Further, most of these cytokines are considered pro-inflammatory and have been associated with TNFa mediated NFKB signaling pathways (Figure 3-8A)[86]. Several of these significantly enhanced cytokines in NF1 mutant mouse GBM were also enhanced at the transcript level in NF1 mutant human GBM (Figure 3-9C). Overall, this data supports the developing notion that enhanced inflammation in the NF1 mutant TIME is mediated by NFKB pathway activation via TNF.

Next, we investigated increased cytokines and chemokines in human GBMs. We extracted protein from 9 NF1 mutant human tumor biopsies, 18 NF1 WT human tumor biopsies and 10 non-pathological brain samples. We examined the levels of several immune proteins by employing a targeted proteomics assay for 92 known immune-oncology related proteins (Supplementary Table 4). With this analysis, we observed that CXCL1, CXCL5, CCL23, CCL17, IL8, CD70, MCP-4 (CCL13), ANGPT1, TNFRSF12A, EGF, and MMP7 are significantly increased in NF1 mutant human tumor samples (Figure 3-8C, Figure 3-10A). Again, upon running TRRUST analysis on the list of significantly increased proteins, NFKB family members come up as likely transcriptional regulators, further emphasizing the role of NFKB signaling in mediating the enhanced inflammation seen in NF1 mutant GBM (Figure 3-8D). Although these cytokines are distinct from those increased in NF1 mutant mouse GBM, many still fall within the NFKB pathway. It is possible that more samples are required to see the same set of increased

cytokines in NF1 mutant mouse GBM in NF1 mutant human GBMs, as they do appear to be increased at the transcript level (Figure 3-9C).

In parallel to comparing NF1 mutant and WT GBMs, we identified significantly enriched immune-oncology related proteins in human GBM compared to non-pathological brains as well (3-10B, Supplementary Table 4). These include cytokines (IL8, CCL4, CCL3), immune marker proteins (CD4), and angiogenic factors (VEGFA), among others (Figure 3-10B, Supplementary Table 4).

In summary, we identify several NFKB pathway target cytokines that are concordantly, significantly enriched in mouse and human NF1 mutant GBM.

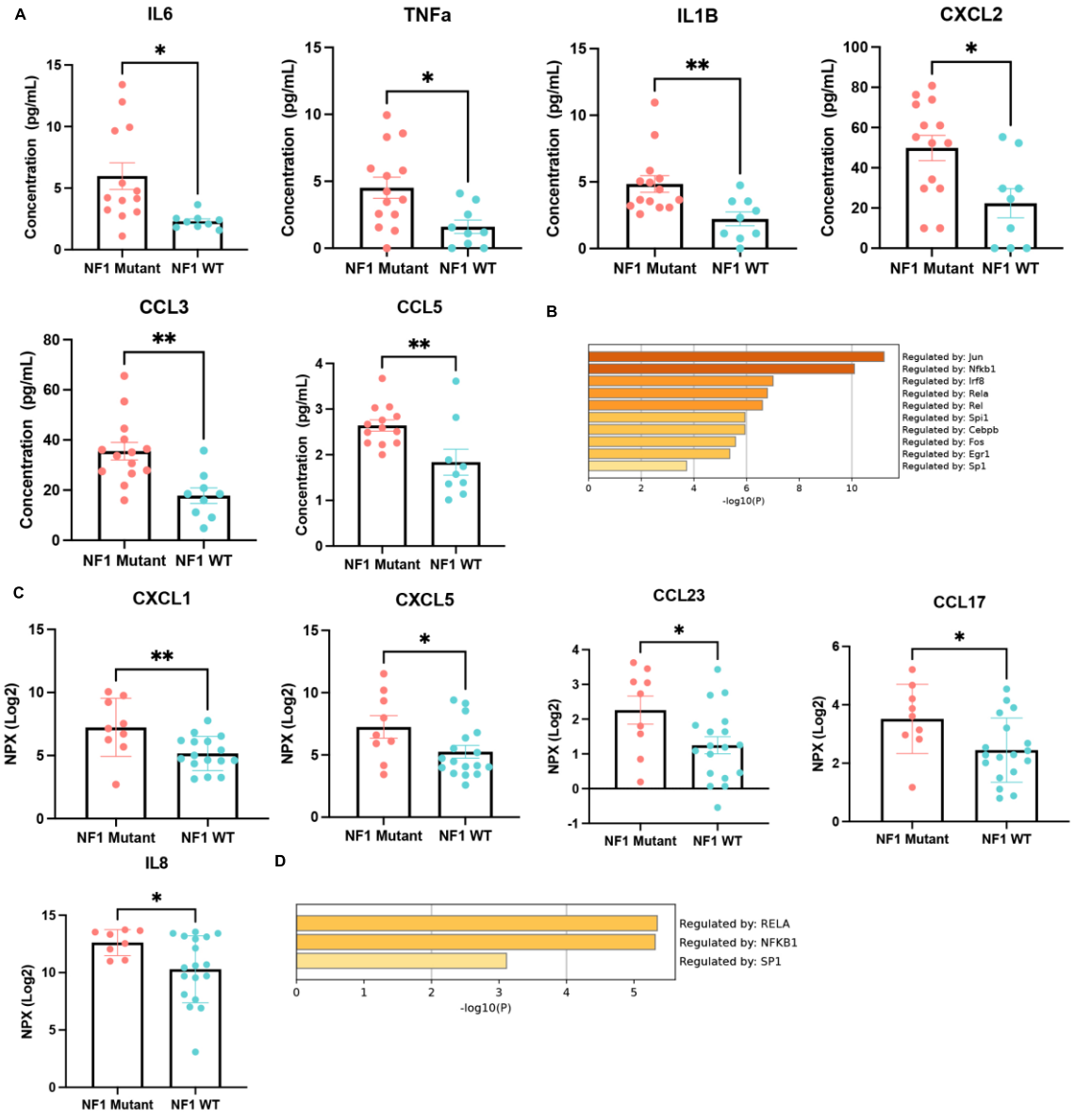

Figure 3-8 NF1 mutant mouse and human GBMs have higher levels of NFKB target cytokines.

A, Graphs showing the significantly increased cytokines in NF1 mutant mouse GBM tumor tissue samples; IL6(p=0.0118), TNFa(p=0.0129), IL1B(p=0.0076), CXCL2(p=0.0105), CCL3 (p=0.0020), and CCL5(p=0.0086). **B,** TRRUST analysis on list of significantly increased factors in NF1 mutant mouse GBM. **C,** Graphs showing significantly increased cytokines when comparing 9 NF1 mutant GBMs vs. 18 NF1 WT GBMs; CXCL1 (p=0.0091), CXCL5 (p=0.048), CCL23 (p=0.033), CCL17 (p=0.028), IL8 (p=0.041). **D,** TRRUST analysis on list of significantly increased factors in NF1 mutant human GBM.

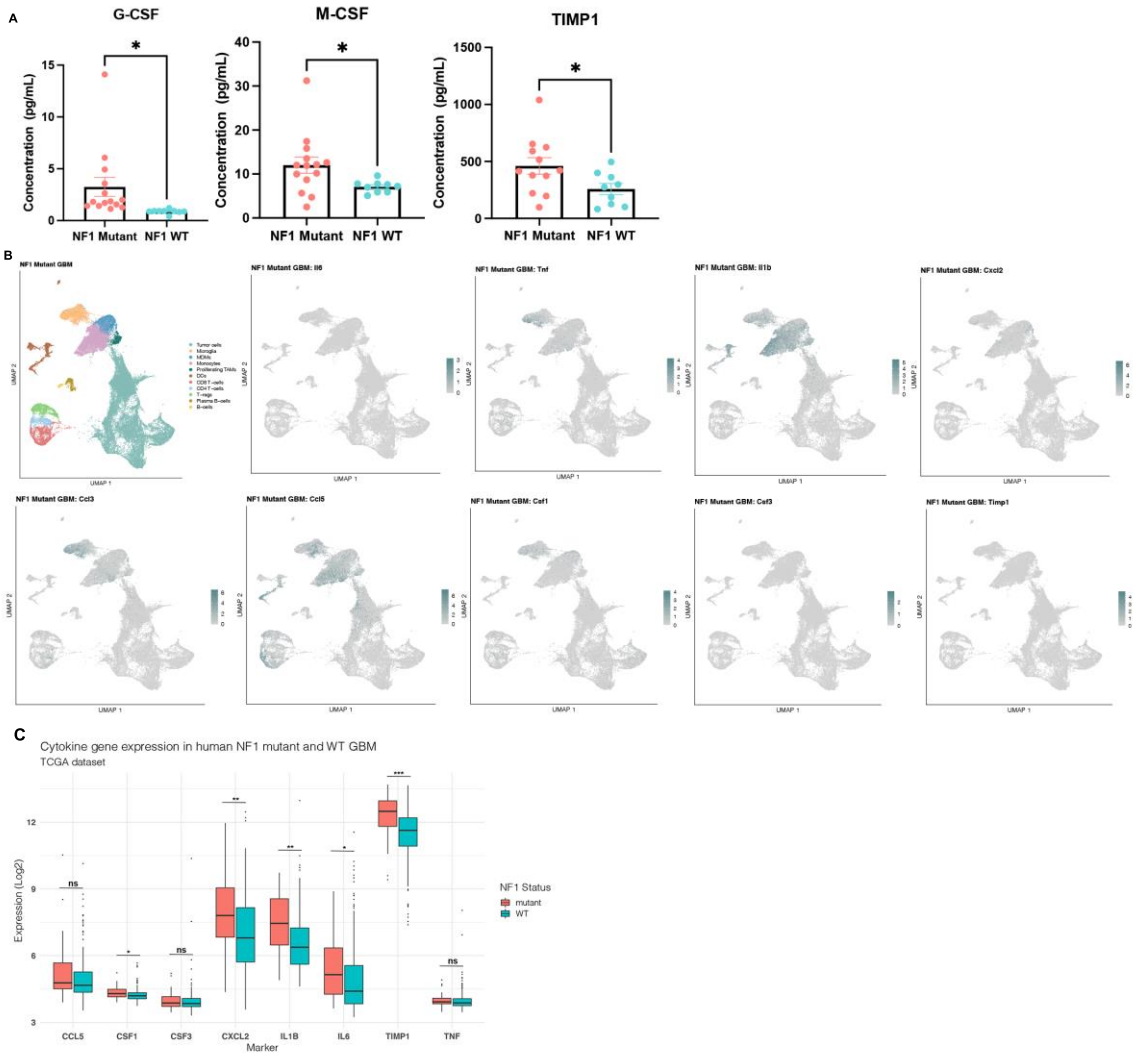

Figure 3-9 TIME cells express most increased cytokines in NF1 mutant mouse GBM.

A, Graphs showing the additional significantly increased cytokines in NF1 mutant mouse GBM tumor tissue samples; G-CSF(p=0.05), M-CSF(p=0.0477), TIMP(p=0.0445). **B,** Feature plots showing the expression of the significantly increased cytokines in NF1 mutant mouse GBM. **C,** Graph showing the expression of the significantly changed cytokines in mouse NF1 mutant GBM in human NF1 mutant vs. WT GBM (N= 28 NF1 mutant vs. 260 WT GBMs from TCGA cohort).

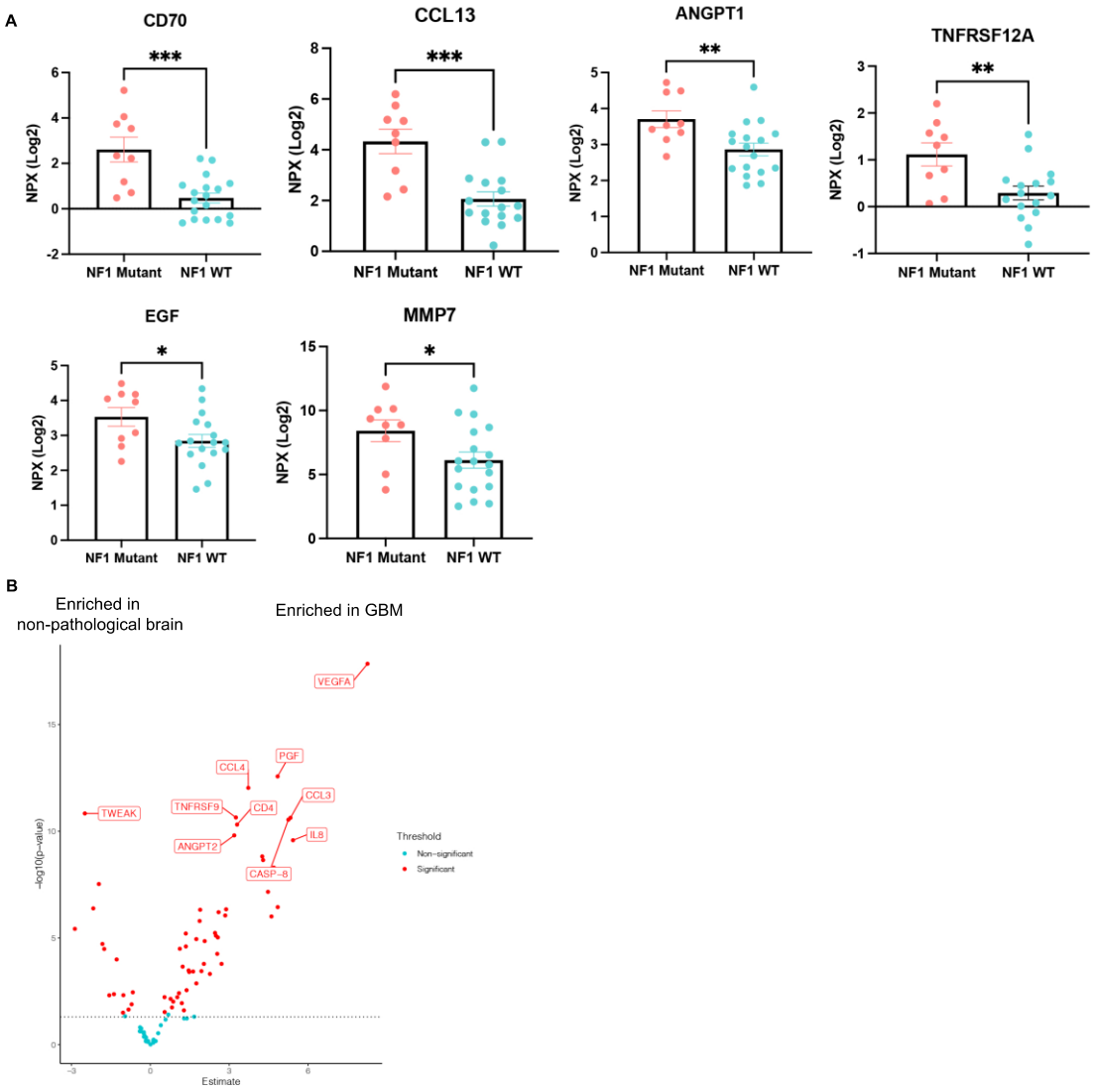

Figure 3-10 Additional cytokines increased in NF1 mutant human GBM.

A, Graphs showing the additional significantly increased cytokines in NF1 mutant human GBM tumor tissue samples; CD70 (p=0.0002), CCL13 (p=0.0002), ANGPT1 (p=0.009), TNFRSF12A (p=0.0054), EGF (p=0.039), MMP7 (p=0.042). **B**, Volcano plot showing select significantly increased immune oncology factors in GBM compared to non-pathological human brain. The rest of the significantly increased factors can be found in Supplementary Table 4.

CEBPB and NFKB transcriptional activity is elevated in NF1 mutant GBMs.

To examine potential drivers of the pro-inflammatory cytokine secretion phenotype in NF1 mutant GBM immune cells, we performed differential gene

expression analysis between the immune populations in the NF1 mutant vs. WT GBM TIME (Figure 3-12A-C). We performed GSEA using hallmark pathways and found that the “TNFA signaling via NFKB” and “Epithelial to mesenchymal” pathways were enriched in all NF1 mutant immune populations examined (Fig. 3-11A, Figure 3-11C). The “TNFA signaling via NFKB” again reinforces the role for this pathway in modulating inflammation in NF1 mutant GBMs. Interestingly, “Epithelial to mesenchymal transition” was up regulated in all of the NF1 mutant GBM tumor immune cells, as NF1 alterations have been linked to the “Mesenchymal” GBM state defined by the TCGA[15]. Notably, we did not see any “Mesenchymal” specific gene enrichment in the NF1 mutant tumor cells (data not shown), suggesting that this transition could potentially start with the microenvironment cells.

Upon further examination of the list of genes associated with “TNFA signaling via NFKB”, we found elevated expression of pro-inflammatory transcription factors *Nfkb1* and *Cebpb* in NF1 mutant GBM immune populations, also predicted regulators of the elevated cytokines (Figure 3-11B, D, Figure 3-8B, D). *Nfkb1* and *Cebpb* have been associated with NF1 mutant GBMs before, but in the context of the tumor cells and not the immune cells[87, 88, 89]. Further, NFKB and CEBPB have been shown in numerous studies to interact when regulating inflammatory gene transcription in the context of GBM[88] and in the context of other diseases[90, 91]. To further validate this finding, we performed immunofluorescence staining on NF1 mutant and WT GBM tumor samples and found that NF1 mutant GBM CD45+

cells had significantly greater nuclear localization of CEBPB and NFKB1 than NF1 WT GBMs (Fig. 3-11C, E). Next, we examined the correlation of *Nf1* expression with *Nfkb* and *Cebpb* expression in human TCGA GBM samples[83]. We found that *Cebpb* significantly correlated with low *Nf1* expression, and *Nfkb1* did not (Figure 3-12D). In sum, we have identified CEBPB and NFKB1 as potential transcriptional regulators of the enhanced inflammation in NF1 mutant GBMs.

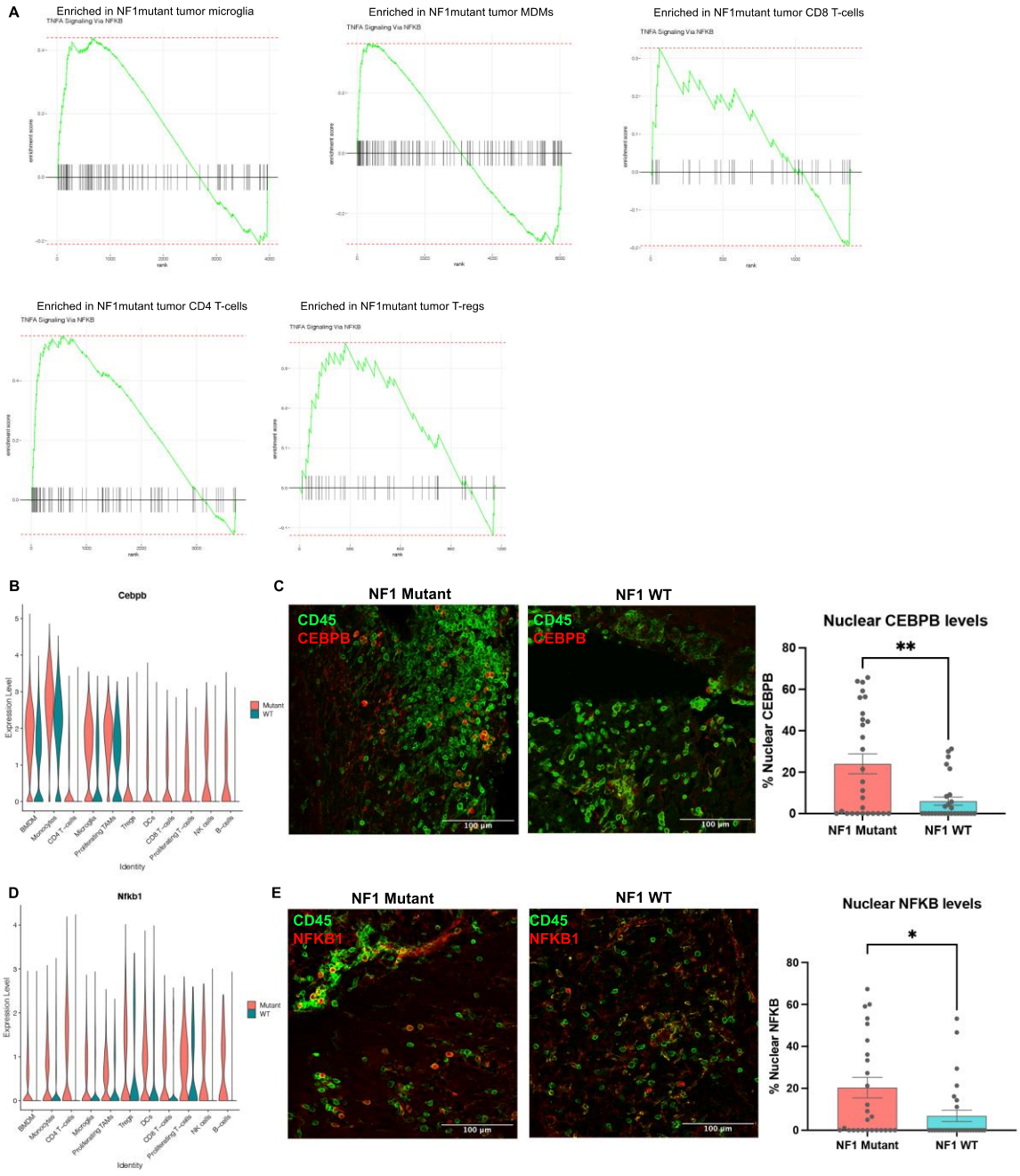

Figure 3-11 CEBPB and NFKB transcriptional activity is elevated in NF1 mutant GBMs.

A, GSEA analysis showing hallmark pathway "TNF signaling via NFKB" as being enriched in NF1 mutant GBM tumor immune populations (Microglia: NES=1.67, padj=0.37, MDMs: NES=1.37, padj=0.12, CD8 T-cells: NES=1.0, padj=0.8, CD4 T-cells: NES=1.64, padj=0.036, T-regs: NES=1.27, padj=0.72). **B,** Gene expression of Cebpb transcription factor in NF1 mutant vs. WT immune populations. **C,** IF staining images and quantification of nuclear localization of CEBPB transcription factor in CD45+ cells (N=8 NF1 mutant GBMs, 9 NF1 WT, 3 FOVs quantified per tumor). **D,** Gene expression

of Nfkb1 transcription factor in NF1 mutant vs. WT immune populations. **E,** IF staining images and quantification of nuclear localization of NFKB1 transcription factor in CD45+ cells (N=8 NF1 mutant GBMs, 9 NF1 WT, 3 FOVs quantified per tumor).

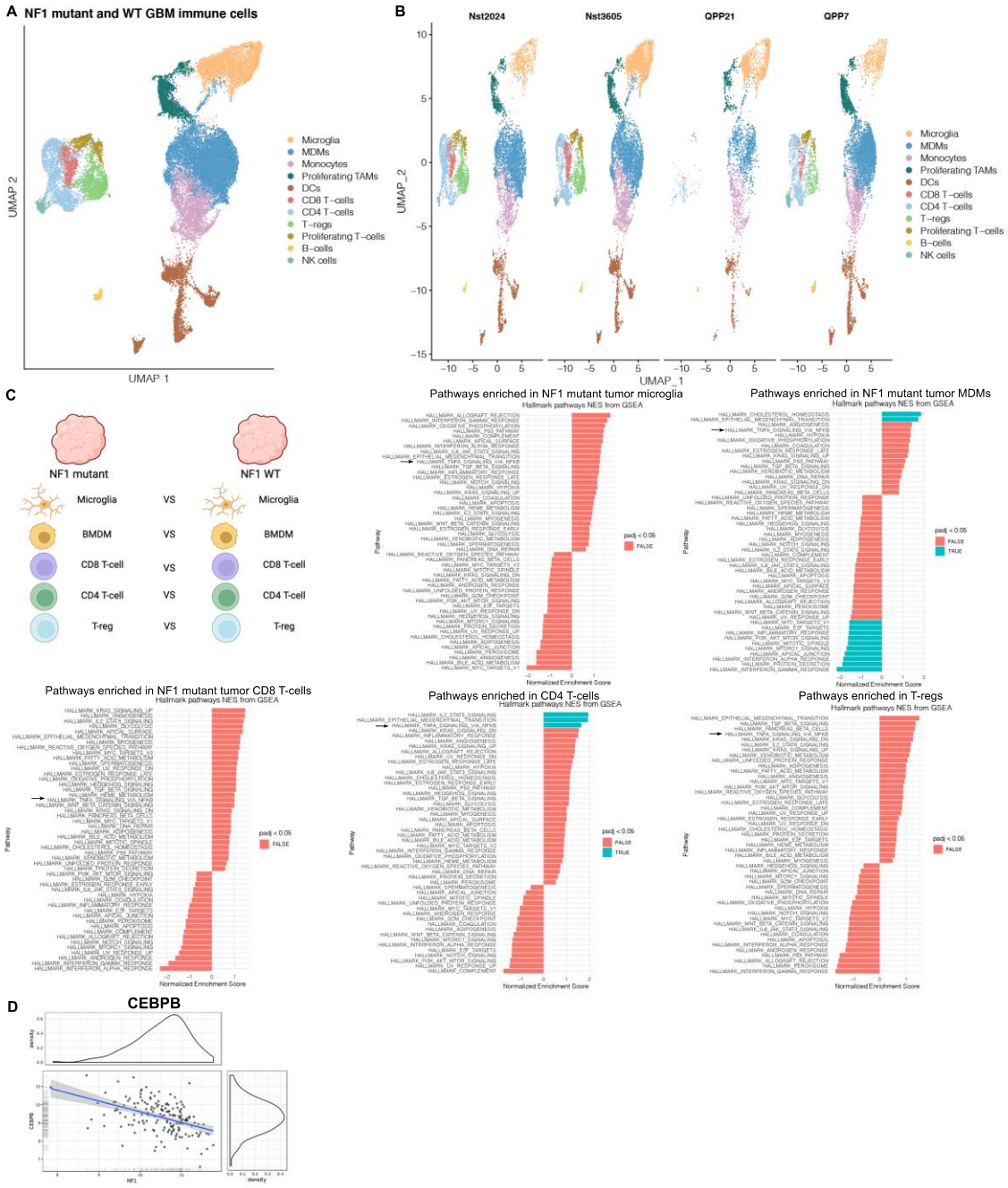

Figure 3-12 Dataset integration and correlation of NF1 loss with transcription factors in NF1 mutant human GBM.

A, UMAP showing the integration of all immune cells sequenced. **B,** UMAPs showing contribution of each NF1 mutant and WT tumor type to the total integrated dataset. **C,** Schematic illustrating comparisons for DEG analysis and full hallmark pathway GSEA analysis for the comparison between NF1 mutant and WT Microglia, MDMs, CD8 T-

cells, CD4 T-cells, and T-regs. **D,** Correlation of NF1 expression with CEBPB (correlation=-0.45, p-value = 0.0).

Discussion

Thus far, immunotherapies have failed to produce significant population wide responses in GBM. To improve patient outcomes, uncovering methods to identify potential responders to immunotherapy are critical. Correlations between prominent tumor genetic alterations and immunotherapy response or immune microenvironment composition have been observed in human GBM[15, 78]. Due to the heterogeneous nature GBM mutational profiles in human patients, preclinical studies using mouse models are necessary to fully explore the impact of genetic alterations on the GBM TIME. Here we use several mouse models of NF1 mutant and NF1 WT GBM to understand the impact of NF1 loss on the GBM TIME.

First, we demonstrate that NF1 loss causes increased immune infiltration in the GBM TIME. We show that NF1 mutant GBMs have greater levels of monocytes, CD4 T-cells, T-regs, B-cells, and NK cells. Upon knocking out NF1 in NF1 WT GBMs, we can induce greater infiltration of these populations. This demonstrates that NF1 loss causes the increased levels of monocytes, CD4 T-cells, T-regs, B-cells, and NK cells. Previous studies have observed increased levels of TAMs in NF1 mutant GBMs[15]. Because monocytes also express AIF1 and CD11B, genes used to distinguish TAMs in these studies, it could be an increased recruitment of monocytes, and not differentiated microglia and MDMs, that is occurring in NF1 mutant GBM. Further study is necessary to understand the role of monocytes vs. differentiated TAMs in GBM.

Next, we perform CITEseq to further investigate the transcriptional states of tumor and immune cells in NF1 mutant vs. WT GBM. We find that NF1 loss induces pro-inflammatory cellular cross talk between the microenvironment cells in NF1 mutant GBM. The enhanced inflammatory gene transcription observed here is consistent with prior studies showing the correlation between NF1 mutations and inflammatory genes[15, 61, 92]. Additionally, we observed that this cross talk takes place predominantly between immune microenvironment cells. This is consistent with a previous report that showed that most cytokine and cytokine receptor expression was by immune microenvironment cells as opposed to tumor cells[32]. The mechanism by which tumor cells influence the composition and activation of the immune microenvironment becomes complicated and is likely indirect as the tumor cells themselves are not necessarily secreting the immune attracting/activating cytokines. Despite the increased presence of T-cells in NF1 mutant GBM, we did not find unique tumor cell-T-cell interactions in NF1 mutant GBMs compared to NF1 WT GBMs. This suggests that the effect of NF1 loss on T-cell recruitment may be indirect. We then focused on macrophage signaling with T-cells and were able to find a promising potential mechanism. Although we did not see a significant increase in TAMs in NF1 mutant GBMs, it is plausible that NF1 deficient tumor cells could influence their polarization and cause them to attract more T-cells to the tumor. Linking NF1 loss in tumor cells to the observed phenotypes here will be an important future direction of this work.

Next, we demonstrated that TNF-TNFR signaling is enhanced in NF1 mutant GBMs. TNF plays a significant role in orchestrating the immune response in homeostatic and disease states. We observed that NF1 mutant GBMs had increased predicted TNF-TNFR interactions. This was further corroborated on the protein level with increased TNFR2 and TNF levels seen in NF1 mutant GBMs. Further, recent work has shown that delivery of an antibody-TNF fusion protein to the brains of GBM patients increased CD4 and CD8 T-cells[60], highlighting the importance of TNF in increasing the proportions of T-cells in the TIME. Future clinical trials of immunotherapies targeting T-cells, such as checkpoint inhibitors, should consider adding delivery of TNF to enhance the number of T-cells in the TIME.

We then validate several in silico predicted cytokine signaling interactions by profiling the intratumoral cytokines by targeted proteomics. Several of the cytokines found to be significantly elevated in NF1 mutant mouse and human GBM were NFKB target genes, again reinforcing the notion that enhanced inflammation in NF1 mutant GBMs is mediated by TNF activation of the NFKB pathway. We also found angiogenic factors and proteinases to be significantly elevated in NF1 mutant mouse and human GBM as well. We find many of these factors to be expressed by TAMs, suggesting an important role for the activation state of TAMs in influencing the GBM TIME composition.

CD70, transmembrane glycoprotein and ligand for CD27, was at significantly higher levels in NF1 mutant human GBM. Currently, Car-T cells against CD70 are in development[93, 94]. If CD70 targeted Car-T cells are tested in clinical trials for glioblastoma, patients should be segmented based on NF1 status, as we have demonstrated that NF1 mutant GBM patients have significantly higher levels of CD70.

Next, we further probed the differential states of immune cells in NF1 mutant vs. WT GBMs. We found that hallmark pathway “TNF signaling via NFKB” and “Epithelial to Mesenchymal transition” was enriched in all immune populations in NF1 mutant GBM. Upon further analysis, we found *Nfkb1* and *Cebpb* to be significantly enriched in several NF1 mutant GBM immune cells. This was confirmed with immunofluorescence staining. This is interesting as *Nfkb* family transcription factors and *Cebpb* have been shown in several instances to interact and be co-dependent[90, 91]. One report demonstrated that NFKB activation through TNFa induced higher CEBPB levels in several glioblastoma cell lines[88]. It appears a similar phenomenon is occurring in NF1 mutant GBMs, except it is induced in immune cells as opposed to tumor cells. Additionally, *Cebpb* has previously been associated with NF1 loss, again expressed by tumor cells as opposed to immune cells[87, 89]. In these reports[87, 88], studies were performed in cell lines and immune cell expression of *Nfkb* and *Cebpb* were not examined. Also, its been shown before that GBM tumor and immune cells can express similar gene signatures[95].

Collectively, our results reveal the impact of NF1 loss on the glioblastoma tumor immune microenvironment and highlight an important role for NFKB and CEBPB induced pro-inflammatory cytokine-mediated crosstalk in enhancing inflammation in GBM. Our work increases understanding of how NF1 loss influences the tumor immune microenvironment and opens up new therapeutic possibilities targeting NF1 mutant glioblastomas.

Methods

Mice.

All mouse experiments were approved and performed according to the guidelines of the Institutional Animal Care and Use Committee of Memorial Sloan Kettering Cancer Center. Tumor suppressor mice with Nestin-CreER^{T2} [8, 73, 74] or NG2-CreER^{TM} [9, 75] transgenes were crossed with conditional *Trp53* allele. Nestin-CreER^{T2}*; Nf1*$^{fl/+}$*; Trp53*$^{fl/fl}$; *Pten*$^{fl/+}$ mice or NG2-CreER^{TM}; *Nf1*$^{fl/+}$*; Trp53*$^{fl/fl}$; *Pten*$^{fl/+}$ mice were generated by breeding Nestin-CreER^{T2};*Trp53*$^{fl/fl}$ or NG2-CreER^{TM};*Trp53*$^{fl/fl}$ mice with *Nf1*$^{fl/fl}$*; Trp53*$^{fl/fl}$; *Pten*$^{fl/fl}$ mice. *Nst-CreER*^{T2}*; Qk*$^{fl/fl}$*; Trp53*$^{fl/fl}$*; Pten*$^{fl/fl}$ [40] breeder mice were gifted by the Jian Hu lab. QPP7 mouse tumor cell line was also gifted by the Jian Hu lab. All mice were maintained under formal MSKCC IACUC protocols.

For all 10x chromium scRNAseq and CITEseq studies, tumor lines were injected into 4–6-week-old C57BL/6J mice purchased from Jackson Laboratories. Mice were housed in individually ventilated cages and had free access to water and

food with 12:12 hour light-dark cycle. All mouse studies included both sexes in approximately equal proportions.

Mouse primary cell culture.

Mice with tumor suppressor alleles were induced with tamoxifen at 4-6 weeks of age and aged until they developed symptoms of GBM as described previously. Mouse primary tumor tissues were freshly dissected from symptomatic mice. Harvested tissues were minced and incubated with Accutase in 37C water bath for 20 minutes, dissociated, and cultured in serum free medium supplemented with B27 and N2 (SFM), plus EGF, FGF and PDGF-AA (10 ng/ml each) in 5% oxygen, 37C incubator. Primary cultures were established as tumor spheres at P0, later passages were as spheres in non-coated plates, or as monolayer in laminin pre-coated plates (10 ng/mL Laminin diluted in DPBS with Ca2+/Mg2+).

Mouse stereotactic GBM cell injection.

The NF1 mutant and WT cell lines were derived from spontaneous GBM mice and cultured as described above. For intracranial injection, mice were anesthetized (Isoflurane) and placed on a stereotactic frame. A midline incision was made on the skin to expose the scalp, and a microdrill was used to perform craniotomy. For intracranial injection, 1×10^4 cells were injected in the striatum (coordinates: 1.0 AP, -1.8 ML, 4.5 DV with respect to the bregma). Minimum cells were injected to avoid inducing inflammation and model physiologic conditions as

closely as possible. Mice were monitored and euthanized for tissue collection when neurologic symptoms were displayed.

Tumor dissociation.

Mice injected with NF1 mutant or NF1 WT cell lines were monitored until neurologic symptoms emerged. Mice were anesthetized and transcardially perfused with ice cold HBSS. Tumors were dissected, chopped up on ice, and dissociated using the Miltenyi Brain Tumor Dissociation Kit. Following dissociation, the myelin was removed with the Miltenyi myelin removal beads and magnetic separator. Next, red blood cells were removed with red blood cell lysis buffer (Sigma). Tumor cell suspensions were frozen with BamBanker cell freezing media and placed at -80 for < 1 month prior to genomic or flow cytometry studies.

10X Chromium ScRNAseq and CITEseq.

Frozen cell suspensions were dethawed and stained with CITEseq antibody panel (see Supplementary Table 1), CD45, and Zombie NIR and Calcien violet viability dyes. Cells were washed and then sorted for viability and CD45 positivity and negativity. Equal numbers of CD45+ and CD45- cells were combined and loaded onto the 10X chromium. The single-cell RNA-Seq of FACS-sorted cell suspensions was performed on Chromium instrument (10X genomics) following the user guide manual for 3′ v3 or v3.1. In brief, FACS-sorted cells were washed once with PBS containing 1% bovine serum albumin (BSA) and resuspended in

PBS containing 1% BSA to a final concentration of 700–1,300 cells per µl. The viability of cells was above 80%, as confirmed with 0.2% (w/v) Trypan Blue staining (Countess II). Cells were captured in droplets. Following reverse transcription and cell barcoding in droplets, emulsions were broken and cDNA purified using Dynabeads MyOne SILANE followed by PCR amplification per manual instruction.

Between 6,000 to 30,000 cells were targeted for each sample. Tumor biological replicates of the same injected cell line were multiplexed together on one lane of 10X Chromium (using Hash Tag Oligonucleotides - HTO) and specific extracellular protein epitope characterized (using Antibody Derived Tag - ADT) following previously published protocol[96]. Final libraries were sequenced on Illumina NovaSeq S4 platform (R1 – 28 cycles, i7 – 8 cycles, R2 – 90 cycles). The cell-gene count matrix was constructed using the Sequence Quality Control (SEQC) package[97].

Data processing

The Cell Ranger pipeline (10x Genomics) was used to perform sample demultiplexing and to generate FASTQ files. Seurat v4 was used for all downstream analysis. Viable cells were identified on the basis of library size and complexity, whereas cells with >15% of transcripts derived from mitochondria were excluded from further analysis.

Protein level analysis

To aid with clustering and explore the protein levels of the CITEseq antibodies used in this study, protein levels were normalized using the Seurat NormalizeData function. Violin plots and feature plots were used to compare protein levels between different cell populations.

Characterization of NF1 mutant vs. WT TAM populations

For characterization of NF1 mutant specific and NF1 WT specific populations, the cells from the NPP3605 and NPP2024 NF1 mutant lines were integrated and the cells from QPP7 and QPP21 NF1 WT lines were integrated using Seurat reciprocal PCA integration (RPCA).

CellChat analysis

CellChat algorithm was used to examine ligand-receptor interactions in the NF1 mutant and NF1 WT integrated datasets[80]. Integrated NF1 mutant and WT tumor datasets were analyzed separately and in an integrated fashion. In order to perform the CellChat integrated dataset comparison analysis, clusters in the NF1 mutant and NF1 WT integrated datasets had to have the same names, so clusters of the same cell type were combined for this analysis (i.e. “Microglia”, as opposed to “Microglia 1”, “Microglia 2”). The T-reg cluster from the NF1 mutant tumors was combined with the CD4 T-cells cluster to make the “CD4 T-cell cluster”. This is because T-regs did not come out as a unique cluster with UMAP analysis for the NF1 WT tumors. The package was then used according to the GitHub tutorial.

TRRUST Analysis

TRRUST analysis was performed on the metascape.org website using the complete list of significantly increased factors found by targeted proteomics in mouse and human NF1 mutant GBM. Mouse and human analysis was performed separately.

Differential gene expression analysis

For differential gene expression analysis between NF1 WT and NF1 mutant immune cell populations, immune populations from NPP3605, NPP2024, QPP7 and QPP21 were integrated using RPCA. For differential expression analysis, the Seurat object RNA slot was used. Seurat default FindConservedMarkers was used to compare differentially expressed genes between NF1 mutant and NF1 WT immune populations. A LogFC cutoff of 0.25 and Padj cutoff of 0.05 was used for analysis.

GO and GSEA analysis.

GSEA was performed using the Fgsea package. GO was performed using the ClusterProfiler, TopGO, and DOSE packages.

Analysis of TCGA GBM data.

TCGA samples with both mutational information and mRNA expression data were compiled from the TCGA database. Samples with and without NF1

mutations were identified. R was used to look at differences in gene expression data between NF1 mutant and WT human GBM samples.

Multicolor Flow Cytometry.

Tumor cell suspensions were dethawed and stained with a fixable viability dye. Cells were then washed, blocked with CD16/32 Fc block for 5-10 minutes, and stained with extracellular antibodies for 20 minutes on ice. Cells were then washed and either resuspended in FACS buffer or Fluorofix buffer (BioLegend) for analysis (myeloid panel) or moved on for staining with intracellular antibody FoxP3 (lymphoid panel). For intracellular staining, cells were fixed and permeabilized with the FoxP3/transcription factor staining kit (eBioscience). Then, cells were stained with FoxP3 for 30 minutes on ice, washed, and resuspended in FACS buffer for analysis. Flow cytometry data was acquired using BD Biosciences LSRFortessa analyzers and BD FACSDiva software. Data was analyzed using FlowJo. Flow cytometry antibodies used for the myeloid panel include CD45(Alexafluor 700, BD Biosciences, #56010), CD11B (BV785, Biolegend, #101243), Ly6C (APC Cy7, BD Biosciences, #560596), Ly6G (PE Cy7, Tonbo Biosciences, #60-1276-U100), MHCII (BV711, Biolegend, #107643), CD49D (BV650, BD Biosciences, #740458), and PDL1 (APC, R&D Systems, #FAB1019A-025). Flow cytometry antibodies used for the lymphoid panel include CD45(Alexafluor 700, BD Biosciences, #56010), CD11B (Alexa 647, Biolegend, #101218), CD3 (PE Cy7, BD Biosciences, 560591), CD4 (APC Cy7, BD Biosciences, #561830), CD8 (BV711, BD Biosciences, #563046), CD19 (BV786,

BD Biosciences, #563333), NK1.1 (BB700, BD Biosciences, #566503), FoxP3 (PE Cy5, Thermo Fisher Scientific, #15-5773-80).

Histology and immunohistochemistry.

Mice were perfused with PBS and brains were fixed in 4% paraformaldehyde, processed, and embedded into paraffin blocks. Blocks were sectioned into 10µM sections and stored at 4 degrees until staining. DAPI was used to stain the nucleus (ThermoScientific, 1ug/ml). Immunofluorescent antibodies used include TNFR2 (R&D systems, #AF-426-SP), CEBPB (Santa Cruz, #sc-7962), NFKB1 (Santa Cruz, #sc-8414). The sections were then imaged with a Zeiss LSM 510 confocal microscopy using Argon 488, He543, and He 633. Images were quantified using Fiji.

Cytokine assays.

For cytokine experiments with mouse NF1 WT and mutant GBM tumors, protein was extracted from tumors by lysing tissue with RIPA buffer and protease inhibitor cocktails. Protein samples were then normalized to contain the same concentration of protein per sample. Once all samples were normalized, they were sent to Eve Technologies Corp. for the Mouse Cytokine/Chemokine 44-plex discovery assay (MD-44). For data analysis, T-Tests were performed between NF1 mutant vs. NF1 WT in prism to determine which cytokines were significantly different between groups. ROUT outlier analysis (Q=1%) in prism was used to remove outliers from the data.

For human cytokine assays, 9 NF1 mutant, 18 NF1 WT, and 10 normal brain tissue pieces were lysed, normalized to contain the same amount of protein per sample, and shipped to Olink Proteomics. Olink proteomics then performed their Target 96 Immuno-oncology panel. All mutations for the samples analyzed are listed in Supplementary Table 7. For data analysis, Olink Proteomics sample analysis software was used. An Anova was performed between NF1 mutant GBMs, NF1 WT GBMs, and normal GBMs. This analysis was used to determine the upper and lower fences. Cytokine readings above or below the upper and lower fences were removed as outliers. Once outliers were removed, direct comparisons and graphs were made using standard T-Tests in prism.

Genetic KO of NF1

Custom lentiviral Cas9/sgRNA expression constructs were ordered from Cellecta. Plasmids contained a Tag RFP construct for selection. NF1 targeted (sgNF1) and non-targeting (sgNT) plasmids were packaged into lentivirus. QPP21 tumor line was then transduced with either NF1 targeted or non-targeting sgRNAs. Transduced cells were grown up and sorted for RFP positivity. Western blot was then performed to confirm NF1 knock out (Cell Signaling, Cat #14623).

Human sample acquisition.

NF1 mutant and WT patient tumor tissue was acquired from the MSKCC Pathology core facility. Normal brain samples were obtained from the MSKCC

Last Wish research autopsy program. All experiments with human tissue samples were approved by the MSKCC institutional review board.

Statistical analysis.

Statistical analysis between groups was performed using two-tailed unpaired Student's t-test. Kaplan-Meier survival curves were analyzed using log-rank (Mantel-Cox) test. For bar figures presented, the center line represents mean ± SEM, as indicated. Data were analyzed using Excel, GraphPad Prism v.9 and Fiji. P-values less than 0.05 were considered significant. Assays are representative of ≥3 independent and biological replicates.

Chapter 4 Perspectives and Future Directions

Summary

In this work, we studied the tumor immune microenvironment of GBM in a basic context using several highly physiologically relevant mouse model systems to gain insights that could influence future immunotherapeutic approaches in GBM. Several recent clinical trials for immunotherapeutics in GBM have failed. As none of these clinical trials have attempted patient stratification, we identified this as a possible strategy to improve outcomes. We have demonstrated here that GBM cell lineage and GBM NF1 status can influence the composition of the tumor immune microenvironment and thus could potentially serve as a useful patient segmentation strategy for immunotherapies. We have also made several insights along the way regarding the function and communication networks of tumor immune microenvironment cells.

In Chapter 2, we demonstrated that GBM cell lineage could influence the tumor immune microenvironment of GBM; Type 2, oligodendrocytic progenitor lineage-derived GBMs have greater overall immune infiltration and specifically MDMs, than Type 1, SVZ NSC lineage-derived GBMs. We then devised a TAM depletion system that offered a more robust and sustained TAM depletion than used in previous studies. We depleted TAMs in Type 1 and Type 2 GBMs, and survival was not impacted. Additionally, we also depleted TAMs in an NF1-sufficient model, and survival was again not impacted. We performed bulk RNAseq on TAM depleted vs. control GBMs and found that cell lineage had more impact on

tumor transcriptome than TAM depletion status. Further, TAM depletion decreased overall tumor inflammation, with pathways such as “TNFa signaling via NFKB” and “Interferon gamma response” being decreased in TAM depleted tumors. Few genes were increased in TAM depleted tumors, with pro-growth pathway “Hedgehog signaling” being the only pathway significantly enriched. In sum, this data suggests that although TAMs support tumor growth and development, GBMs are not dependent on them for growth and survival, and do not have to significantly adapt to survive in their absence.

In Chapter 3, we explored the impact of NF1 loss on the TIME of GBM. We showed that NF1 loss can indeed cause increased immune infiltration in GBM, with CD4+ and FOXP3+ T-lymphocytes, B-cells, NK-cells, and monocytes being the primary populations impacted. To gain more mechanistic insight into the differences between NF1 mutant and WT GBMs, we performed CITEseq on several NF1 mutant and WT GBM tumors. We used CellChat to examine the ligand-receptor interactions between the microenvironment cells and tumor cells in NF1 mutant vs. WT GBM. NF1 mutant GBMS had a greater amount and strength of ligand receptor interactions than NF1 WT GBM, many of them being pro-inflammatory. NF1 mutant GBMs had greater predicted TNF signaling due to broader expression on TNFRs on immune microenvironment cells. Next, we validated several predicted cytokine-mediated signaling pathways increased in NF1 mutant GBMs in silico by profiling the cytokines of human and mouse GBMs with targeted proteomics. We found that NF1 loss can also induce an increase in

the levels of pro-inflammatory cytokines, extracellular matrix components, and angiogenic factors, all potential mechanisms leading to the increased immune recruitment observed in NF1 deficient GBMs. Upon further investigation of the differentially expressed genes between the NF1 mutant and WT TIME cells, we found that NF1 mutant GBMs enhanced pro-inflammatory gene transcription through NFKB1 and CEBPB transcription factors. In sum, NF1 mutant GBMs recruit greater amounts of immune infiltrates through increased secretion of pro-inflammatory cytokines mediated by NFKB1 and CEBPB transcription factor activity.

Implications

In Chapter 3, we demonstrate the GBM cell lineage can influence the tumor immune microenvironment composition, and that TAM depletion does not afford survival benefit to several lineage-based mouse models of GBM. First, the revelation that GBM cell-lineage can influence tumor immune microenvironment composition opens the possibility of future immunotherapy clinical trials being segmented by Type 1 and Type 2 GBM. Immunotherapies that target MDMs may work better in the MDM-rich Type 2 GBM microenvironment. Future pre-clinical or clinical stage trials may reveal greater efficacy for immunotherapies in Type 2 GBMs.

Greater consensus on the preclinical data for CSF1R inhibitor therapies is needed. Here, we demonstrate in several mouse models of GBM that robust TAM depletion with the combination of a genetic and pharmacologic approach

does not lead to survival extension. This adds to recent reports of CSF1R inhibitor inefficacy in a PDGFRA and HRas-driven model of GBM[29]. Ultimately, given the failure of CSF1R inhibitor therapy in several additional models of GBM, broadly depleting TAMs in GBM is not likely to have clinical success, and the data presented here and elsewhere[29] explain the recent clinical trial failures of CSF1R inhibitor therapies. It remains to be seen if the combination of CSF1R inhibitor with other therapies is effective. Current data suggests that focusing future preclinical studies on depleting or augmenting specific TAM populations in GBM will likely be more effective than pan-TAM targeting strategies.

In Chapter 3, we demonstrated that *Nf1* loss in GBM endows a pro-inflammatory tumor immune microenvironment with greater infiltration of monocytic and lymphocytic populations and enhanced cytokine signaling. Given the increased immune activity observed in *Nf1* mutant GBMs, we propose prioritizing these patients for future GBM immunotherapy clinical trials. Because we see greater infiltration and activation of both myeloid and lymphoid populations, immunotherapies targeting either population could potentially show greater success in *Nf1* mutant GBMs.

Interestingly, recent work has shown that NF1 mutations do not correlate with patient response to checkpoint blockade therapy. However, other MAPK pathway alterations, such as BRAF and PTPN11, do correlate with checkpoint blockade therapy response[78]. Additionally, *PTEN* mutations were shown to negatively correlate with immune checkpoint blockade response[78]. Here, our mouse models also contained Pten mutations, however, they did not appear to mask the impact

of *Nf1* loss on the microenvironment. Considering all the available data, one segmentation strategy for future GBM immunotherapy clinical trials targeting T-cells could segment GBMs with MAPK pathway alterations (*NF1, BRAF, PTPN11)* vs. GBMs without MAPK alterations to examine if patients with MAPK alterations responded better.

Emerging drug targets and therapeutic strategies

In Chapter 2, we highlighted that TAM depletion may only be an effective therapeutic strategy for a small subset of GBMs (potentially PDGFB-driven GBMs). More work needs to be done to determine if TAM depletion is effective as a combination therapy, such as when paired with radiation or chemotherapy.

As better understanding of the heterogeneity of TAM populations in GBM evolves, more refined therapeutic targeting of TAMs may be effective. For example, it was recently discovered that CD169+ TAMs are anti-tumor[33]. As such, future therapeutic strategies could aim to bolster this anti-tumor population of TAMs. This could then be potentially combined with checkpoint blockade therapy to heighten anti-tumor immunity.

Several interesting drug targets emerge from our studies on NF1 mutant GBMs. Using targeted proteomics, we uncover several secreted proteins that are at higher levels in NF1 mutant human and mouse GBM. One protein of interest, CD70, was at significantly higher levels in NF1 mutant GBMs. CD70 is the

membrane bound ligand for receptor, CD27, and plays a role as an immune checkpoint[94]. CD70 has been shown to be expressed by tumor cells and immune cells[93]. CAR T cells targeting CD70 have been developed preclinically and have shown success in GBM[93]. If CD70 CAR T-cells make it to the clinic, it would be logical to stratify the clinical trial to observe differences in responses between NF1 mutant and WT patients.

We also highlight the potential importance of the TNFa signaling pathway and other pro-inflammatory cytokine signaling networks in promoting inflammation in the GBM TIME. One way to make the GBM TIME “Hot” and thereby more responsive to immunotherapies is to engineer methods to deliver cytokines to the TIME. One study did this by engineering an oncolytic virus that expressed cetuximab-CCL5. The combination of the oncolytic viral therapy with the secretion of cetuximab-CCL5 induced greater microenvironment inflammation and survival than oncolytic viral therapy alone[59]. Other methods of delivering immune-activating cytokines to the GBM TIME include engineering hematopoietic cells ex vivo to secrete high levels of that cytokine[98]. Additionally, antibody-cytokine fusion proteins have been delivered to GBM patients and have been safe and effective at enhancing T-cell presence[60]. In sum, adding immune-activating cytokines to complement immunotherapies in GBM is a promising approach to enhance patient responses.

Future directions

In chapter 2, we demonstrated that GBM cell lineage can influence the composition of the TIME, and that cell-lineage based mouse models of GBM were inherently insensitive to TAM depletion therapy. In the future, it would be beneficial to test more immunotherapies on Type 1, SVZ, NSC lineage derived GBMs vs. Type 2, oligodendrocytic lineage derived GBMs. Despite the Type 1 and Type 2 tumors having the same response to TAM depletion therapy, we hypothesize that they may respond differentially to other immunotherapies given the difference in microenvironment composition.

In addition to testing more immunotherapies on Type 1 and Type 2 tumors, it would also be beneficial to work out the mechanism responsible for causing increased immune cell recruitment to Type 2 tumors. Understanding the mechanism would enhance our basic understanding of how immune cells are recruited to the GBM TIME. This could be done by identifying differentially expressed cytokines between Type 1 and Type 2 GBMs to determine if Type 2 GBMs secreted higher levels of monocyte attracting cytokines. Then, the monocyte attracting cytokine could be knocked out of the Type 2 tumor primary cells, transplanted into mice, and then tumors measured for MDM recruitment levels.

In Chapter 3, we demonstrated that NF1 loss causes greater immune infiltration, partially through enhanced pro-inflammatory cytokine secretion by the NF1 mutant GBM TIME cells mediated by NFKB1 and CEBPB transcription factor

activity. For future experiments, it would be meaningful to determine the role of the cytokines differentially secreted by tumor and immune cells in NF1 mutant GBMs compared to NF1 WT GBMs. This could be done by knocking out the cytokine of interest in tumor cells or microenvironment cells. Alternatively, pharmacologic approaches could also be used, such as treating GBMs with a TNF inhibitor to determine how this impacted the TIME.

Additionally, several immunotherapies can be tested on NF1 mutant vs. WT GBMs to determine if NF1 mutant GBMs respond better. This can be done using checkpoint blockade therapy, CAR T-cell based therapies, and oncolytic virus therapy.

In addition to further exploring the roles of various cytokines in impacting the TIME in GBM, the transcription factor activity can also be further explored. For example, CEBPB could be knocked out in TAMs to see how this impacts their cytokine secretion and the overall recruitment of immune cells to the GBM TIME. In parallel, this could be done with NFKB1 as well. This would provide a better mechanistic understanding of the roles of these two transcription factors in controlling inflammation status in GBM.

Bibliography

1. Ostrom, Q.T. *et al.* CBTRUS Statistical Report: Primary Brain and Other Central Nervous System Tumors Diagnosed in the United States in 2009-2013. *Neuro Oncol* **18**, v1-v75 (2016).

2. Stoyanov, G.S. *et al.* Cell biology of glioblastoma multiforme: from basic science to diagnosis and treatment. *Med Oncol* **35**, 27 (2018).

3. Stupp, R. *et al.* Effect of Tumor-Treating Fields Plus Maintenance Temozolomide vs Maintenance Temozolomide Alone on Survival in Patients With Glioblastoma: A Randomized Clinical Trial. *JAMA* **318**, 2306-2316 (2017).

4. Vanderbeek, A.M. *et al.* The clinical trials landscape for glioblastoma: is it adequate to develop new treatments? *Neuro Oncol* **20**, 1034-1043 (2018).

5. Chen, R., Smith-Cohn, M., Cohen, A.L. & Colman, H. Glioma Subclassifications and Their Clinical Significance. *Neurotherapeutics* **14**, 284-297 (2017).

6. Bond, A.M., Ming, G.L. & Song, H. Adult Mammalian Neural Stem Cells and Neurogenesis: Five Decades Later. *Cell Stem Cell* **17**, 385-395 (2015).

7. Nishiyama, A., Shimizu, T., Sherafat, A. & Richardson, W.D. Life-long oligodendrocyte development and plasticity. *Semin Cell Dev Biol* **116**, 25-37 (2021).

8. Alcantara Llaguno, S. *et al.* Malignant astrocytomas originate from neural stem/progenitor cells in a somatic tumor suppressor mouse model. *Cancer Cell* **15**, 45-56 (2009).

9. Alcantara Llaguno, S.R. *et al.* Adult Lineage-Restricted CNS Progenitors Specify Distinct Glioblastoma Subtypes. *Cancer Cell* **28**, 429-440 (2015).

10. Wang, Z. *et al.* Cell Lineage-Based Stratification for Glioblastoma. *Cancer Cell* **38**, 366-379 e368 (2020).

11. Alcantara Llaguno, S. *et al.* Cell-of-origin susceptibility to glioblastoma formation declines with neural lineage restriction. *Nat Neurosci* **22**, 545-555 (2019).

12. Lee, J.H. *et al.* Human glioblastoma arises from subventricular zone cells with low-level driver mutations. *Nature* **560**, 243-247 (2018).

13. Verhaak, R.G. *et al.* Integrated genomic analysis identifies clinically relevant subtypes of glioblastoma characterized by abnormalities in PDGFRA, IDH1, EGFR, and NF1. *Cancer Cell* **17**, 98-110 (2010).

14. Brennan, C.W. *et al.* The somatic genomic landscape of glioblastoma. *Cell* **155**, 462-477 (2013).

15. Wang, Q. *et al.* Tumor Evolution of Glioma-Intrinsic Gene Expression Subtypes Associates with Immunological Changes in the Microenvironment. *Cancer Cell* **32**, 42-56 e46 (2017).

16. Yang, F.C. *et al.* Nf1-dependent tumors require a microenvironment containing Nf1+/-- and c-kit-dependent bone marrow. *Cell* **135**, 437-448 (2008).

17. Klemm, F. *et al.* Interrogation of the Microenvironmental Landscape in Brain Tumors Reveals Disease-Specific Alterations of Immune Cells. *Cell* **181**, 1643-1660 e1617 (2020).

18. Pombo Antunes, A.R. *et al.* Understanding the glioblastoma immune microenvironment as basis for the development of new immunotherapeutic strategies. *Elife* **9** (2020).

19. Hambardzumyan, D., Gutmann, D.H. & Kettenmann, H. The role of microglia and macrophages in glioma maintenance and progression. *Nat Neurosci* **19**, 20-27 (2016).

20. Liu, H. *et al.* Pro-inflammatory and proliferative microglia drive progression of glioblastoma. *Cell Rep* **36**, 109718 (2021).

21. Zhu, C., Kros, J.M., Cheng, C. & Mustafa, D. The contribution of tumor-associated macrophages in glioma neo-angiogenesis and implications for anti-angiogenic strategies. *Neuro Oncol* **19**, 1435-1446 (2017).

22. Shi, Y. *et al.* Tumour-associated macrophages secrete pleiotrophin to promote PTPRZ1 signalling in glioblastoma stem cells for tumour growth. *Nat Commun* **8**, 15080 (2017).

23. Chen, P. *et al.* Symbiotic Macrophage-Glioma Cell Interactions Reveal Synthetic Lethality in PTEN-Null Glioma. *Cancer Cell* **35**, 868-884 e866 (2019).

24. Takenaka, M.C. *et al.* Control of tumor-associated macrophages and T cells in glioblastoma via AHR and CD39. *Nat Neurosci* **22**, 729-740 (2019).

25. Mathewson, N.D. *et al.* Inhibitory CD161 receptor identified in glioma-infiltrating T cells by single-cell analysis. *Cell* **184**, 1281-1298 e1226 (2021).

26. Pyonteck, S.M. *et al.* CSF-1R inhibition alters macrophage polarization and blocks glioma progression. *Nat Med* **19**, 1264-1272 (2013).

27. Quail, D.F. *et al.* The tumor microenvironment underlies acquired resistance to CSF-1R inhibition in gliomas. *Science* **352**, aad3018 (2016).

28. Butowski, N. *et al.* Orally administered colony stimulating factor 1 receptor inhibitor PLX3397 in recurrent glioblastoma: an Ivy Foundation Early Phase Clinical Trials Consortium phase II study. *Neuro Oncol* **18**, 557-564 (2016).

29. Rao, R. *et al.* Glioblastoma genetic drivers dictate the function of tumor-associated macrophages/microglia and responses to CSF1R inhibition. *Neuro Oncol* **24**, 584-597 (2022).

30. Pombo Antunes, A.R. *et al.* Single-cell profiling of myeloid cells in glioblastoma across species and disease stage reveals macrophage competition and specialization. *Nat Neurosci* **24**, 595-610 (2021).

31. Ochocka, N. *et al.* Single-cell RNA sequencing reveals functional heterogeneity of glioma-associated brain macrophages. *Nat Commun* **12**, 1151 (2021).

32. Yeo, A.T. *et al.* Single-cell RNA sequencing reveals evolution of immune landscape during glioblastoma progression. *Nat Immunol* (2022).

33. Kim, H.J. *et al.* Blood monocyte-derived CD169(+) macrophages contribute to antitumor immunity against glioblastoma. *Nat Commun* **13**, 6211 (2022).

34. Bayik, D. *et al.* Myeloid-Derived Suppressor Cell Subsets Drive Glioblastoma Growth in a Sex-Specific Manner. *Cancer Discov* **10**, 1210-1225 (2020).

35. Miao, X. *et al.* CD103(+) Cell Growth Factor Flt3L Enhances the Efficacy of Immune Checkpoint Blockades in Murine Glioblastoma Model. *Oncol Res* **26**, 173-182 (2018).

36. Wang, H. *et al.* Different T-cell subsets in glioblastoma multiforme and targeted immunotherapy. *Cancer Lett* **496**, 134-143 (2021).

37. Ravi, V.M. *et al.* T-cell dysfunction in the glioblastoma microenvironment is mediated by myeloid cells releasing interleukin-10. *Nat Commun* **13**, 925 (2022).

38. Jacobs, J.F. *et al.* Prognostic significance and mechanism of Treg infiltration in human brain tumors. *J Neuroimmunol* **225**, 195-199 (2010).

39. Gao, J. *et al.* Integrative analysis of complex cancer genomics and clinical profiles using the cBioPortal. *Sci Signal* **6**, pl1 (2013).

40. Shingu, T. *et al.* Qki deficiency maintains stemness of glioma stem cells in suboptimal environment by downregulating endolysosomal degradation. *Nat Genet* **49**, 75-86 (2017).

41. Zamler, D.B. *et al.* Immune landscape of a genetically engineered murine model of glioma compared with human glioma. *JCI Insight* **7** (2022).

42. Ausman, J.I., Shapiro, W.R. & Rall, D.P. Studies on the chemotherapy of experimental brain tumors: development of an experimental model. *Cancer Res* **30**, 2394-2400 (1970).

43. Seyfried, T.N., el-Abbadi, M. & Roy, M.L. Ganglioside distribution in murine neural tumors. *Mol Chem Neuropathol* **17**, 147-167 (1992).

44. Hambardzumyan, D., Amankulor, N.M., Helmy, K.Y., Becher, O.J. & Holland, E.C. Modeling Adult Gliomas Using RCAS/t-va Technology. *Transl Oncol* **2**, 89-95 (2009).

45. Genoud, V. *et al.* Responsiveness to anti-PD-1 and anti-CTLA-4 immune checkpoint blockade in SB28 and GL261 mouse glioma models. *Oncoimmunology* **7**, e1501137 (2018).

46. Szatmari, T. *et al.* Detailed characterization of the mouse glioma 261 tumor model for experimental glioblastoma therapy. *Cancer Sci* **97**, 546-553 (2006).

47. Khalsa, J.K. *et al.* Immune phenotyping of diverse syngeneic murine brain tumors identifies immunologically distinct types. *Nat Commun* **11**, 3912 (2020).

48. Reardon, D.A. *et al.* Glioblastoma Eradication Following Immune Checkpoint Blockade in an Orthotopic, Immunocompetent Model. *Cancer Immunol Res* **4**, 124-135 (2016).

49. Aslan, K. *et al.* Heterogeneity of response to immune checkpoint blockade in hypermutated experimental gliomas. *Nat Commun* **11**, 931 (2020).

50. Omuro, A. *et al.* Radiotherapy Combined With Nivolumab or Temozolomide for Newly Diagnosed Glioblastoma With Unmethylated

MGMT Promoter: An International Randomized Phase 3 Trial. *Neuro Oncol* (2022).

51. Haddad, A.F. *et al.* Mouse models of glioblastoma for the evaluation of novel therapeutic strategies. *Neurooncol Adv* **3**, vdab100 (2021).

52. Martinez-Murillo, R. & Martinez, A. Standardization of an orthotopic mouse brain tumor model following transplantation of CT-2A astrocytoma cells. *Histol Histopathol* **22**, 1309-1326 (2007).

53. Chen, Z. *et al.* Genetic driver mutations introduced in identical cell-of-origin in murine glioblastoma reveal distinct immune landscapes but similar response to checkpoint blockade. *Glia* **68**, 2148-2166 (2020).

54. Chen, D.S. & Mellman, I. Oncology meets immunology: the cancer-immunity cycle. *Immunity* **39**, 1-10 (2013).

55. Reardon, D.A. *et al.* Effect of Nivolumab vs Bevacizumab in Patients With Recurrent Glioblastoma: The CheckMate 143 Phase 3 Randomized Clinical Trial. *JAMA Oncol* **6**, 1003-1010 (2020).

56. Todo, T. *et al.* Intratumoral oncolytic herpes virus G47Δ for residual or recurrent glioblastoma: a phase 2 trial. *Nat Med* **28**, 1630-1639 (2022).

57. Liau, L.M. *et al.* Association of Autologous Tumor Lysate-Loaded Dendritic Cell Vaccination With Extension of Survival Among Patients With Newly Diagnosed and Recurrent Glioblastoma: A Phase 3 Prospective Externally Controlled Cohort Trial. *JAMA Oncol* (2022).

58. Song, E. *et al.* VEGF-C-driven lymphatic drainage enables immunosurveillance of brain tumours. *Nature* **577**, 689-694 (2020).

59. Tian, L. *et al.* Specific targeting of glioblastoma with an oncolytic virus expressing a cetuximab-CCL5 fusion protein via innate and adaptive immunity. *Nat Cancer* **3**, 1318-1335 (2022).

60. Weiss, T. *et al.* Immunocytokines are a promising immunotherapeutic approach against glioblastoma. *Sci Transl Med* **12** (2020).

61. Luoto, S. *et al.* Computational Characterization of Suppressive Immune Microenvironments in Glioblastoma. *Cancer Res* **78**, 5574-5585 (2018).

62. Christofides, A. *et al.* The complex role of tumor-infiltrating macrophages. *Nat Immunol* **23**, 1148-1156 (2022).

63. Chen, Z., Ross, J.L. & Hambardzumyan, D. Intravital 2-photon imaging reveals distinct morphology and infiltrative properties of glioblastoma-associated macrophages. *Proc Natl Acad Sci U S A* **116**, 14254-14259 (2019).

64. Bowman, R.L. *et al.* Macrophage Ontogeny Underlies Differences in Tumor-Specific Education in Brain Malignancies. *Cell Rep* **17**, 2445-2459 (2016).

65. Buttgereit, A. *et al.* Sall1 is a transcriptional regulator defining microglia identity and function. *Nat Immunol* **17**, 1397-1406 (2016).

66. Hammond, T.R. *et al.* Single-Cell RNA Sequencing of Microglia throughout the Mouse Lifespan and in the Injured Brain Reveals Complex Cell-State Changes. *Immunity* **50**, 253-271 e256 (2019).

67. Bennett, M.L. *et al.* New tools for studying microglia in the mouse and human CNS. *Proc Natl Acad Sci U S A* **113**, E1738-1746 (2016).

68. Chen, Z. *et al.* Cellular and Molecular Identity of Tumor-Associated Macrophages in Glioblastoma. *Cancer Res* **77**, 2266-2278 (2017).

69. Parkhurst, C.N. *et al.* Microglia promote learning-dependent synapse formation through brain-derived neurotrophic factor. *Cell* **155**, 1596-1609 (2013).

70. Galarneau, H., Villeneuve, J., Gowing, G., Julien, J.P. & Vallieres, L. Increased glioma growth in mice depleted of macrophages. *Cancer Res* **67**, 8874-8881 (2007).

71. Hanahan, D. & Weinberg, R.A. Hallmarks of cancer: the next generation. *Cell* **144**, 646-674 (2011).

72. Bruttger, J. *et al.* Genetic Cell Ablation Reveals Clusters of Local Self-Renewing Microglia in the Mammalian Central Nervous System. *Immunity* **43**, 92-106 (2015).

73. Chen, J., Kwon, C.H., Lin, L., Li, Y. & Parada, L.F. Inducible site-specific recombination in neural stem/progenitor cells. *Genesis* **47**, 122-131 (2009).

74. Groszer, M. *et al.* Negative regulation of neural stem/progenitor cell proliferation by the Pten tumor suppressor gene in vivo. *Science* **294**, 2186-2189 (2001).

75. Zhu, X. *et al.* Age-dependent fate and lineage restriction of single NG2 cells. *Development* **138**, 745-753 (2011).

76. Buch, T. *et al.* A Cre-inducible diphtheria toxin receptor mediates cell lineage ablation after toxin administration. *Nat Methods* **2**, 419-426 (2005).

77. Love, M.I., Huber, W. & Anders, S. Moderated estimation of fold change and dispersion for RNA-seq data with DESeq2. *Genome Biol* **15**, 550 (2014).

78. Zhao, J. *et al.* Immune and genomic correlates of response to anti-PD-1 immunotherapy in glioblastoma. *Nat Med* **25**, 462-469 (2019).

79. Zhang, Y. *et al.* An RNA-sequencing transcriptome and splicing database of glia, neurons, and vascular cells of the cerebral cortex. *J Neurosci* **34**, 11929-11947 (2014).

80. Jin, S. *et al.* Inference and analysis of cell-cell communication using CellChat. *Nat Commun* **12**, 1088 (2021).

81. Yang, Y., Islam, M.S., Hu, Y. & Chen, X. TNFR2: Role in Cancer Immunology and Immunotherapy. *Immunotargets Ther* **10**, 103-122 (2021).

82. Skartsis, N. *et al.* IL-6 and TNFalpha Drive Extensive Proliferation of Human Tregs Without Compromising Their Lineage Stability or Function. *Front Immunol* **12**, 783282 (2021).

83. Bowman, R.L., Wang, Q., Carro, A., Verhaak, R.G. & Squatrito, M. GlioVis data portal for visualization and analysis of brain tumor expression datasets. *Neuro Oncol* **19**, 139-141 (2017).

84. Hoesel, B. & Schmid, J.A. The complexity of NF-kappaB signaling in inflammation and cancer. *Mol Cancer* **12**, 86 (2013).

85. Han, H. *et al.* TRRUST: a reference database of human transcriptional regulatory interactions. *Sci Rep* **5**, 11432 (2015).

86. Turner, M.D., Nedjai, B., Hurst, T. & Pennington, D.J. Cytokines and chemokines: At the crossroads of cell signalling and inflammatory disease. *Biochim Biophys Acta* **1843**, 2563-2582 (2014).

87. Marques, C. *et al.* NF1 regulates mesenchymal glioblastoma plasticity and aggressiveness through the AP-1 transcription factor FOSL1. *Elife* **10** (2021).

88. Bhat, K.P.L. *et al.* Mesenchymal differentiation mediated by NF-kappaB promotes radiation resistance in glioblastoma. *Cancer Cell* **24**, 331-346 (2013).

89. Carro, M.S. *et al.* The transcriptional network for mesenchymal transformation of brain tumours. *Nature* **463**, 318-325 (2010).

90. Acosta, J.C. *et al.* Chemokine signaling via the CXCR2 receptor reinforces senescence. *Cell* **133**, 1006-1018 (2008).

91. Kuilman, T. *et al.* Oncogene-induced senescence relayed by an interleukin-dependent inflammatory network. *Cell* **133**, 1019-1031 (2008).

92. Wang, L.B. *et al.* Proteogenomic and metabolomic characterization of human glioblastoma. *Cancer Cell* **39**, 509-528 e520 (2021).

93. Seyfrid, M. *et al.* CD70 as an actionable immunotherapeutic target in recurrent glioblastoma and its microenvironment. *J Immunother Cancer* **10** (2022).

94. Starzer, A.M. & Berghoff, A.S. New emerging targets in cancer immunotherapy: CD27 (TNFRSF7). *ESMO Open* **4**, e000629 (2020).

95. Hara, T. *et al.* Interactions between cancer cells and immune cells drive transitions to mesenchymal-like states in glioblastoma. *Cancer Cell* **39**, 779-792 e711 (2021).

96. Stoeckius, M. *et al.* Cell Hashing with barcoded antibodies enables multiplexing and doublet detection for single cell genomics. *Genome Biol* **19**, 224 (2018).

97. Azizi, E. *et al.* Single-Cell Map of Diverse Immune Phenotypes in the Breast Tumor Microenvironment. *Cell* **174**, 1293-1308 e1236 (2018).

98. Birocchi, F. *et al.* Targeted inducible delivery of immunoactivating cytokines reprograms glioblastoma microenvironment and inhibits growth in mouse models. *Sci Transl Med* **14**, eabl4106 (2022).